DURBAN UNIVERSITY OF TECHNOLOGY
INYUVESI YASETHEKWINI YEZOBUCHWEPHESHE

DESALINATION OF A LOCAL OIL REFINERY EFFLUENT TO MEET DISCHARGE LIMITS

Submitted in fulfillment of the requirements for the degree of:

Master of Engineering in the Department of Chemical Engineering,

Faculty of Engineering
and the Built Environment

at Durban University of Technology

By

Elorm Obotey Ezugbe (21959409)

Date: June 2021

Supervisor: Prof S. Rathilal

Preface

This research was carried out under the collaboration of the Durban University of Technology, Department of Chemical Engineering and FFS Refiners (Pty) Ltd, under the supervision of Prof. Sudesh Rathilal. Preliminary analyses, including effluent characterization were conducted at FFS Refiners' Production laboratory, Jacobs. Experimental runs and analyses of results were conducted in the Department of Chemical Engineering, Faculty of Engineering and The Built Environment, DUT.

Declaration

I, **Elorm Obotey Ezugbe** the undersigned candidate declare that

i. The research reported in this dissertation, except where otherwise indicated, is my original work.

ii. This dissertation has not been submitted for any degree or examination at any other university.

iii. This dissertation does not contain other persons' data, pictures, graphs or other information, unless specifically acknowledged as being sourced from other persons.

iv. This dissertation does not contain other persons' writing, unless specifically acknowledged as being sourced from other researchers. Where other written sources have been quoted, then:

   a) their words have been re-written but the general information attributed to them has been referenced;

   b) where their exact words have been used, their writing has been placed inside quotation marks, and referenced.

v. Where I have reproduced a publication of which I am an author, co-author or editor, I have indicated in detail which part of the publication was actually written by myself alone and have fully referenced such publications.

vi. This dissertation does not contain text, graphics or tables copied and pasted from the Internet, unless specifically acknowledged, and the source being detailed in the dissertation and in the References sections.

Signature: …… Date: 21/09/2021……..

Prof S. Rathilal

Signature: …… Date: 21 September 2021……..

Acknowledgements

My foremost thanksgiving goes to God, the Lord of Host for His providence, mercy and grace. Thank You Lord for how far You have brought me.

I wish to express my heartfelt gratitude to my supervisor, Prof Sudesh Rathilal for his immense support, guidance, encouragement and care through this period of research. Prof, your impact is indelible. Thank you.

Special thanks to Mr. Emmanuel K. Tetteh, Dr. Edward K. Armah, Mr. Dennis Asante-Sackey, Mr. Jeremiah Adedeji, Dr Dennis Amoah and Mr. Samuel Ofori Frimpong for being a solid bulwark for me and providing useful tidbits that made my work easier and better. God bless you in abundance.

Many thanks to the staffs of FFS Refiners - Jacobs, especially to Ms. Keshnee Naik and April Pather of the R&D department, Mr. Arish and Mr. Luntu of the production laboratory. I appreciate the urgency with which you responded to my questions and needs during my period of training and throughout this research.

To the members of the Green Engineering and Sustainability research group, especially Ms. Gloria Amo-Duodu, Ms. N. Sibiya and Dr Martha, I say, thank you for your valuable contributions to my research.

Mr. Mohamed Jaafar Bux, Mr. Vishnu Krbagaran Moodley and Ms. Seshna Sewsanker, technicians at the department of chemical engineering, you were very supportive. I appreciate your contributions.

Now to Durban University of Technology for providing financial support, Chemical Engineering postgrads and entire the department of Chemical Engineering, thank you for creating a friendly environment for me to carry out my research.

Last but not least, I would like to say thank you to the entire Ezugbe family for their love and prayers, Mr. George F. Agordzo, Mr. Gorge Tsevi and Ms. Veronica Agbesi-Elloh for their constant checkups, advice and endless love. And to all those whose names are not written here, please know that your support and efforts are deeply appreciated. God bless you all in abundance.

Dedication

This dissertation is dedicated to my parents, Mr. & Mrs. Ezugbe, Mr. George F. Agordzo, Ms. Veronica Agbesi-Elloh and Dela Aku Ezugbe (Mrs. Agbeve). You gave everything to see this dream come true.

And to you my nephew, George Dzordzormenunya Agbeve, mummy gave birth to you while I was away. I hope this inspires you! The world awaits your impact.

Abstract

The Sustainable Development Goal Six (SDG 6) – "ensure availability and sustainable management of water and sanitation for all" places huge responsibilities on stakeholders (industry, domestic and agricultural) to prioritize water saving, water reuse and proper wastewater treatment to make potable water accessible everywhere in the world.

With the industrial sector consuming nearly 20% of the fresh water available, there is a corresponding generation of large volumes of effluents. This has been projected to increase, as population is skyrocketing and more economies are becoming more industrialized to accommodate the needs of the ever-increasing population.

Over the years, stringent effluent discharge limits have been imposed on the industrial sector to minimize the pollution of the receiving environments, especially the water bodies. In addition, wastewater treatment for reuse is being encouraged, which will ease the stress on freshwater resources.

The oil refinery industry is noted for the generation of large volumes of effluents. These effluents are heavy laden with toxic and refractory materials as well as high concentrations of salts which pose huge environmental risks and detrimental ripple effects on humans and animals if these effluents are not properly treated before discharge. Unfortunately, the use of conventional treatment methods to treat downstream oil refinery effluent (ORE) has been unsuccessful in the removal of these materials, especially the salts.

This research therefore, aimed at desalinating the effluent from the effluent treatment plant (ETP) of a local South African waste oil refinery to meet discharge limits. The ETP, even though successful in the removal of organics (COD, turbidity and colour), consistently records high levels of sulphates, chlorides and carbonates as a result of the source of their raw material and other in-house processes that take place during the treatment process.

The study assessed and compared the feasibility of applying three membrane processes, viz forward osmosis (FO), reverse osmosis (RO) and hybrid FO-RO systems in desalinating the ORE. The FO and RO were first run as standalone processes, where models were generated and used to optimize the important factors using the Box-Benhken design (BBD) of response surface methodology (RSM). Based on the optimized conditions, the hybrid FO-RO was investigated. The basis of comparison was their permeation fluxes, salt rejection and flux recoverability after membrane cleaning. A total of 45 experimental runs were

conducted which catered for pure water flux tests of virgin membranes, optimization studies and confirmatory runs. The factors of interest for FO were feed solution flow rate (FS-FR) (7.5 – 9.4 L/h), draw solution flow rate (DS-FR) (7.5 – 9.4 L/h) and draw solution concentration (DS-C) (20, 35 and 50 g/L NaCl). With RO, focus was placed on operating pressure (14 – 18 bar), feed concentration and operating time (4-6 h).

The results showed an average permeation flux of 3.64 ± 0.13 L/m^2h, Cl^- enrichment (reverse solute diffusion (RSD)) of 35.5 ± 5.15%, SO_4^{2-} rejection of 100%, CO_3^{2-} rejection of 94.59 ± 0.32 and flux recovery of 86.01 ± 2.66% for FO. For RO, the average permeation flux achieved was 2.29 ± 0.24 L/m^2h, Cl^- rejection efficiency was 90.54 ± 0.81%, SO_4^{2-} rejection efficiency was 95.1%, CO_3^{2-} rejection efficiency was 97.3 ± 0.4 and flux recovery after membrane cleaning was 62.52 ± 2.62%. The FO-RO hybrid process proved unsuccessful due to constraints from the filtration unit. As an intervention to make the hybrid process work, NF was used as the recovery process. However, results show a low permeation flux of 0.69 ± 0.10 L/m^2h on average.

From the results obtained, it was concluded that RO presents the best desalination option for treating the ORE using low pressure of between 14 – 18 bar. This will require no post treatment and there will be no contamination of feed due to RSD.

Research outputs

Conferences

i. **Ezugbe E. O**., Rathilal S., Ishwarlall S. and Kweinor Tetteh E., 2020. Removal of Cl^-, SO_4^{2-} and CO_3^{2-} salts from oil refinery effluent using forward osmosis. 18th Johannesburg International Conference on Science, Engineering, Technology and Waste Management (SETWM-20), 16 – 17 November, 2020, Johannesburg, South Africa.

ii. **Ezugbe E. O**., Rathilal S., Ishwarlall S. and Kweinor Tetteh E., 2020. Desalination of oil refinery effluent using forward osmosis; effects of cross flowrate on process efficiency. 5th Interdisciplinary Research and Innovation Conference, 15 – 17 September 2020, Durban, South Africa.

Publications

i. **Ezugbe, E. O**., Kweinor Tetteh, E., Rathilal, S., Asante-Sackey, D. and Amo-Duodu, G. 2021. Desalination of municipal wastewater using forward osmosis. *Membranes,* 11(2): 119. Available: https://www.mdpi.com/2077-0375/11/2/119

ii. **Ezugbe, E. O.** and Rathilal, S. 2020. Membrane technologies in wastewater treatment: A review. *Membranes* 10(5): 89. Available: https://www.mdpi.com/2077-0375/10/5/89

Table of contents

List of figures

List of tables

Nomenclature

AEM	Anion exchange membrane
AGMD	Air gap membrane distillation
BBD	Box-Behnken Design
BOD	Biochemical oxygen demand
CA	Cellulose acetate
Cd	Cadmium
CEB	Chemically enhanced backwashing
CECP	Concentrative external concentration polarization
CEM	Cation exchange membrane
CICP	Concentrative internal concentration polarization
CIP	Cleaning in place
Cl^-	Chloride ion
CO_3^{2-}	Carbonate ion
COD	Chemical oxygen demand
CP	Concentration polarization
DCMD	Direct contact membrane distillation
DECP	Dilutive external concentration polarization
D_f	Dilution factor
DI	De-ionized
DICP	Dilutive internal concentration polarization
ED	Electrodialysis
EDR	Electrodialysis reversal

FO	Forward osmosis
FO-RO	Forward osmosis-reverse osmosis
ICP	Internal concentration polarization
LGMD	Liquid gap membrane distillation
MD	Membrane distillation
MF	Microfiltration
MWCO	Molecular weight cut off
NF	Nanofiltration
PE	Polyethylene
PTFE	Polytetraflourethylene
PV	Pervaporation
PWF	Pure water flux
RO	Reverse osmosis
rpm	Revolution per minute
RSM	Response surface methodology
TDS	Total dissolved solids
TFC	Thin film composite
TOC	Total organic carbon
TSS	Total suspended solids
Sn	Tin
SO_4^{2-}	Sulphate ion
SS	Stainless steel
UF	Ultrafiltration

VMD	Vacuum membrane distillation

Chapter 1

INTRODUCTION

1.1 Background

Industrial effluent treatment for reuse or discharge provides a great option for water conservation and environmental sustainability. Generation of effluents is unavoidable, as it forms a fundamental part of the value chain in all sectors of life. As population grows, there is also a corresponding growth in industrial, domestic and agricultural activities which rely heavily on freshwater resources. These activities deplete the limited freshwater resources. Also, these activities produce large volumes of effluents which cause severe environmental problems when disposed of without proper treatment. As a result, there is imbalance in the distribution of freshwater across all sectors. This is obvious in most parts of the world especially Africa and parts of Asia, as acute water shortage is recorded frequently throughout the year, amidst serious environment issues accompanied by water scarcity (UN Water 2019; Ezugbe and Rathilal 2020)

One of the major industries that utilize much water in their processes is the oil refinery industry. It is reported that for every one barrel of oil refined, about 10 barrels of wastewater is produced (Pendashteh *et al.* 2011). During the process of refining petroleum into useful products, refineries use large volumes of water for processes such as distillation, cracking, polymerization, alkylation, hydrotreating, desalting, treatment and finishing of petroleum products. In addition, wastewater is generated through cleaning activities ranging from housekeeping to cleaning of crude storage tanks and crude transportation vessels (Kuyukina, Krivoruchko and Ivshina 2020). By virtue of the sources of these effluents, their composition is highly complex and inconsistent. This highly contaminated water is made up of high concentrations of residual free and emulsified oils, hydrocarbons (representing the main organic load), dissolved salts (halides, phosphates, sulphates and sulfides), carcinogenic and mutagenic substances which require rigorous treatment for their proper removal (Barthe *et al.* 2015).

Over the years, many treatment processes have been employed in ORE treatment. Mostly, the effluent treatment train consists of pretreatment or primary treatment processes such as oil water separation, dissolved air floatation coagulation and flocculation. In addition, further clarification of the effluent is done to reduce suspended materials and colloids.

These help in recovery of residual oils, while making the effluent better suited for discharge or other treatment processes such as biological treatment. However, as stringent regulations for wastewater discharge are becoming stricter, effluent treatment plants (ETPs) are faced with the challenge of further treatment of their effluents. Coupled with the stringent discharge limits, the need for industry to treat its effluents for reuse to enhance water conservation and reduce the stress on freshwater sources drives ETPs to explore more advanced options in treatment of their effluents (Kuyukina, Krivoruchko and Ivshina 2020).

In addition to recalcitrant organic and refractory materials that present a major challenge to ORE treatment, salinity of oil refinery effluents equally poses a great challenge in treating the effluent to meet discharge standards. Salinity is the mass of salt dissolved in a unit mass of water (Singh and Hankins 2016a). Salinity of oil refinery effluents (ORE) can be as high as 35,000 ppm (Tetteh *et al.* 2020). This is clearly problematic for conventional ORE treatment processes to treat effectively. These saline wastewaters have devastating effects on their receiving environments. On top of this, failure of treatment plants to meet discharge limits leads to the imposition of sanctions by the municipality and payment of huge fines.

1.2 Problem Statement

In their attempt to meet stringent discharge standards, save cost on effluent disposal and conserve water, most oil refineries subject their effluents to at least the basic treatment processes such as oil-water separation, dissolved air floatation, coagulation/flocculation, and sedimentation. However, these processes seldom treat the effluents to discharge limits or to reuse standards. At best, some treatment plants employ biological treatment processes to degrade the high organic content of ORE. This leaves the effluent with high concentration of dissolved salts as the conventional treatment processes do not remove these dissolved salts.

In the effluent treatment plant of a local waste oil refinery in Durban, KwaZulu Natal Province, 20 kiloliters of wastewater is processed per hour. The source of this wastewater is from ship slops, bottoms of tankers, refinery off-specs, housekeeping activities within the refinery, surface runoffs etc. This makes the effluent very complex, high in residual oil concentration and varied concentrations of organics and dissolved salts. Before being discharged into the municipal sewers, the effluent undergoes a series of treatment processes

as shown in Figure 1-1. Consequently nearly 95% of residual oil is recovered and processed into other useful products. Similarly, chemical oxygen demand (COD), soap oil and grease (SOG), total suspended solids (TSS) and turbidity are removed to below the required discharge limits (Tetteh, Rathilal and Robinson 2018).

To manage the high levels of sulfide, which is characteristic of the plant's effluents, hydrogen peroxide (H_2O_2) is dosed into the effluent at the municipal sewer inlet as shown in figure 1.1. The hydrogen peroxide, as an oxidizing agent, oxidizes the sulfide to sulphates. This intervention in turn, causes the generation of sulphates in high concentrations (855.756 ± 138.23 mg/L) in the effluent discharged into the municipal sewer. In addition to the sulphates, high chloride concentration (714.4 ± 126 mg/L), which is an intrinsic nature of the effluent due to its source and high carbonate concentrations (206 ± 23 mg/L) generated from the in-house processes such as the incessant use of large quantities of lime during the process of clarification, make the final effluent fall short of discharge limits (Cl^- = 250 mg/L, SO_4^{2-} = 250 mg/L and CO_3^{2-} = 61 mg/L) and ISO:14001 regulations (environmental management systems) (EPA 2015).

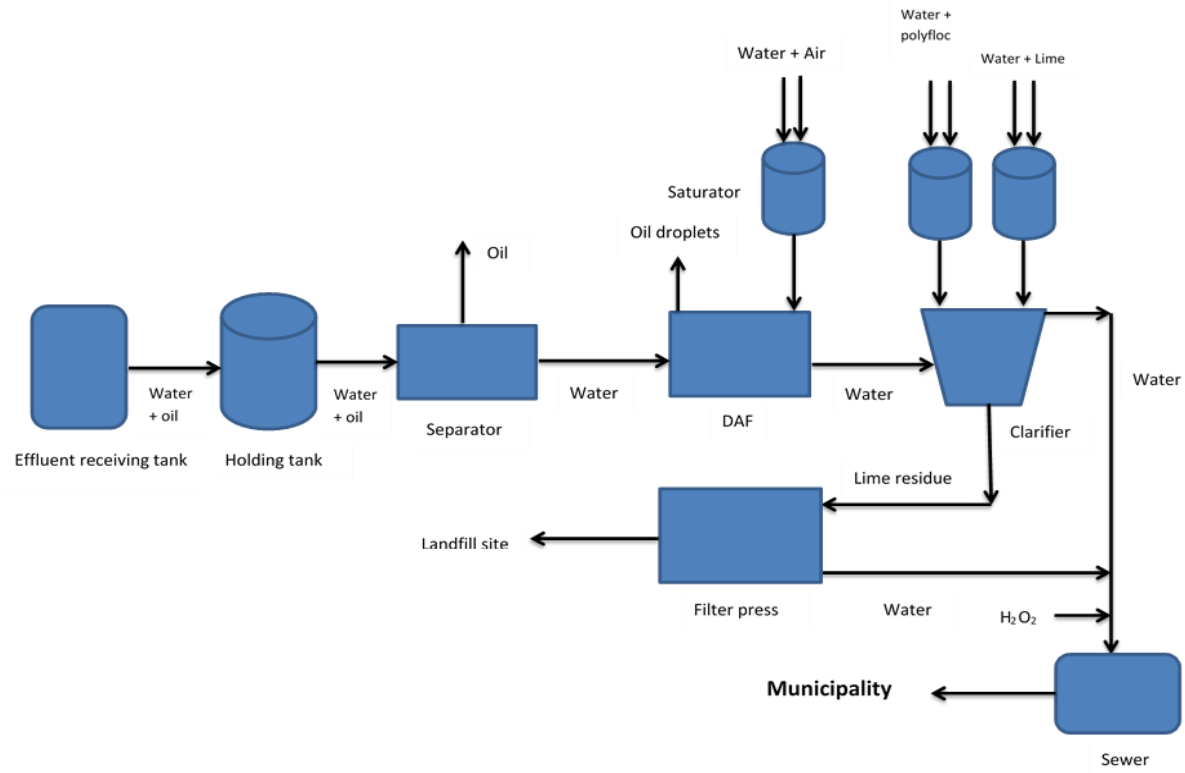

Figure 1-1: Block flow diagram of local waste oil refinery ETP

This poses an immediate risk to the ETP, as it invites high fines from the municipality. In addition, this limits the possibility of the plant to reuse its effluent due to the hardness and

corrosive propensity of the water. Again, the ripple effects of the saline effluent on the environment are detrimental, and as such it is imperative to find an efficient desalination technique to remove the salts for safe disposal before the effluent is discharged or reused.

1.3 Desalination processes

Desalination is the removal of dissolved salts from saline water, be it seawater, brackish water or wastewater, to make it useable for domestic, agricultural or industrial activities. Desalination is either by thermal means, like vapor compression (VC), multistage flash (MSF), or multi-effect distillation (MED) or by membrane technology, mainly reverse osmosis (RO) (Singh and Hankins 2016a). However, due to the energy intensity of thermal desalination processes, there has been a great shift to membrane desalination processes over the past couple of decades (Burn and Gray 2015).

1.4 Membrane technology for desalination

Membrane technology encompasses the use of a barrier (membrane) to selectively separate two phases from each other based on factors such as size or volatility. Membrane technology presents many attractive features that make desalination of any saline stream relatively cheap, compared to thermal desalination processes. In addition, the use of membrane processes guarantees the removal of at least 95% of contaminants than any treatment process can achieve (Noble and Stern 1995; Chollom, Rathilal and Pillay 2014). Basically, membrane technology is classified as either pressure driven (RO, NF, ultrafiltration (UF), microfiltration (MF)), where external hydraulic pressure is applied to cause separation or osmotically driven (forward osmosis (FO), pressure retarded osmosis (PRO)), where movement of water is driven by osmotic pressure gradient (Wang *et al.* 2008).

In RO desalination, an external pressure is generated that overcomes the osmotic pressure of the feed. This forces water molecules to move across the membrane while leaving behind the salt. For a feed of salinity 500 – 10,000 ppm, a pressure of 10 – 20 bar is required whereas for salinities above 10,000 ppm, pressures of above 20 bar would be required. RO has a proven efficiency of desalination, removing univalent ions up to 99.5% (Lee, Arnot and Mattia 2011; Singh and Hankins 2016a).

FO is a dilution process in which two solutions having different osmotic pressures are circulated at opposite sides of a semi permeable membrane. The more concentrated

solution known as the draw solution (DS) draws water from the less concentrated one known as the feed solution (FS). The movement of the water molecules continues until equilibrium is reached (Ezugbe *et al.* 2021). Since the FO process does not require an external pressure for separation, the process provides many opportunities for low energy desalination (Linares *et al.* 2014). In most cases however, FO requires a recovery process, unless for niche applications, where the permeate forms part of the product and therefore, needs no recovery.

It is worthy to note, that reducing the osmotic pressure of the feed to RO can significantly reduce the energy for desalination. This can be achieved by dilution of the feed. This makes the combination of RO with dilution processes like FO very promising. The hybrid FO-RO process has the potential of simultaneously treating wastewater while desalinating a saline stream (Bamaga, Yokochi and Beaudry 2009; Cath, Drewes and Lundin 2009). In the hybrid FO-RO combination, the water drawn from the FS dilutes the DS. This water is recovered during the RO process. At the same time, the DS is reconstituted to ensure maintenance of the DS osmotic pressure (Al-Zuhairi *et al.* 2015).

This research therefore seeks to explore the application of membrane technology, specifically FO, RO, and a combination of the two (FO-RO), to desalinate ORE effluent. Effects of operating variables such as feed solution flow rate, draw solution flow rate and draw solution concentration on performance of FO is studied while for RO, the effects of feed concentration, operating time and operating pressure on the process performance is studied.

1.5 Aims and Objectives

The main aim of the research was to investigate and recommend a desalination process for treatment of a local oil refinery effluent to meet discharge limits. The specific objectives are;

i. To determine the optimum operating conditions for each process using Design Expert Software.
ii. To evaluate the permeation flux of FO, RO and hybrid FO-RO/NF system based on optimum conditions.
iii. To evaluate and compare salt rejection of the three membrane processes at optimum conditions.
iv. To evaluate flux recoverability of the three processes after membrane cleaning.

1.6 Approach

Effluent for this project was collected at the three-phase separator (sewer) of a local waste oil refinery in Durban, in the KwaZulu Natal Province, South Africa. At this point (sewer), the effluent had gone through some form of treatment stages. Residual oil was removed at the oil-water separator as well as the dissolved air floatation (DAF) units. Suspended solids were removed by means of coagulation and flocculation at the clarifier. The effluent was then passed into the sewer for onward discharge into the municipal treatment systems.

In total, 45 experimental runs were conducted. The first round of experiments included the determination of pure water flux for both FO and RO virgin membranes. These were run in triplicates. This was then followed by 15 runs each for FO and RO using the Box Behnken Design of response surface methodology (RSM), utilizing a synthetic feed to optimize the entire treatment process. The final stage of the experiment, which involved 3 confirmatory runs each for FO and RO and 3 runs for the hybrid FO-RO was conducted with real effluent at the obtained optimum conditions.

To achieve membrane cleaning towards flux recoverability, both physical and chemical cleaning processes were adopted. For FO, physical cleaning was by manual flushing of the membrane under running water while scrubbing the surface. This was followed by osmotic backwash to reverse the flow of permeate and dislodge foulants that may be within the membrane pores. For RO, physical cleaning was achieved by forward flushing at low pressure while chemical cleaning was performed using NaOH and HCl solutions as prescribed by membrane manufacturers.

1.7 Organization of dissertation

The dissertation consists of five chapters which are organized as follows;

Chapter One:

This chapter gives an introduction and background to the entire study, highlighting the need for the study and the expected outcome.

Chapter Two:

This chapter presents a comprehensive review of the literature related to the generation and effects of ORE on the environment, membrane desalination techniques (their advantages and disadvantages and the factors that affect their performance) and experimental design.

Chapter Three:

Research methodology, materials, methods, and equipment description as well as the procedures for experiment are captured here. For the first part, procedures for FO and RO as standalone processes are presented. This is followed by the procedures for hybrid FO-RO/NF at optimum conditions.

Chapter Four:

This chapter presents the results and discussions of the study. First, the performance efficiency of FO and RO are highlighted based on the studied operating conditions. Then comparative studies between the FO, RO and FO-RO/NF hybrid process are presented. Interpretation of results was done through quantitative and qualitative data analysis.

Chapter Five:

This chapter concludes the entire study, declaring new findings, making deductions as well as recommendations for further studies in desalination of ORE.

Chapter 2

Literature Review

2.1 Introduction

The Petroleum refinery industry has been instrumental in providing energy to the world, driving industrial activities and world economies for centuries now. Statistics show that about 57.3% of the world's energy requirements are met by the petroleum industry (Hannah 2020). There are however, huge environmental risks associated with the large volumes of effluents produced by this industry if discharged without adequate treatment. Much work has been done in the treatment of oil refinery effluents (ORE) especially the organic components. However, the high concentrations of salts (TDS) in ORE remains a challenge as efficient and cost-effective treatment processes are still difficult to come by. This is the challenge with the effluent treatment plant (ETP) of a local South African waste oil refinery treatment plant. This chapter reviews relevant literature on the oil refinery industry, oily effluent generation and characteristics, treatment processes and their various advantages and disadvantages. Particularly, much focus is given to literature on membrane technology and its application in desalination of oil refinery effluent. Finally, an exposition is made on experimental design, taking into consideration multifactorial interactions and their effects on the removal of the targeted salt.

2.2 The oil refinery industry and oily wastewater generation – The South African perspective.

The global petroleum production has been reported to reach 4.4 billion tons (Tian *et al.* 2020). Even though South Africa does not have its own crude oil reserves, the refining of crude oil supplied from other countries like Saudi Arabia, Angola, Nigeria, Ghana etc., is a major activity within the country (SAPIA 2021). Up to 60% of the country's crude oil requirements are supplied by the above-mentioned countries. A year-on-year breakdown of the refining capacity of the major refineries in South Africa since 2010 is shown in Table 2-1.

Table 2-1: Year-on-year break down of oil refining capacity (bbl/day) of South Africa (SAPIA 2021).

Refinery	2010	2013	2014	2015	2016	2017	2018	2019
Sapref	180 000	180 000	180 000	180 000	180 000	180 000	180 000	180 000
Enref	120 000	120 000	120 000	120 000	135 000	135 000	135 000	135 000
Chevref	100 000	100 000	100 000	100 000	100 000	100 000	100 000	100 000
Natref	108 000	108 000	108 000	108 000	108 000	108 000	108 000	108 000
Sasol*	150 000	150 000	150 000	150 000	150 000	150 000	150 000	150 000
PetroSA*	45 000	45 000	45 000	45 000	45 000	45 000	45 000	45 000
Total	703 000	703 000	703 000	703 000	718 000	718 000	718 000	718 000

*crude equivalent

Basically, petroleum refining entails the conversion of crude oil into useful products such as LPG, kerosene, base oils, gasoline, jet fuel, diesel fuel, other fuel oils, lubricating oils and feedstock for the petrochemical industry. Before the achievement of these finished products, crude oil goes through a series of separation and treatment processes. These processes include thermal and catalytic cracking, steam and catalytic reforming, isomerization, sour water stripping, catalyst regeneration, naphtha and gas oil desulphurization, distillation, polymerization, alkylation, hydrotreating, desalting, treatment, finishing of petroleum products, among others (Al Zarooni and Elshorbagy 2006; Kuyukina, Krivoruchko and Ivshina 2020). These processes use large quantities of water; in the range of 0.2 m^3/t to 25 m^3/t of water per feed processed; as such there is generation of tons of wastewater which are sent to the ETP for treatment. In addition, wastewater is generated through storm water, sewage, dilution water and contaminated water from all technological units, cleaning activities ranging from housekeeping to cleaning of crude storage tanks and crude transportation vessels, etc. (Kriipsalu, Marques and Maastik 2008; Radelyuk *et al.* 2019; Kuyukina, Krivoruchko and Ivshina 2020). All these make the final effluent very complex and heavily contaminated. A typical water balance for an oil refinery is shown is Figure 2-1.

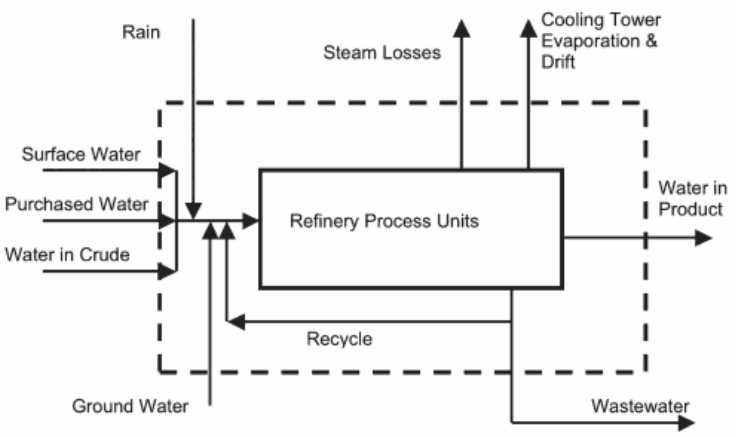

Figure 2-1: Typical water balance for an oil refinery (AECOM 2010).

2.3 Oil refinery wastewater characteristics

The petroleum and petrochemical industry is accustomed to using complex and complicated raw materials, processes, and side reactions in their activities. As a result, wastewater from this sector generally contains many poisonous substances that are classified as inorganic and organic pollutants (Tian *et al.* 2020). Inorganic pollutants include heavy metals such as cadmium, lead, nickel, and vanadium. These metals form organometallic complexes within the wastewater (Varjani and Upasani 2017). Other inorganic pollutants include dissolved salts, nitrates, sulphides, fluorides, ammonia and waste catalysts (Varjani *et al.* 2020). Organic pollutants on the other hand include grease and petroleum products like paraffin (very few carbons, C1- C4), naphthene (such as cyclohexane – C_6H_{12} and dimethyl cyclopentane- C_7H_{14}), aromatics (such as benzene- C_6H_6), methane, xylene, commonly summarized as BTEX and PAHs, etc. (Alijuboury *et al.* 2017). These make the effluent to have high biochemical oxygen demand (BOD), high chemical oxygen demand (COD) and volatile organic compounds (VOCs) (Varjani *et al.* 2020). Upon discharge into the environment without proper treatment, these effluents cause devastating effects on their receiving environments. They contain hazardous and toxic substances, having carcinogenic and mutagenic effects in living organisms (Kuyukina, Krivoruchko and Ivshina 2020).

2.4 Salt concentration of ORE and its effects on the environment.

ORE, by virtue of its source, has a wide range of salinity. Before transport of crude oil from its source either by pipeline or by any other forms of transport, stringent regulations regarding salt concentration must be met (Pereira *et al.* 2015). Desalting is usually carried out to reduce the salt content of the crude oil prior to its transport. This process involves

mixing of heated crude oil with washing water (known as dilution water). The mixture is later separated where the dilution water is later processed for proper disposal. Desalting is carried out both at the production field and the refinery (Pereira *et al.* 2015). At the refinery, the dilution water is sent to the ETP for further treatment or transported to third party treatment facilities for proper treatment and disposal.

The main salts making up ORE include chlorides, sulphates and carbonates of magnesium, calcium, sodium, etc. Exposure of these salts in high concentrations into the environment threatens environmental stability. Some adverse environmental impacts include salinization of receiving water bodies, leading to abrupt changes in the pH which endangers aquatic life, altering the growth of freshwater adapted species like amphibians and micro algae sodification of agricultural soils and ion toxicity in plants leading to ill plant growth (Ezugbe *et al.* 2020; Ezugbe *et al.* 2021).

2.5 Oil refinery wastewater treatment processes

Treatment of ORE can be divided into two major parts - pretreatment processes and further treatment. Pretreatment recovers residual oils and remove all forms of suspended materials, grease, colloidal substances, etc. Further treatment minimizes, if not eliminates totally, effluent contaminants, hence making the water viable for reuse or discharge into the environment (Diya'uddeen, Daud and Abdul Aziz 2011; Pathak and Mandalia 2012).

2.6 Pretreatment processes for oily wastewater treatment

Pre-treatment is the initial treatment given to oily wastewater prior to the application of main purification processes (Ezugbe and Rathilal 2020). Due to the high concentrations of residual oils and grease in ORE, pretreatment processes are mainly targeted towards the removal or recovery of residual oils. Commonly used pretreatment processes include gravity separation followed by skimming. This process allows for the separation of oil from water through the settling of the heavier one freely under gravity. The API oil-water separator is most commonly used in this process. The use of corrugated plate interceptor (CPI) is fairly common too (Al-Shamrani, James and Xiao 2002). This is followed by skimming, which recovers the oil for further refining while the wastewater goes for further treatment (Varjani *et al.* 2020). Further recovery of residual oils is done by applying the dissolved air floatation (DAF) or induced air floatation (IAF) technique. This process employs air to enhance the separation of smaller oil droplets. During this process, coagulation/flocculation agents are used to increase the coalition of smaller particles

(suspended materials, colloids, etc.) into bigger flocs that can be easily separated (Al-Shamrani, James and Xiao 2002; Hanafy and Nabih 2007; Tetteh, Rathilal and Robinson 2018). Pretreatment processes usually form the primary treatment train of wastewater treatment.

2.7 Secondary and tertiary treatment Processes.

After pretreatment of ORE, further treatment is needed to get the effluent to discharge limits or for reuse. Secondary treatment processes are usually targeted towards the further reduction of suspended materials and refractory components of the ORE. Coagulation and flocculation are very important steps in further treatment of ORE. These help in the removal of turbidity, colour, COD, and total suspended solids (TSS) (Farajnezhad and Gharbani 2012; Varjani *et al.* 2020). At this stage, addition of chemicals such as polyaluminum chloride, ferric chloride, aluminum hydroxide, aluminum sulphate, etc., causes the agglomeration of smaller particles into bigger ones for easy settling or sedimentation in the clarifying tanks (Kriipsalu, Marques and Maastik 2008).

Biological treatment is another process adopted for the further treatment of ORE. The use of microorganisms such as bacteria has been found to be very effective in degrading the dissolved organic components of ORE (Jamaly, Giwa and Hasan 2015). Some of the commonly applied biological treatment methods include aerated lagoon, membrane bioreactor (MBR), sequencing batch reactor (SBR) and activated sludge (Varjani *et al.* 2020). The ultimate aim of this process is to degrade the waste into more stable products like CO_2, H_2O and other products (Alijuboury *et al.* 2017; Varjani *et al.* 2020). Biological processes have been successfully applied in many instances to degrade ORE (Zhao *et al.* 2006; Xie, Zhong and Chen 2007; da Cruz, dos Santos Neto and Marsaioli 2008; Shokrollahzadeh *et al.* 2008; Jamaly, Giwa and Hasan 2015) with varying degrees of success. The main challenges faced with biological systems are the generation of large quantities of sludge and their inability to degrade recalcitrant contaminants and remove dissolved solids.

Membrane filtration, sand filtration, advanced oxidation processes (AOPs) etc., are classified as tertiary or advanced treatment processes. The tertiary/advanced treatment step is responsible for the removal of contaminants that could not be removed during the secondary treatment step (coagulation/flocculation, biological treatment). These may include finer suspended particles and metals (Yu, Han and He 2017). Advanced treatment

steps are considered if the refinery is required to meet stringent discharge limits for specific contaminants such as dissolved salts and metals, COD or polyaromatic hydrocarbons (PAHs) (AECOM 2010).

Sand filtration employs a column of sand of varying coarseness and smoothness as filtration medium with support from pebbles and gravel (Verma, Daverey and Sharma 2017). During the process, water to be treated is fed at the top of the column and treated water is collected at the bottom of the column. As the water being treated passes through the layers of sand, the contaminants are trapped. The process uses physical, chemical, and biological methods to purify water (Adin 2003). Sand filters have proven efficiency in the retention of suspended materials like algae, organic matter, fine sand, silt, micro-plastics, pesticides, and nitrates (Aslan 2005; Teixeira and Ghisi 2019; Wolff *et al.* 2021). However, sand filtration does not remove dissolved salts from ORE.

AOPs are processes that use highly reactive free radicals to oxidize organic compounds and break them down into less toxic forms such as H_2O or CO_2 (Andreozzi *et al.* 1999). In principle, AOPs work by generating a highly electrophilic species (OH·), which has a high redox potential of 2.8 eV. These species react rapidly with organic compounds and break them down (Garrido-Cardenas *et al.* 2020). Examples of AOPs are shown in Table 2-2.

Table 2-2: Examples of AOPs (Palaniandy and Feroz 2019)

Hydrogen peroxide/UV light	Ozone/Titanium dioxide
Hydrogen peroxide/ozone	Fenton's reactions (Fe^{2+}/H_2O, $H_2O_2/Fe^{2+}/UV$)
Titanium dioxide/UV	Sonolysis
Ozone/UV	Ozone sonolysis
Ozone/UV/Hydrogen peroxide	Catalytic oxidation
Ozone/Titanium dioxide/Hydrogen peroxide	Supercritical water oxidation

Basically, AOPs work through the following pathways, viz hydrogen abstraction, addition of radicals and electron transfer. The OH· species attacks organic materials and generates carbon radicals like R· or R·-OH. Ultimately, these radicals are further involved in other reactions which destroy or mineralize target pollutants (Garrido-Cardenas *et al.* 2020).

AOPs have been applied in ORE treatment (Stepnowski *et al.* 2002; Coelho *et al.* 2006; Souza *et al.* 2011; Tony, Purcell and Zhao 2012; Palaniandy and Feroz 2019; Tetteh *et al.*

2020). It is however noteworthy, that the focus of AOPs is the organic component of the ORE. Consequently, dissolved salts remain a challenge within the final effluent to be discharged.

2.8 Desalination of ORE

Desalination is the removal of dissolved minerals from water (brackish, sea, ground or wastewater), to make it fresh, useable for industry, drinking or for other purposes such as agriculture (Greenlee *et al.* 2009; Essien 2010). Desalination has received a lot of attention in recent years due to its promising nature of reclaiming useable water from wastewater and making sea and brackish water potable, for which reason is it considered important in meeting the world's water demands. The Department of Water and Sanitation (DWS), South Africa, noted that desalination has become an option for water conservation and reuse(South Africa Yearbook 2018). Similarly, Quist-Jensen, Macedonio and Drioli (2015) and Quist-Jensen, Macedonio and Drioli (2015) underpinned the importance of desalination as an opportunity to avoid a complete degradation of natural water resources and reduce the stress being put on these resources.

Desalination of ORE is mainly achieved using membrane-based processes or a combination of membrane-based processes and thermal or electrical techniques (Youssef, Al-Dadah and Mahmoud 2014). Thermal desalination processes like multistage distillation (MED), multistage flash (MSF) and vapor compression (VC) are energy intensive with high susceptibility to scaling and are hardly used in ORE desalination. Alternative desalination processes such as microbial desalination cells (MDCs), capacitive deionization technologies, clathrate hydrates, and Ion concentration polarization are still under investigation and as such, information is lacking in terms of their efficiency and large scale application potentials (Subramani and Jacangelo 2015; Elsaid *et al.* 2020).

2.9 Membrane technologies for ORE desalination

A membrane is defined as a selective barrier that separates two phases from each other by restricting the movement of materials across it based on pre-defined conditions like size or volatility. Membrane processes can be classified based on their driving forces viz, pressure driven, osmotically driven and hybrid membrane processes with a combination of driving forces – membrane distillation, Electrodialysis, etc. (Wang *et al.* 2008; Baker 2012; Ezugbe and Rathilal 2020).

2.9.1 Pressure driven membrane processes:

These are processes that depend on external hydraulic pressure to achieve separation. These are microfiltration (MF), ultrafiltration (UF), nanofiltration (NF) and reverse osmosis (RO). By far, pressure driven membrane processes are the most used membrane processes in effluent treatment processes (Chollom 2014; Aliyu, Rathilal and Isa 2018).

2.9.1.1 Microfiltration (MF)

MF is a filtration technique, where particles having micron size are removed from a suspension. These may include bacteria, fats, oils, grease, colloids, organics, micro-particles, yeast cells, etc. MF membranes have pore sizes within the range of 0.1 – 10 µm. The separation mechanism is based on the sieving effect, where particles are separated largely based on size exclusion. MF requires the least pressure when compared to other pressure driven membrane processes (Huisman 2000; Fane, Wang and Jia 2011). MF membranes are made from polymers such as cellulose acetate, polysulfone, polyvinylidene fluoride (PVDF), etc. Comparison of all the pressure driven membrane processes is shown in Table 2-3.

2.9.1.2 Ultrafiltration (UF)

This is a membrane filtration technique that separates particles of molecular weight cut-off (MWCO) within the range of 20 – 150 kilo Daltons. UF separation falls between MF and NF, being able to reject materials such as proteins, pigments, oils, sugar, organics, colloids, and micro plastics. The osmotic pressure generated by these micro and macro materials is usually low, and thus UF requires pressures within the range of 2 – 6 bars to cause the needed separation. Materials larger than the pore size of the membrane are rejected whereas those with smaller sizes are transported as part of the permeate water. Like MF membranes, UF membranes are porous in nature. They are usually asymmetric in structure commonly made from a wide range of polymer materials such as polysolfone, polyethersulfone, polyvinylidene fluoride, polyacrylonitrile, cellulose acetate and inorganic materials such as alumina, zirconia and titania. In the asymmetric structure, the top layer, or ‘skin’ (thickness within range of 0.1-0.2 µm) controls separation of materials while the support layer provides mechanical support for the membrane (Lee and Koros 2003; Spivakov and Shkinev 2005).

Table 2-3: Comparison of pressure driven membrane processes and their characteristics (Muro, Riera and del Carmen Díaz 2012; Singh and Hankins 2016a)

Membrane process	MWCO (kilo Dalton)	Retained diameters (µm)	Pressure required (bar)	Membrane type	Average permeability (L/m^2 h bar)	Solutes retained
MF	100-500	10^{-1} – 10	1-3	Porous, asymmetric, or symmetric	500	Bacteria, fat, oil, grease, colloids, organics, micro-particles
UF	20-150	10^{-3} – 1	2-5	Micro porous, asymmetric	150	Proteins, pigments, oils, sugar, organics, microplastics
NF	2-20	10^{-3} – 10^{-2}	5-15	tight porous, asymmetric, thin film composite	10-20	Pigments, sulfates, divalent cations, divalent anions, lactose, sucrose, sodium chloride
RO	0.2-2	10^{-4} – 10^{-3}	15-75	Semi porous, asymmetric, thin film composite	5-10	All contaminants including monovalent ions

MWCO = molecular weight cut-off

2.9.1.3 Nanofiltration (NF)

Separation by NF falls between UF and RO. As such, the mechanism of separation is either by pore flow (sieving effects) or solution diffusion. NF selectivity is within MWCO of 2 – 20 kilo Daltons, showing a near perfect rejection for multivalent ions and 70-90% rejection for univalent ions like NaCl and KCl. Transport in the NF membrane may be due to the availability of larger free spaces, small pores or nanovoids. The sizes of the pores form a transition between microporous and dense membranes. Due to its ability to reject materials with low MWCO, NF operates within relatively higher hydrostatic pressures of 5 – 15 bars, as compared to MF and UF. Common materials used in NF membrane make up include polysolfone, polyethersulfone (PES), polyvinylidene fluoride (PVDF), polyacrylonitrile, cellulose, polyvinyl alcohol (PVA), polyamide (PA) (Nagy 2012; Wu *et al.* 2017).

2.9.1.4 Reverse Osmosis (RO)

RO is a membrane separation process where an external hydrostatic pressure is applied to a solution of high concentration of solute to produce pure water. The pressure applied is higher than the osmotic pressure of the feed, which causes water molecules to diffuse through the membrane. This is illustrated in Figure 2-2.

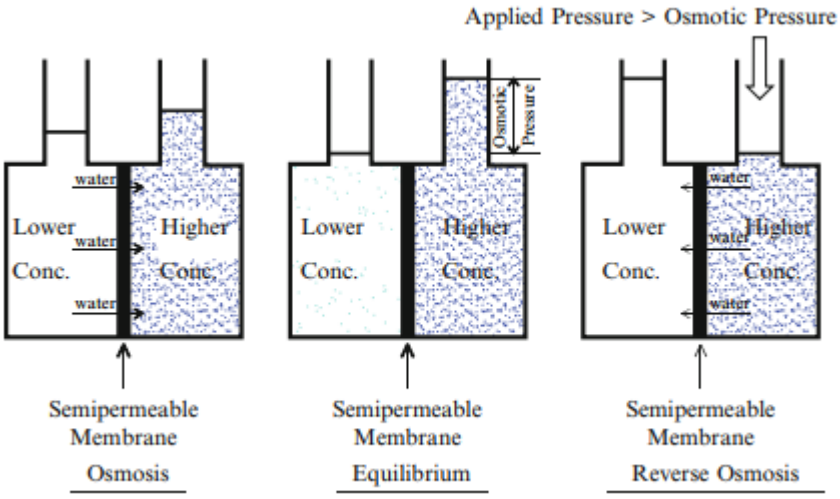

Figure 2-2: Principle of reverse osmosis (Fane, Wang and Jia 2011)

RO membranes are considered dense and non-porous. By this, the membrane consists of polymer networks through which water molecules can diffuse. Consequently, flow of permeate through the membrane is governed by the solution diffusion principle (Baker 2012), which is described in detail in section 2.9.1.7. RO membranes may be asymmetric or thin film composite. Asymmetric RO membranes are made up of a dense skin layer (0.1 – 1 µm) and a porous support layer. The dense skin layer controls flux and rejection of solutes while the support layer provides mechanical support for the membrane (Fane, Wang and Jia 2011). The thin film composite (TFC) membrane is made of two or more layers. The first layer is the extremely thin surface layer (0.5 µm or less, usually made of polyamide). This layer is responsible for the separation of the feed to produce permeate. Subsequent layers of the TFC provide support to the thin layer. These may vary in thickness from 50 – 100 µm, and they provide mechanical support during variations in temperature and pressure. Support layers are made from polysulfone, polyester or polypropylene (Burn and Gray 2015; Kucera 2015).As shown in Table 2-3, the main difference between these processes is the pressure range within which they operate and their pore sizes. MF and UF are considered low pressure filtration processes. They are mostly used as pre-filtration steps before the application of NF or RO which are considered high pressure filtration processes.

2.9.1.5 Factors affecting performance of RO

The performance of RO depends on factors like feed water pressure, temperature, feed concentration, and pH. These factors affect the flux, salt rejection and salt passage during the process.

i. Effects of feed pressure:

Feed pressure, also known as the net driving force, is the amount of hydrostatic pressure generated to overcome the intrinsic osmotic pressure of the feed water. When the osmotic pressure is overcome, the flow of water is reversed and water molecules are forced through the membrane as permeate. Holding all other conditions constant, feed pressure is directly proportional to the permeation flux as shown in Figure 2-3. That is, the flow through the membrane is proportional to the net driving pressure (NDP) differential ($\Delta P - \Delta \pi$) (Al-Mutaz and Al-Ghunaimi 2001).

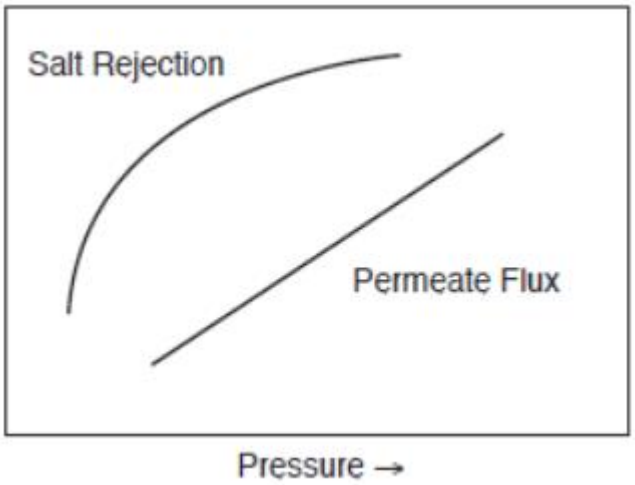

Figure 2-3: Effects of pressure on permeation flux and salt rejection. Adapted from (DOW Water 2010)

The variation of pressure with salt rejection is equally shown on Figure 2-3 Increase in pressure leads to increase in salt rejection. However, unlike for permeation flux, the relationship between pressure and salt rejection is not a linear one. When feed pressure increases, more water is pushed through the membrane. As this goes on, the amount of salt to pass through the same membrane pores as the water molecules are reduced. However, there is a limit to how much salt can be rejected while pressure increases. As shown in Figure 2-3, the plateau on the salt rejection curve shows that above certain pressures, salt rejection becomes constant (DOW water solutions 2010).

ii. Effects of feed temperature

Figure 2-4 shows the effects of feed temperature on permeation flux and salt rejection. Increase in feed temperature leads to increase in permeation flux. At higher temperatures,

the feed viscosity reduces, and the rate of water diffusion increases. This leads to an increase in permeation flux (Al-Mutaz and Al-Ghunaimi 2001).

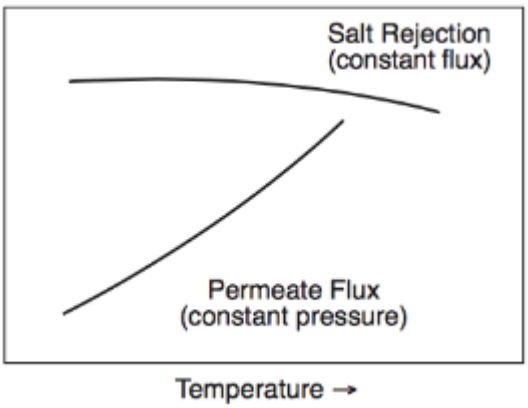

Figure 2-4: Effects of temperature on permeation flux and salt rejection (Sterlitech 2018)

Salt rejection reduces with increasing temperature as shown in Figure 2-4. As feed temperature is increased, the rate of diffusion of the salt also increases, leading to high salt passage across the membrane. Consequently, salt rejection is reduced.

iii. Effects of feed concentration

Increase in feed concentration leads to reduction in permeation flux and salt rejection as shown in Figure 2-5. As the osmotic pressure of the feed solution increases due to increased concentration, more external pressure will be required to overcome the feed osmotic pressure. Hence, at constant pressures, an increase in feed concentration will decrease permeation flux. Similarly, when permeation flux decreases, it implies that more dilution of the salts will take place, leading to decreased salt rejection.

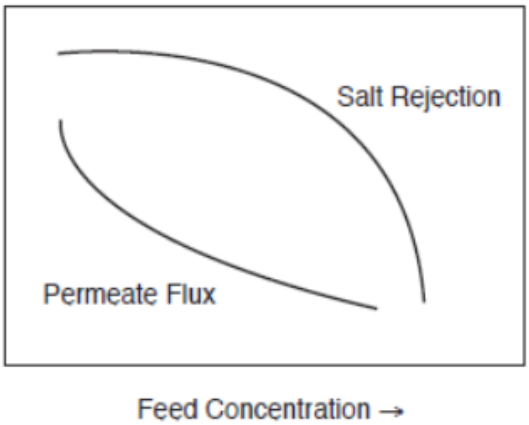

Figure 2-5: Effects of feed concentration on salt rejection and permeation flux (DOW Water 2010)

iv. Effects of feed pH

The main effects of pH are seen in the salt rejection rather than permeation flux. Membrane surfaces are either positively charged or negatively charged. However, the presence of an isoelectric point makes it possible for these charges to change under different conditions of pH. Beyond the isoelectric point of a membrane, the membrane becomes positively charged or negatively charged depending on its initial charge. The isoelectric point of a membrane is reached with variations in pH. When a membrane surface is negatively charged, the rejection of anions will be high. In the same way, for a membrane with a positively charged surface, rejection of cations will be high. This may have little direct effects on permeation flux (Nanda *et al.* 2010).

2.9.1.6 General mass balance equations in RO

For a typical single unit RO system, a mass balance can be performed on the system as flows.

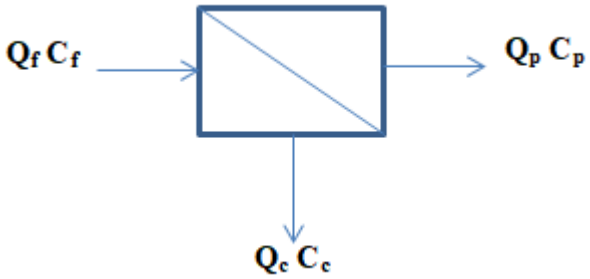

Figure 2-6: General mass balance on a single RO unit

From Figure 2-6:

$$Q_f = Q_p + Q_c \qquad \text{Equation 2.1}$$

$$Q_f C_f = Q_p C_p + Q_c C_c \qquad \text{Equation 2.2}$$

Where Q_f = feed flow rate in L/min, Q_p = permeate flow rate in L/min, Q_c = concentrate (brine) flow rate in L/min. C_f = feed concentration in g/L, C_p = permeate concentration in g/L and C_c = concentration of concentrate in g/L. These equations form the basis of determining other important RO performance parameters such as recovery and the concentration factor (Burn and Gray 2015).

2.9.1.7 The pore flow and the solution diffusion mechanisms

Pore flow (Figure 2-7A) is dominant in MF and UF processes which use microporous membranes. This mechanism describes flow in capillary or porous mediums during pressure driven convective flow. The Darcy's law (equation 2.3) is generally used to describe this kind of flow.

$$J_i = K' c_i \frac{\mathrm{d}p}{\mathrm{d}x} \qquad \text{Equation 2.3}$$

Where, $\frac{dp}{dx}$ is the pressure gradient in the porous medium, c_i is the concentration of the component *i* in the medium and K' is the coefficient reflecting the nature of the medium. With pore flow in microporous membranes, transport of molecules is usually through permanent pathways through the pores of the membrane. Ultimately, during pore flow, separation is achieved due to size exclusion of permeants when they are larger than the pore sizes (Wijmans and Baker 1995; Baker 2012).

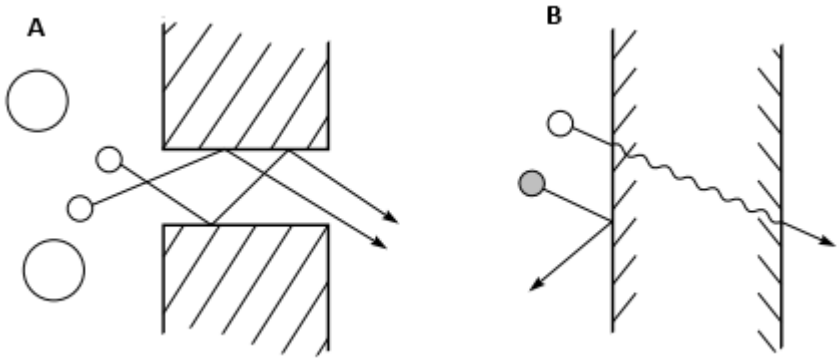

Figure 2-7: (A) Pore flow in microporous membranes and (B) solution diffusion mechanism in dense membranes. Adapted from (Baker 2012)

The solution diffusion mechanism (Figure 2-7B) takes place in dense, non-porous membranes like RO or NF membranes. This mechanism works on the principle of diffusion, where solute materials move from a region of their higher concentration to a region of their lower concentration across a semi-permeable membrane. During the process, permeants dissolve into the membrane material, after which diffusion of these permeants take place through the spaces in the polymer chains based on a concentration gradient to the other side of the membrane. This kind of diffusion transport is described mainly using Fick's law (equation 2.4). The amount of permeant and the rate at which these permeants diffuse through the polymer matrix determine the separation that is achieved.

$$J_i = -D_i \frac{\mathrm{d}c_i}{\mathrm{d}x}$$ Equation 2.4

Where J_i is the rate of transfer of component *i* or flux (g/cm^2·s) and $\frac{\mathrm{d}c_i}{\mathrm{d}x}$ is the concentration gradient of component *i*, D_i is the diffusion coefficient (cm^2/s) and is a measure of the mobility of the individual molecules. The negative sign shows that the direction of diffusion is down the concentration gradient (Wijmans and Baker 1995; Baker 2012; Alon Yeshayahu 2019).

2.9.1.8 Flow modes in membrane processes

The direction of flow in membrane filtration has a great impact on the efficiency of the membrane process. The two kinds of flow modes are (a) dead end filtration and (b) cross flow filtration. In dead end filtration (Figure 2-8A), feed flow is perpendicular to the membrane surface, flowing through the membrane pores. Dead end filtration is known for rapid separation since the feed is forced against the membrane. However, the rejected particles soon build up on the membrane surface causing severe fouling of the membrane. In cross flow filtration (Figure 2-8B), feed flow is tangential to the membrane surface, crossing the pores of the membrane channel. For this reason, only a small fraction of the liquid flowing across the membrane passes through it. Due to the velocity of the flow, materials retained by the membrane are swept along, leading to less accumulation of materials on the membrane, which reduces membrane fouling, enhances high filtration rate and high product recovery rate (Ismail and Yuliwati 2000; Cui, Jiang and Field 2010).

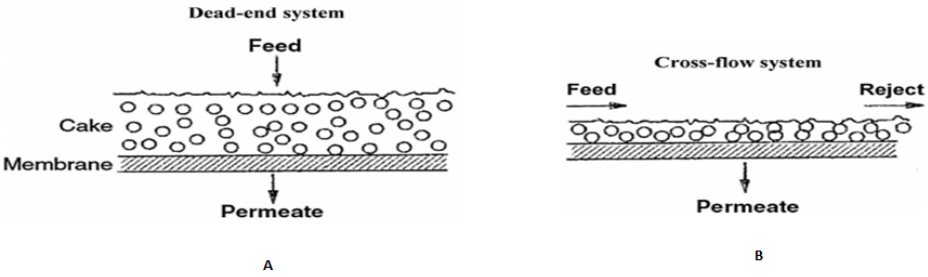

Figure 2-8: Flow modes in membrane processes - A: dead end. B: cross flow (Singh and Hankins 2016b)

2.9.2 Some applications of pressure driven membrane processes in ORE treatment

Table **2-4** shows some applications of pressure driven membrane processes in ORE treatment. In most cases, two or more processes are combined to achieve the desired results.

It is also commonace to see pressure driven membrane processes in combination with other forms of treatment techniques like coagulation/flocculation, sand filters, carbon filters, adsorption, solvent extraction or distillation (Jamaly, Giwa and Hasan 2015).

Table 2-4: Some applications of pressure driven membrane processes in ORE treatment adapted from (Ezugbe and Rathilal 2020)

Membrane process	Type of ORE	Results	Reference
UF/RO	Crude oil desalter effluent	95% TDS removal	(Norouzbahari, Roostaazad and Hesampour 2009)
UF/RO	Outlet from the API unit	Oil and grease (100%), TOC (98%), COD (98%), TDS (95%), Turbidity (100%)	(Salahi *et al.* 2011)
RO	Effluent from sand filter	TDS (87%), TOC (90%), COD (95%), Turbidity (81.8%)	(Salahi, Mohammadi and Rekabdar 2010)
NF	Raw oily wastewater from gasoline tanks	COD (84%), EC (88%)	(Rahimpour *et al.* 2011)
UF	Disposed wastewater from the wastewater treatment unit of Tehran refinery	Oil and grease (97%), TSS (100%), turbidity (97%), TDS (23%)	(Noshadi *et al.* 2013)
MF	Outlet of the API unit of Tehran refinery	TOC removal > 95%	(Abadi *et al.* 2011)
UF/RO	Bilge water, oil content of 100 – 500 ppm	90% removal of all cations (Na^+, K^+, Mg^{2+}, Ca^{2+}, Zn^{2+}, Mn^{2+}, Al^{3+}, Li^+).	(Tomaszewska, Orecki and Karakulski 2005)

2.9.3 Osmotically driven membrane processes (ODMPs)

ODMPs depend on osmotic pressure difference between two solutions to transfer water molecules from one point to the other through a semipermeable membrane (Xie, Cath and Ladner 2021). The osmotic pressure is the pressure possessed by a solution that prevents it from diffusing through a semipermeable membrane. When two solutions of different concentrations are in contact with a semipermeable membrane, the solution with the higher chemical potential (referred to as draw solution) draws water from the solution with the lower chemical potential (referred to as the feed solution) until equilibrium is reached. The two main ODMPs are pressure retarded osmosis (PRO) and FO (Cath *et al.* 2013; Wei, She and Liu 2021). PRO is mainly applied in production of energy. In this process, the DS is partially pressurized with external hydrostatic pressure. This pressure helps to convert the

pressure within the permeate stream into mechanical or electrical energy (Cui, Jiang and Field 2010; Achilli and Hickenbottom 2016).

2.9.4 Forward Osmosis (FO)

Unlike PRO, FO depends only on the osmotic pressure gradient between the draw solution (DS) and the feed solution (FS) to drive the movement of water across a semipermeable membrane. In most FO applications, there is always the need for a recovery unit, which recovers the permeate water and at the same time regenerate and recycle the draw solutes (Mohammadifakhr *et al.* 2020). Figure 2-9 shows the principle of FO.

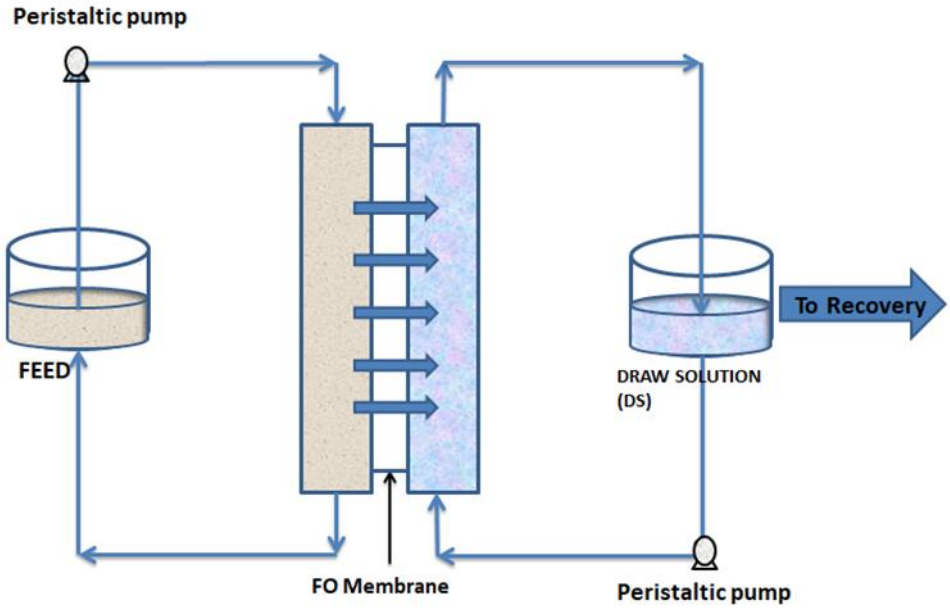

Figure 2-9: Principle of FO. Adapted from (Ezugbe and Rathilal 2020).

FO is advantageous in several ways. Firstly, the process depends on osmotic pressure not external hydraulic pressure like in pressure driven membrane processes (for example in niche applications of FO like fertigation) (Zou and He 2016), which makes energy consumption lower compared to pressure driven processes. Again, fouling in FO membranes is easily reversed and water cleaning is easier since the use of osmotic pressure for separation causes less compaction of foulants than hydraulic pressure. Selection of an osmotic agent gives FO the flexibility in operation. It makes customization of products like pharmaceuticals and beverage production easy, in which case properties of products are maintained, since no pressure or heat is applied. The regeneration and recycling of DS is another added advantage of FO. This helps in saving cost (Akther *et al.* 2015; Shaffer *et al.* 2015; Shen, Hankins and Nicholas 2016; Iskander *et al.* 2017; Wang *et al.* 2018).

2.9.4.1 Draw solution and draw solutes: properties and recovery.

Draw solution is the osmotic agent that provides the driving force for water movement in FO. The draw solution may be formed by homogeneously dissolving the appropriate draw solute or draw agent in water. Sometimes, draw solutions may be saline streams from seawater desalination or other industrial processes (Alejo *et al.* 2017).

The draw solution plays an important role in flux production and recovery of draw solutes. Not only do draw solutes contribute significantly to process improvement but also radical cost reduction. As such, important properties are taken into consideration when draw solutes are being selected for draw solution preparation. Firstly, draw solutes should be able to generate high osmotic pressure to drive the FO process; this is the most important property of draw solutes. As FO relies on the osmotic pressure gradient, the osmotic pressure generated by the draw agent should be significantly higher than the osmotic pressure within the feed solution to produce enough driving force for water movement (Chekli *et al.* 2012; Cai and Hu 2016). Figure 2-10 shows some common draw solutes and their osmotic pressures.

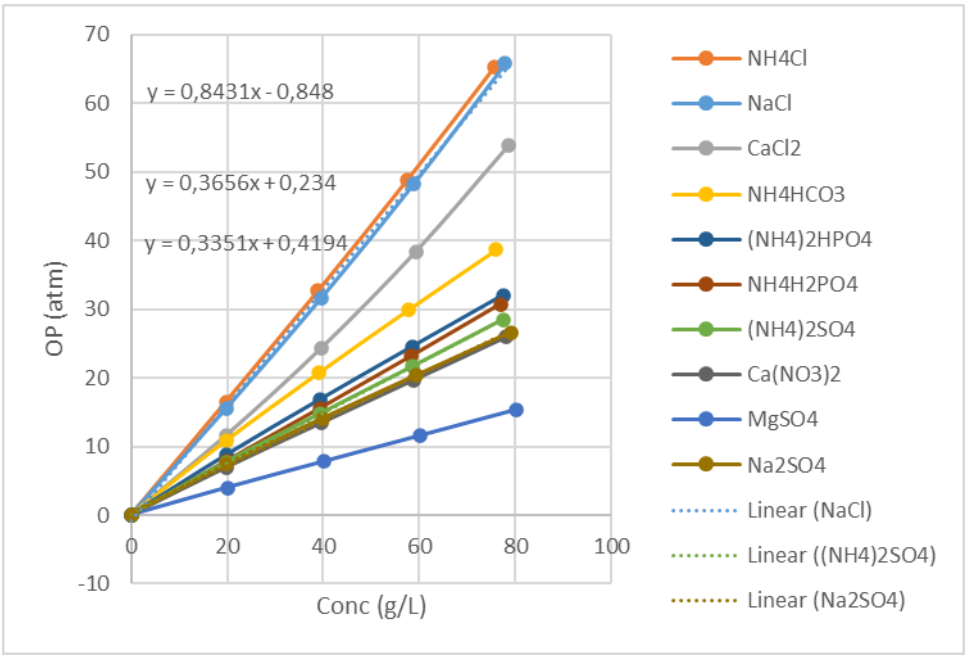

Figure 2-10: Osmotic pressure of some common draw solutes (Mogashane *et al.* 2020)

Trendlines:

NaCl: 0.843 x Conc (g/L) – 0.848 Equation 2.5

$(NH_4)_2SO_4$: 0.366 x Conc (g/L) + 0.234 Equation 2.6

Na_2SO_4: 0.3351 x Conc (g/L) + 419 Equation 2.7

It is observed, that for a draw solute to generate high osmotic pressure, there should be good water solubility and a high degree of dissociation in water. This favors draw agents such as NaCl and $CaCl_2$, which are most used as draw agents (Mogashane *et al.* 2020).

Another important property of draw solutes is their ability to be recovered easily and at a low cost. Draw solutes must be recovered for reuse. Doing so also recovers the permeate water for use. Draw solute recovery takes place in a post treatment of the DS. The type of recovery process adopted depends on the type of draw solute used. For example, if univalent draw solutes such as NaCl or KCl are used, high pressure membrane processes (NF, RO) or membrane distillation are usually employed as post treatment for recovery of permeate as well as the draw solute. Multivalent salt-based draw solutes may be recovered using UF. For draw agents that are gasses or volatile, thermal separation is used. Other recovery methods include precipitation for sulphate-based draw agents and magnetic recovery for magnetic draw agents (Chekli *et al.* 2012; Luo *et al.* 2014).

Low reverse solute flux (RSF) is also an important property considered when choosing draw solutes. RSF is caused by the reverse diffusion of solutes (RSD), where there is the backward movement of draw solutes into the FS due the difference in concentration of the solute between the FS and the DS. Details of RSD are discussed in the section 2.9.6.1. RSF is associated with a high cost of operation and can cause contamination of the FS. Other considerations for selecting a draw solute include non-toxicity, commercial potential, and availability (Chekli *et al.* 2012; Gwak and Hong 2018).

2.9.4.2 Classification of draw solutes

Draw solutes come in different forms. The most widely used draw solutes are inorganic-based draw solutes such as NaCl, KCl, $MgCl_2$, $CaCl_2$, Na_2SO_4, $CuSO_4$, $KHCO_3$, $MgSO_4$, $Ca(NO_3)_2$, $NH_4H_2PO_4$, etc. The wide usage of these solutes is due to their ability to produce high fluxes and availability of recovery methods (Johnson *et al.* 2018). In specific niche applications like fertigation (dilution of fertilizer for agricultural application), some inorganic draw agents are used directly after osmotic dilution with no need for regeneration.

Organic-based draw solutes such as sucrose, glucose, fructose, EDTA, sodium formate, etc., have seen their applications in many fields like potable water production, food

production, wastewater treatment, etc. These draw agents are characterized by large molecular sizes and as such, their tendency of causing reverse solute diffusion (RSD) is very low compared to inorganic draw agents (Luo *et al.* 2016; Ju and Kang 2017).

Apart from inorganic and organic draw solutes, draw solutes may come in the form of thermolytic compounds (NH_4HCO_3, SO_2) and polyectrolytes (poly acrylic and sodium salt (PAANa), sodium lignin sulfonate (NaLS), etc.). All these draw agents are explored for various reasons to enhance the efficiency of the FO process (Ge *et al.* 2012; Orme and Wilson 2015).

2.9.4.3 FO membranes and membrane orientation

In general, any dense, nonporous and selectively permeable material can be used as a FO membrane. The membrane should consist of a high-density active layer for high solute rejection and a support layer with minimum porosity for higher water fluxes and low internal concentration polarization (CP). The membrane should also be hydrophilic (Rastogi and Nayak 2011; Li, Shi and Yu 2020). Typically, FO membranes are asymmetric, having a rejection layer made up of a highly hydrophilic polymer and a porous support layer. The most common FO membranes are the cellulose triacetate (CTA) membranes and the thin film composite membranes. FO membranes are defined by their intrinsic properties known as the water permeability (A), solute permeability (B) and structural parameter (S) of the support layer (Roest 2017).

Membrane orientation during FO affects the results of the process. The membrane is either oriented in the FO mode, such that the active layer faces the FS while the support layer faces the DS or in the PRO mode, where the active layer faces the DS and the porous support layer faces the FS. Many studies have demonstrated that membrane orientation contributes largely to internal concentration polarization, fouling and solute transport (Gray, McCutcheon and Elimelech 2006; Zhao, Zou and Mulcahy 2011). In a study conducted by Zhao *et al.* (2014) to investigate the effects of membrane orientation on FO performance, the authors showed that both water flux and solute flux in the PRO mode was higher than the FO mode especially at higher concentrations. Wang *et al.* (2010) studied the effects of membrane orientation on fouling and ICP. The authors observed that the FO mode was more fouling resistant than the PRO mode. Their observation also extended to the stability of permeation flux in FO mode than in PRO mode. In terms of ICP (which

occurs in the support layer of the membrane), it was found that the FO mode was more prone to ICP than the PRO mode.

2.9.5 Concentration polarization (CP)

CP occurs when particle concentration at the membrane surface is higher than in the bulk of the fluid. CP is a common phenomenon in all membrane filtration processes. CP has negative effects on permeation flux and promotes membrane fouling. When solutes build up on the membrane surface, they cause resistance to permeate flow, leading to high pressure requirements and rigorous pretreatment procedures (Cath, Childress and Elimelech 2006). Figure 2-11 summarizes the various types of CP.

2.9.5.1 External concentration polarization (ECP)

ECP is the type of concentration polarization that occurs at the surface of the membrane active layer. As shown in Figure 2-11, ECP occurs both in osmotically driven and pressure driven membranes. In pressure driven membranes, only CECP occurs due to the convective flow of feed at the surface of the membrane. That is, as the feed flows over the active layer of the membrane, there is accumulation of solutes as water from the FS permeates the membrane (Song and Elimelech 1995; Giacobbo *et al.* 2018).

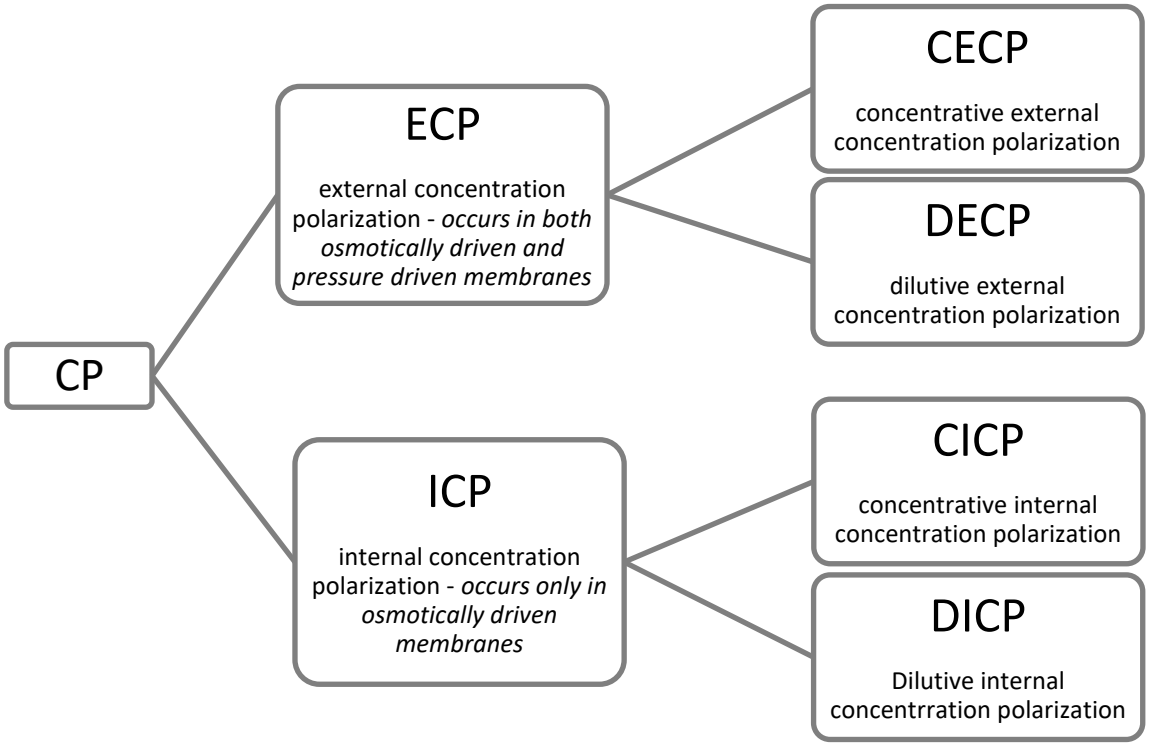

Figure 2-11: Classification of concentration polarization

In osmotically driven membrane processes, both CECP and DECP may occur depending on the membrane orientation. Just like in PD membranes, when the active dense layer of the ODMPs membrane faces the feed, CECP occurs. On the other hand, when the dense active layer of the OD membrane faces the DS, DECP occurs. In DECP, the permeating water from the FS to the DS dilutes the DS at the DS-membrane interface (Sablani *et al.* 2001; Cath, Childress and Elimelech 2006).

2.9.5.2 Internal concentration polarization (ICP)

ICP occurs within the porous support layer of ODMPs membranes as shown in Figure 2-11. Similar to the mechanism of ECP, ICP occurs due to the deposition of solutes, in this case, within the porous support layer of the membrane. DICP occurs when the DS is circulated at the porous support side of the membrane. In this case, water permeating from the FS side dilutes DS within the porous support layer. On the other hand, CICP occurs when the membrane active layer faces the DS (Mohammadifakhr *et al.* 2020).

ICP is known to cause a more severe decline in flux than ECP. Up to 80% of flux decline was observed in previous studies due to ICP (Mehta and Loeb 1978). The main challenge in dealing with ICP is the difficulty in accessing the deposited solutes since they are within the porous support layer. Unlike the ECP, which can be mitigated by using high cross flow velocities and other flow dynamics, mitigating ICP will require the reduction of the support layer, yet ensuring that mechanical strength of the membrane is not compromised (Mikulášek 1994; Klyuchnikov *et al.* 2020). Figure 2-12 shows a schematic diagram of ECP and ICP on a membrane element.

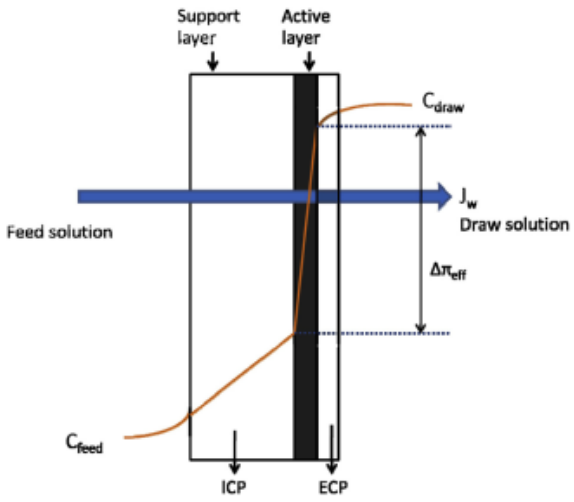

Figure 2-12: ICP within the membrane support layer and ECP at the membrane active layer. Adapted from (Zhao *et al.* 2012).

2.9.6 Mass transport in FO membranes

Movement of materials across the FO membrane can be classified into two forms, viz solvent transport and solute transport (Bui, Arena and McCutcheon 2015) as shown in Figure 2-13. Transport of these components mainly depend on intrinsic membrane properties like water permeability designated as *A*, solute permeability *B*, and the structural parameter of the support layer, *S* of the membrane (Nagy 2019a).

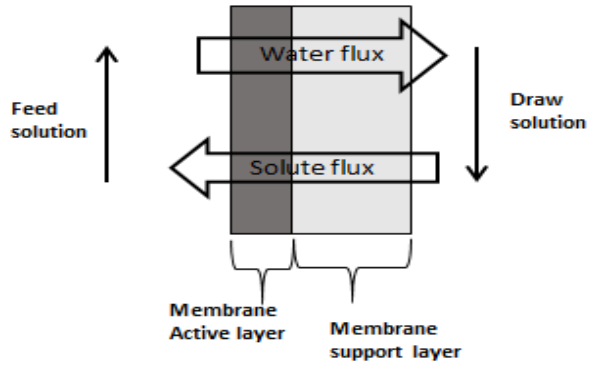

Figure 2-13: Mass transport across the FO membrane. Modified from Roest (2017)

Solvent (water) transport through the semipermeable membrane is generally governed by equation 2.8

$$J_w = A(\Delta\pi - \Delta P) \qquad \text{Equation 2.8}$$

Where J_w is water flux (L/m^2·h - LMH), A is the water permeability coefficient of the membrane (LMH/bar), $\Delta\pi$ is the osmotic pressure differential in bar across the membrane and ΔP is the hydraulic pressure differential in bar across the membrane. In FO, $\Delta P = 0$, hence the dependence of J_w on $\Delta\pi$. In RO, $\Delta P > \Delta\pi$, hence the dependence of J_w on ΔP. Ultimately, the direction of flow of permeate will be in line with the net pressure as shown in Figure 2-14.

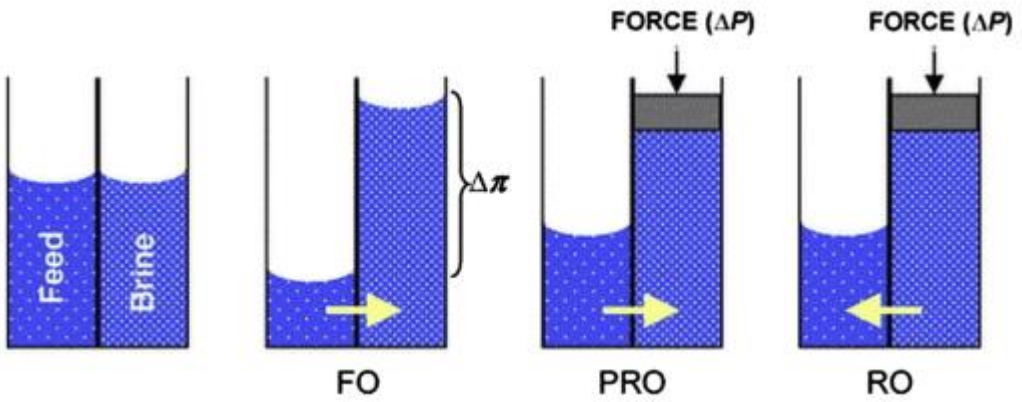

Figure 2-14: Driving force in different membrane processes. Adapted from (Singh and Hankins 2016b)

Solute transport across the FO semipermeable membrane is bidirectional. Solute diffuses across the membrane simultaneously in both directions (Hancock and Cath 2009). This solute diffusion is generally governed by Fick's law of diffusion;

$$J_s = B(\Delta c) \qquad \text{Equation 2.9}$$

Where J_s is the flux (g/m^2·h) of an individual species of salt diffusing through a semipermeable membrane, B is solute permeability coefficient (m/s) and Δc is the trans-membrane concentration differential (Merten, Lonsdale and Riley 1964; Hancock and Cath 2009).

2.9.6.1 Reverse Solute diffusion (RSD)

In the FO process, as water molecules move into the DS across the semipermeable membrane under osmotic pressure, some of the draw solutes also diffuse from the DS into the FS under the influence of concentration gradient. The forward movement of water (water flux) and the backwards diffusion of solute (RSF) are inevitable due to the system's tendency to reduce concentration difference between the FS and the DS. The RSD is undesirable, as it tends to contaminate the FS, leads to loss of draw solute as well as causes a reduction in osmotic pressure of the system (She *et al.* 2012; Zhang *et al.* 2017).

Figure 2-15 shows a schematic diagram of the leakage of solutes from the DS into the FS. During this process, the draw solute first diffuses into the support layer of the asymmetric membrane (FO mode). This diffusion continues until it reaches the interface between the support layer and the active layer, where the draw solutes spread within the active layer before finally diffusing into the FS (Yong, Phillip and Elimelech 2012).

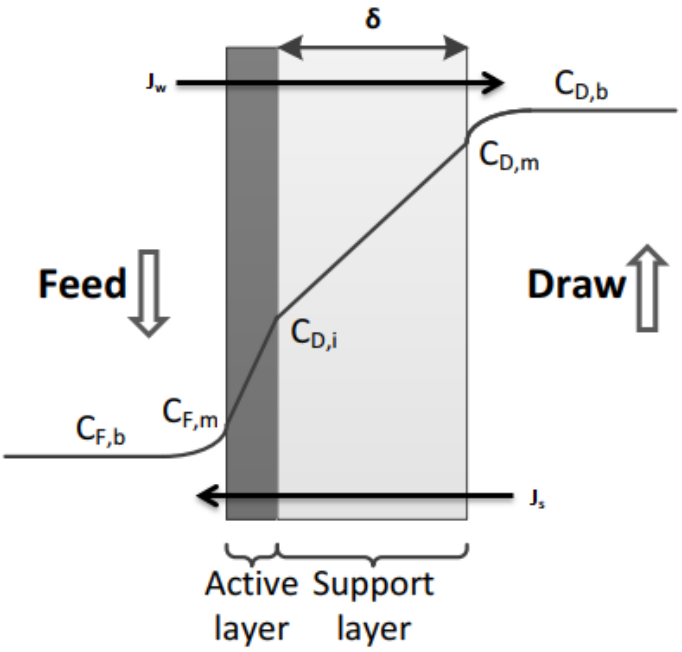

Figure 2-15: Schematic diagram of the leakage of solutes from the DS into the FS
Modified from Roest (2017)

2.9.6.2 Layer by layer considerations for water transport and reverse solute diffusion in FO membranes.

Equations 2.8 and 2.9 form the bases for transport across the FO membrane. From equation 2.9, an expression for reverse solute across the active layer of the membrane (as shown in figure 2-15) can be written as follows;

$$-J_s = -B(C_{D,i} - C_{F,m}) \qquad \text{Equation 2.10}$$

Where $-J_s$ is the reverse solute flux, B is the solute permeability coefficient, $C_{D,i}$ is the concentration of solute at the porous support layer-active layer interface and $C_{F,m}$ is the concentration of solute at the feed-membrane interface.

The salt flux across the porous support is the combination of the diffusive component, driven by the salt concentration gradient, and the convective component, resulting from the movement of water through the membrane (McCutcheon and Elimelech 2007). This implies that;

$$-J_s = -D^S \frac{dc(x)}{dx} + J_w\, c(x) \qquad \text{Equation 2.11}$$

Where D^S is the effective solute diffusion coefficient in the support layer (m^2/s) and *c(x)* is the solute concentration at position *x* within the membrane. The effective solute diffusion coefficient is related to the bulk diffusion coefficient (*D*) by the porosity (ε) and tortuosity (τ) of the support layer according to equation 2.12 (Yong, Phillip and Elimelech 2012).

$$D^S = \frac{D\varepsilon}{\tau} \qquad \text{Equation 2.12}$$

At steady state conditions, the RSF within the active layer and the porous layer should be equal. Mathematically, this yields the following equation;

$$\frac{dc(x)}{dx} - \frac{J_w}{D^S}\, c(x) = \frac{B}{D^S}\,(c_{D,i} - c_{F,m}) \qquad \text{Equation 2.13}$$

Integrating the above equation (equation 2.13), from x = 0 (porous layer-draw solution interface) to x = - δ (porous layer-active layer interface), it follows that;

$$c_{D,i} = C_{D,m}\, exp\left(\frac{J_w S}{D}\right) + \frac{B}{J_w}\,(c_{D,i} - c_{F,m})\left(\exp\left(\frac{J_w}{D}\right) - 1\right) \qquad \text{Equation 2.14}$$

Where $C_{D,m}$ is the solute concentration at the porous support layer-draw solution interface, *S* is the structural parameter (m).

So far, the equations only took into consideration the dilutive ICP and effective water flux. It is however important to account for the concentrative and dilutive ECP. During the FO process, solutes from the feed are retained by the membrane, consequently leading to accumulation of solutes at the membrane active surface, causing ECP at the boundary layer. As such, taking into consideration concentrative and dilutive ECP,

$$-J_s = -D^S \frac{dc(z)}{dz} + J_w\, c(z) \qquad \text{Equation 2.15}$$

Where $c(z)$ is the concentration of solute at the position *z* within the boundary layer. At steady state conditions, the solute flux within the ECP boundary layer and the solute flux within the active layer are the same. Integrating from *z* = 0 (ECP boundary layer, where the solute concentration is $c_{F,m}$) to *z* = - δ (where the solute concentration $C_{F,b}$ is) results in the following;

$$c_{F,m} = C_{F,b}\, exp\left(\frac{J_w}{k}\right) - \frac{B}{J_w}\,(c_{D,i} - c_{F,m})\left(1 - \exp\left(\frac{J_w}{k}\right)\right) \qquad \text{Equation 2.16}$$

Where $C_{F,b}$ is the solute concentration in the bulk of the feed solution and *k* is the boundary layer mass transfer coefficient (m/s). To finally write the general expression for water flux and RSF, the following assumptions were made (Tiraferri *et al.* 2013).

1. Osmotic pressure is linearly proportional to the salt concentration, hence $\Delta\pi = \Delta c$.
2. ECP in the DS is negligible because the support layer thickness is relatively large, thereby dominating the concentration polarization; hence $\pi_{D,S} \approx \pi_{D,b}$.

Substituting equations 2.14 and 2.16 into equations 2.8 and 2.9 yields the following expressions for J_w and J_s respectively;

$$J_w = A\left(\frac{\pi_{D,b}\exp(-J_w k) - \pi_{F,b}\exp\left(\frac{J_w}{k}\right)}{1+\frac{B}{J_w}\left(\exp\left(\frac{J_w}{k}\right)-\exp(-J_w K)\right)}\right) \qquad \text{Equation 2.17}$$

$$J_s = B\left(\frac{C_{D,b}\exp(-J_w k) - C_{F,b}\exp\left(\frac{J_w}{k}\right)}{1+\frac{B}{J_w}\left(\exp\left(\frac{J_w}{k}\right)-\exp(-J_w K)\right)}\right) \qquad \text{Equation 2.18}$$

Application of equations 2.17 and 2.18 are for the determination and simulation of water flux and reverse solute flux in membrane production and fabrication.

2.9.7 Hybrid membrane processes

Membrane processes have been combined in many different fashions for different applications. The hybrid membrane processes may be a combination of two membrane techniques such as FO-RO, FO-NF, FO-UF, UF-RO, etc. It may also be a combination of a membrane technique with thermal, chemical, or biological process as in examples like membrane bioreactors (MBR) and membrane distillation (MD), FO-MD, Electrodialysis (ED) etc. The ultimate aim of hybrid membrane processes is to harness the advantages of other techniques for the overall process improvement and efficiency. In desalination applications, MD, ED, and FO-RO are mostly employed. These are briefly discussed below.

2.9.7.1 Membrane distillation (MD)

MD utilizes heat to separate substances across a microporous hydrophilic membrane based on the volatilities of the substances being separated. The driving force in MD is the partial pressure gradient across the membrane, created as a result of the temperature difference between the two sides of the membrane (Nagy 2019b). As shown in Figure 2-16, during MD, water vapour from a hot aqueous solution is transferred through the membrane based

on the principle of liquid-vapour equilibrium. Due to the hydrophilic nature of the membrane, only vapour molecules are allowed through it, while the liquid phase is prevented from passing through (Khayet and Matsuura 2011).

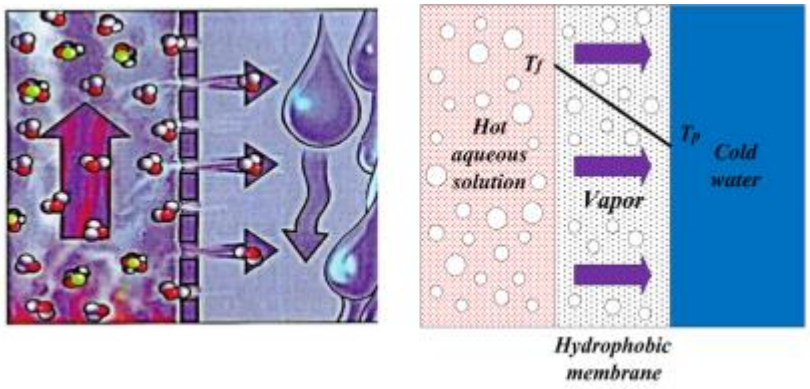

Figure 2-16: Membrane distillation process. Adapted from (Belessiotis, Kalogirou and Delyannis 2016)

The MD process can be classified into four different configurations based on the method of condensation, vapor recovery and application of driving force (Alkhudhiri, Darwish and Hilal 2012; González, Amigo and Suárez 2017). These are as followed.

1. Direct contact membrane distillation (DCMD): like conventional distillation, the membrane in DCMD is in contact with the hot aqueous solution at the feed side, and the cold steam of water at the permeate side. The partial pressure difference created as result of the difference in temperature between the two sides of the membrane drives water molecules from the feed through the membrane. DCMD produces high permeation fluxes but with high heat loss (Hausmann *et al.* 2011; Ashoor *et al.* 2016).
2. Air Gap membrane distillation (AGMD): as the name suggests, the ADMD makes use of an air gap, interposed between the membrane and the cooling surface. Vaporized permeate crosses the stationary air gap and condenses at the cooling surface by natural convection induced by the difference between the air gap and the cooling surface. This configuration has low heat loss ability, however low permeation fluxes are usually achieved (Alkhudhiri, Darwish and Hilal 2013; Leaper *et al.* 2019).

3. Vacuum membrane distillation (VMD): in the VMD, a vacuum pump provides vacuum at the permeate side of the membrane. This vacuum pressure is lower than

the saturated pressure of the components of the feed, causing pressurized permeate-water to be sucked from the membrane pores. With VMD, condensation of the permeate is done externally, outside of the distillation module (González, Amigo and Suárez 2017).

4. Sweeping gas membrane distillation (SGMD): this configuration employs a cold gas, usually an inert gas to constantly sweep the vaporized permeate from the membrane into an external condensation unit. The main drawback of this configuration is the need for an external condenser, which adds to the complexity of the design (Khayet and Matsuura 2011).

MD is highly advantageous in producing pure water from saline streams with low heat requirements (>100 degrees). Again, permeate quality is independent of the feed solution characteristics. The process efficiency is however hampered as the salt content of the feed increases, as the vapor pressure production is hindered. Again, compared with RO, MD produces low fluxes, hence much energy is required to produce large amounts of permeate (Dow *et al.* 2016; Sanmartino *et al.* 2016).

2.9.7.2 Electrodialysis (ED)

The application of ED is based on the combination of electricity and an ion permeable membrane to separate dissolved ions from water. During the process, ions are transferred from a dilute solution into a concentrated solution through an ion permeable membrane under the influence of an electric potential (Akhter, Habib and Qamar 2018; Al-Amshawee *et al.* 2020). A schematic diagram of ED is shown in Figure 2-17.

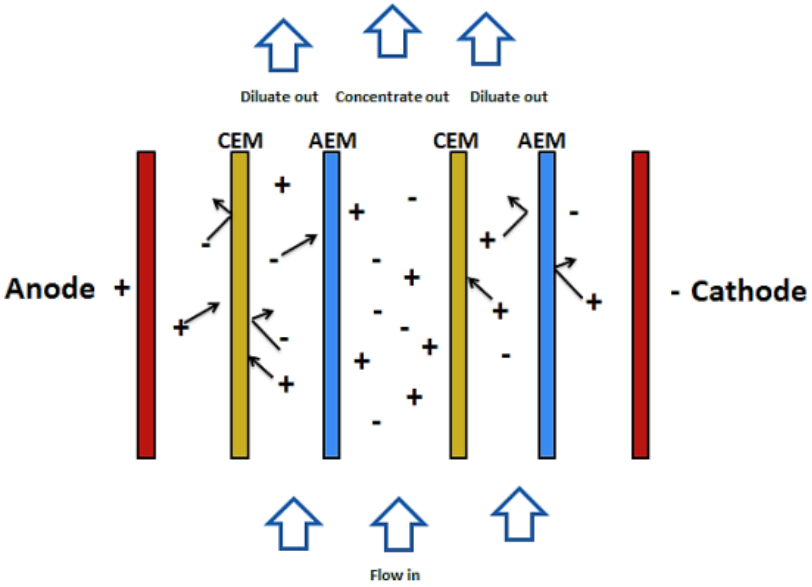

Figure 2-17: Schematic representation of ED. Adapted from (Ezugbe and Rathilal 2020).

A typical ED unit is made up of two ion exchange membranes – cation exchange membrane (CEM) and anion exchange membrane (AEM), and two streams of flow - the product (diluate) stream and the concentrate stream (Chao and Liang 2008). When electric current is passed through the system, ions migrate from the diluate into the concentrate across oppositely charged membranes. That is, cations migrate to the cathode through the CEM but are retained by the AEM whereas anions migrate to the anode through the AEM but are retained by the CEM. The result of this process is a feed stream depleted of ions and an ion-rich concentrate stream (Strathmann 2010; Galama *et al.* 2014).

ED is usually combined with Electrodialysis reversal (EDR), where the electrodes are reversed to reverse the flow of ions. This is done to control the fouling of the ion exchange membranes (Chao and Liang 2008). ED and EDR possess some advantages, such as high water recovery and low fouling propensity. It is however, not suitable for waste streams with high concentration of salts, as the operational cost increases significantly. In addition, the process generates chlorine gas at the electrodes, which cause corrosion of the electrodes (Singh and Hankins 2016a; Campione *et al.* 2018).

2.9.7.3 Forward osmosis - reverse osmosis hybrid system (FO-RO)

Combining FO with high pressure membrane processes like RO and NF has seen many applications over the years. For both desalination and wastewater treatment, this hybrid process has been found to be very useful as a multi-barrier in contaminant rejection and as an energy reduction strategy in desalination (Cath, Drewes and Lundin 2009; Cath *et al.*

2010). Technically, combining these two membrane processes of opposing working principles provides the opportunity of harnessing the advantage in each process to offset their limitations. For direct potable water use (Cath *et al.* 2005; Cartinella *et al.* 2006), landfill leachate treatment (York, Thiel and Beaudry 1999), industrial wastewater treatment (Giagnorio *et al.* 2019), simultaneous desalination and wastewater treatment (Cath *et al.* 2010; Bamaga *et al.* 2011) and oil and gas wastewater treatment (Lampi and Shethji 2014), FO-RO hybrid systems have proved very efficient in contaminant removal and water recovery.

During the FO-RO hybrid process (Figure 2-18), effluent to be treated, serves as the FS to the FO and a more saline stream serves as the DS as described in section 2.9.34. The draw solution can be manually prepared using an appropriate draw agent. The application of RO comes as a recovery method to reclaim water for reuse and at the same time reconstitutes the draw solution by recycling the brine into the DS tank. In simultaneous desalination and wastewater treatment, where the wastewater (which is usually low in osmotic pressure) serves as the FS and the sea or brackish water serve as the DS, water drawn from the FS serves to reduce the osmotic pressure of the DS. This then reduces the pressure required by the RO for desalination (Choi *et al.* 2017).

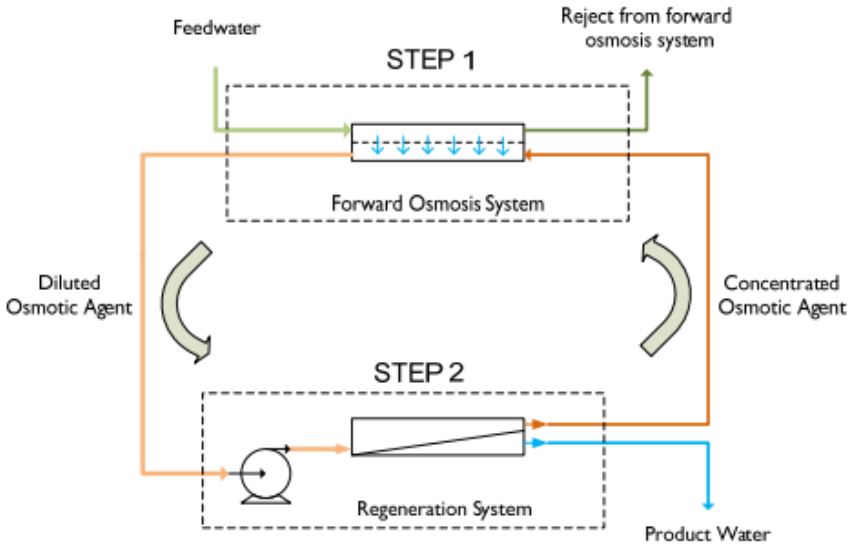

Figure 2-18: Schematic diagram of FO-RO hybrid system. Adapted from (Nicoll 2013a)

The FO-RO hybrid process may be conducted either in batch mode or in continuous mode. In the batch mode, FO process is allowed alone for some time until 60 – 80% of the water is recovered from the FS into the DS. The diluted DS is then fed to the RO process for water recovery and reconstitution of the draw solution. In the continuous mode, the hybrid

process in conducted in a close loop, where the RO constantly reconstitutes the DS until the desired recovery is achieved (Volpin *et al.* 2018).

In an approximately 50 hour extensive study and modeling of FO-RO system for water recovery, Holloway *et al.* (2007), studied the feasibility of the hybrid system in recovering water from a 190 m^3/day anaerobic digestate. The modeling estimated the specific energy, power and membrane area as a function of water recovery. It was observed, that to achieve a 90% water recovery, a corresponded 1900 m^2 of membrane surface area would be required, against 800 m^2 for 50% water recovery. That is, for such high recovery rates, several membrane elements may be required, arranged in series. It was also demonstrated that the power and specific energy requirements for the hybrid system increased as the water recovery rate increased. It was concluded that the hybrid FO-RO system outperformed RO as a standalone process for the same conditions of recovery and feed concentration.

In a 5 month-long study of FO-RO hybrid process on simultaneous wastewater treatment and seawater desalination, Choi *et al.* (2017), studied the long term flux, fouling reversibility, permeation of dissolved organic matter, permeate water quality and energy consumption on the FO-RO process. The study which was set at a fixed FO water recovery rate of 55% and RO water recovery rate of 35% used wastewater from coal fired power plant as FS and seawater as DS. The 21.8 m^3/day pilot plant proved feasible, with sustained permeation flux, 15% energy reduction (comparing to seawater RO operation for same conditions) and excellent fouling controllability which was attributed to the osmotic dilution of the RO feed by the FO process.

Clearly, FO-RO hybrid processes offer great prospects in desalination and wastewater treatment as indicated by the above examples and many other similar applications of the process (Thompson and Nicoll 2011; Nicoll 2013a; Nicoll 2013b; Al-Zuhairi *et al.* 2015; Choi *et al.* 2016).

2.9.8 Membrane modules

Membranes come in different packings known as modules. Membrane modules provide economical packaging mainly for large scale applications. There are mainly four types of membrane modules, viz plate and frame, tubular, spiral wound and hollow fiber membrane

modules (Cui, Jiang and Field 2010). Figure 2-19 - Figure 2-22 show the various types of membrane modules.

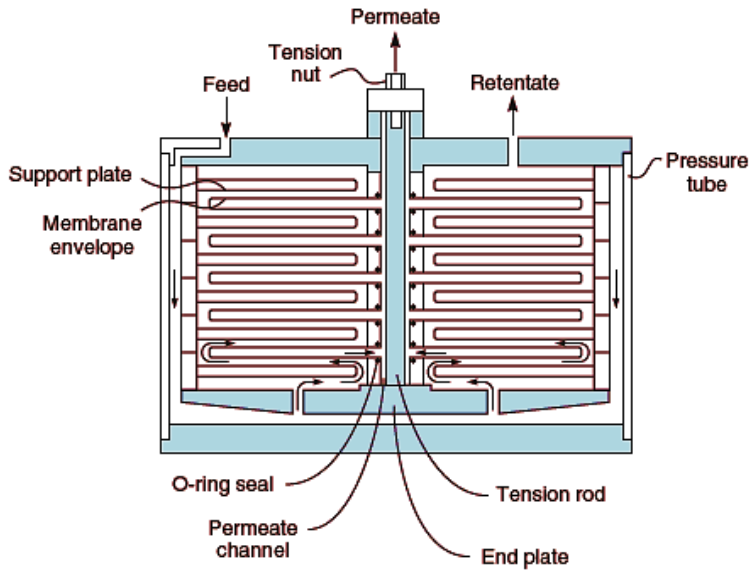

Figure 2-19: Schematic diagram of plate and frame membrane module. Adapted from (Baker 2012)

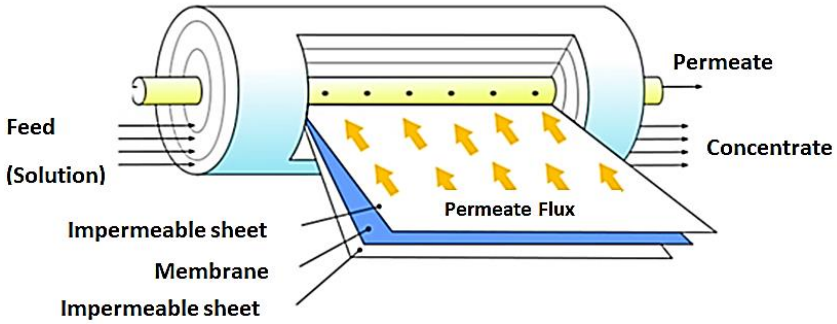

Figure 2-20: Schematic diagram of spiral wound membrane module. Adapted from (Membrane Solutions LLC 2020)

The plate and frame membrane module (Figure 2-19) is hardly used these days, except for special purposes like treatment of wastewaters with high concentration of suspended solids. The most important components of a plate and frame module are the flat membrane, membrane supporting plate, spacer and feed distribution plate. This membrane module has low membrane packing density making it less advantageous to the rest (Yasukawa, Suzuki and Higa 2018).

Figure 2-20 shows the spiral wound membrane module. This is perhaps the most widely used membrane module, especially in NF and RO applications. This module offers high

packing density of membranes and spacers wound around a central collection tube which is perforated for permeate passage (McKeen 2017). Due to the high packing density, permeation flux through the spiral wound module is mainly high.

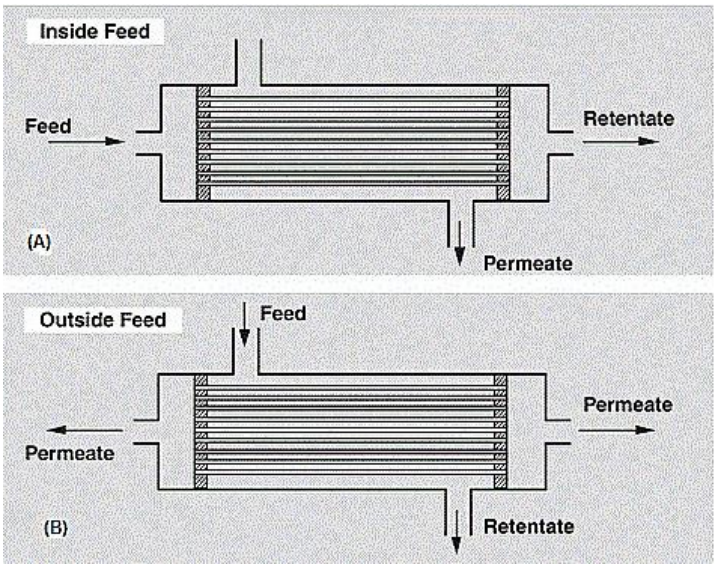

Figure 2-21: Schematic diagram of hollow fiber membrane module. Adapted from (Balster 2016)

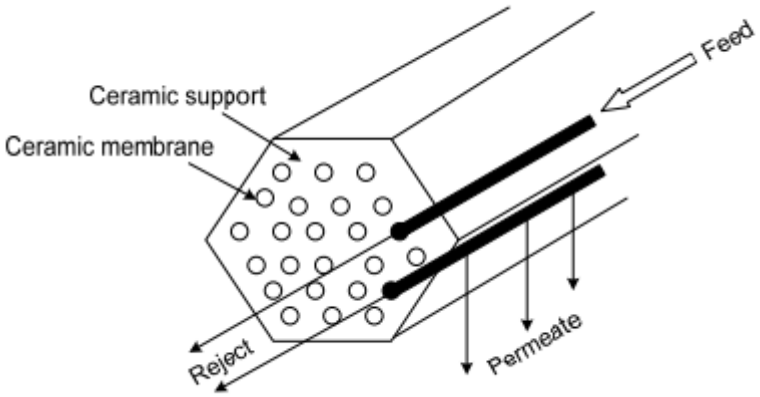

Figure 2-22: Schematic diagram of tubular membrane module. Adapted from (Chollom, Rathilal and Pillay 2014)

The hollow fiber membrane module consists of a bundle of fibers which are enclosed in a pressure vessel as shown in Figure 2-21. Feed enters at one side of the module and the retentate leaves at the other end. This module has the advantage of housing a large number of membranes in one vessel (Rackley 2017). There are two configurations applied in this

membrane module - shell side (outside feed) and bore side (inside feed). The shell side feed type is preferred for operations at high pressures (50 – 70 bar) whereas for moderate pressure operations, the bore side feed type is preferred. Hollow fiber membrane modules are noted for a high cost of production and complexity in the production process (Doran 2013).

Figure 2-22 shows the tubular membrane module. This module consists of smaller tubes enclosed in one bigger one. The feed solution is fed into the vessels under pressure and the permeate flows through the porous tubes into the module housing and collected through an outlet (Langerak, Koehler and Tonelli 1993). The tubular membrane module is mainly used in treating feed with high solid contents (Xue *et al.* 2021).

2.9.9 Fouling in membrane processes

Membrane fouling refers to the accumulation of contaminants (foulants) such as suspended solids, microbes, organic substances, etc. on the surface or within the pores of a membrane leading to reduction of water flux, reduction in water quality and short shelve life of the membrane (Speth, Summers and Gusses 1998). Fouling is either reversible or irreversible depending on position of deposition of the foulants. When foulants are deposited within the pores of the membrane structure, fouling is considered irreversible. When this happens, membrane cleaning hardly restores the permeation flux to its original. On the other hand, when foulant is merely deposited on the membrane surface to form a cake layer, fouling is considered reversible. With reversible fouling, membrane cleaning is usually able to restore permeation flux to its original value (Ezugbe and Rathilal 2020).

Occurrence of fouling is due to complex physical and chemical interactions between the constituents of the foulants in the feed and between the constituents of the foulant and the membrane surface. The extent of membrane fouling is largely dependent on feed characteristics (pH, ionic strength, divalent cation concentration, etc.) and membrane properties such as surface morphology, hydrophobicity, charge and molecular weight cut-off as well as working temperature of the system (Li and Elimelech 2004; Guo, Ngo and Li 2012).

2.9.9.1 Type of fouling

Fouling can be classified as biofouling, colloidal fouling, organic fouling, or inorganic fouling (also known as scaling) depending on the nature of the foulant (Guo, Ngo and Li 2012).

Biofouling can be described as the accumulation and growth of biofilms on a membrane surface. These may be microbial cells, extracellular polymeric substances formed from the attachment of microorganisms to moist surfaces. These organisms then feed on nutrients in this medium, grow and consequently block the pores of the membrane, leading to an increase in resistance of permeate flow (Chang, Lee and Lee 2019).

Inorganic fouling otherwise known as scaling is caused from the deposition of inorganic salts on the surface, or within the pores of a membrane. Examples of these salts include $CaSO_4$, $CaCO_3$ and SiO_2 (Al-Amoudi and Lovitt 2007). During inorganic fouling, poorly soluble salts precipitate out of solution onto the membrane when their concentration exceeds their solubility limits (Shirazi, Lin and Chen 2010). Organic fouling occurs due to the adsorption of organic compounds onto the membrane surface. These organic compounds are usually present as natural organic matter. When these compounds accumulate over time, they cause opposition to permeate flow (Amy 2008).

Colloidal materials range from few nanometers to micrometers. These may include clay minerals, colloidal silica, iron, aluminum, manganese oxides, polysaccharides, lipoproteins, biological debris, etc., which accumulate on the membrane surface or pores over time and cause an increase in resistance to permeate flow (Park *et al.* 2008; Guo, Ngo and Li 2012).

2.9.9.2 Fouling mechanism

Fouling may occur in one of the following forms (Wang and Waite 2008; Peinemann and Nunes 2010):

- Adsorption: this occurs when there is a specific interaction between the solute particles and the membrane material leading to the formation of a monolayer of particles on the membrane surface. This can happen even in the absence of permeation flux.

- Pore blockage: since membrane processes are filtration processes, pore blockage can occur during the filtration process leading to full or partial closure of the membrane pores.
- Deposition: this happens when foulants are deposited on the membrane surface and grow later into a layer, causing more resistance to permeate flow. This is referred to as cake layer formation.
- Gel formation: this is when the fouling layer is present in the form of a cross link three-dimensional network of the deposited materials.

During filtration, blocking of the membrane (especially for porous membranes) may follow any four of the mechanisms described by the filtration laws, illustrated in Figure 2-23 (Wang and Tarabara 2008). The first mechanism (Figure 2-23a) is complete pore blocking or pore sealing, where particles larger than the size of the membrane pores seal the pores completely without superimposing on other particles. The second mechanism is the standard-pore blocking. This mechanism (Figure 2-23b) assumes that pore volume decreases as particles get deposited on the walls of the pores. Subsequently, the decrease in pore volume becomes proportional to the volume of particles deposited within the pores (Vela *et al.* 2008).

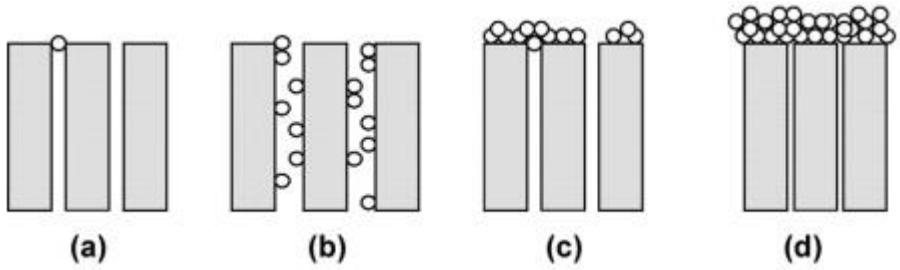

Figure 2-23: Pore blocking mechanisms; (a) complete pore blocking, (b) standard pore blocking, (c) intermediate pore blocking and (d) cake filtration. Adapted from (Wang and Tarabara 2008)

Figure 2-23c illustrates intermediate pore blocking. With this mechanism, the rate at which pores are blocked depends on the number of open pores available. This implies that foulants either plug membrane pores directly when they get to it or deposit on other foulants that are already there (Emami *et al.* 2020). The final pore blocking mechanism is illustrated in Figure 2-23d. This is known as cake filtration. During cake filtration, particles that are deposited onto the membrane surface do not block any pores either due to the dense nature of the membrane (mainly RO membranes) or due to the pores already being blocked by

other particles. The filter cake formed on the membrane surface keeps growing as the filtration process continues and this increases the resistance to permeate flow through the membrane (Civan 2016).

2.9.9.3 Mitigating fouling – pretreatments and membrane cleaning

Fouling in membrane processes is inevitable. Many techniques have been explored for reducing the effects of fouling on membranes. Some of these techniques include boundary layer velocity control, turbulence inducers and membrane modification (Jagannadh and Muralidhara 1996). Other techniques that have been proposed include feed pretreatment, flow manipulation, rotating membrane, and gas sparging (Williams and Wakeman 2000).

2.9.10 Pretreatment methods

Pretreatment processes play vital roles in mitigating membrane fouling and achieving efficient use of energy. Pretreatment is the preliminary treatment given to wastewater before the application of membrane process. Depending on the nature of the feed, pretreatment may be very simple or very rigorous. Pretreatments basically precondition wastewater for further treatment my changing the physical, chemical or biological properties of the wastewater (Koyuncu *et al.* 2015).

The kind of pretreatment method adopted is dependent on the nature of the wastewater to be treated. The most used pretreatment methods include coagulation/flocculation, adsorption, softening and pre-filtration (packed bed filters, strainers, filter cloths etc.) (Koyuncu *et al.* 2015). Specific pretreatment methods for ORE were discussed in the section 2.6.

2.9.10.1 Membrane cleaning

Membrane cleaning is carried out to restore permeation flux which is lost due to fouling. Membrane cleaning clears the foulants on the membrane to allow for the passage of permeate through the membrane. Membrane cleaning may be physical, chemical or biological. There could also be a combination of two or more cleaning methods such as biochemical or physico-chemical cleaning methods. When membrane cleaning is performed without extracting the membrane element from its housing, it is known as in-situ. On the other hand, when the cleaning is performed with the membrane element taken out of its housing, the cleaning process is referred to as ex-situ (Lin, Lee and Huang 2010; Wang *et al.* 2014).

Physical cleaning: these are activities that mechanically dislodge foulants from the membrane. Among physical cleaning methods are periodic back flushing, pneumatic cleaning, ultrasonic cleaning and sponge ball cleaning. Periodic back flushing involves the application of pressure on the permeate side of the membrane causing the membrane to be flushed inside out. The pressure applied to back flush the membrane is usually higher than the filtration pressure. This causes foulants to be lifted off the membrane surface (Ang, Lee and Elimelech 2006). Back flushing is known for its effectiveness in reversing fouling of deposited materials in the form of a gel layer or cake layer (Yan-Jun *et al.* 2000).

Pneumatic cleaning involves the application of pressurized air to clean the membrane. The air loosens and destabilizes the foulant from the membrane surface through the creation of a shear force on the membrane surface. The air can also be used in conjunction with the feed to enhance the cleaning by bubbling of the air through the feed to enhance the creation of the shear force. Pneumatic cleaning has the advantage of being free from chemical usage; however, the energy involved in pumping of air is a huge factor to contend with (An 2010; Lin, Lee and Huang 2010).

Ultrasonic cleaning is the process of using ultrasound to cause disturbance in a liquid medium. During the process, bubbles are formed. The formation, growth and collapse of these bubbles transmit energy to the membrane surface which dislodges the foulants. Ultrasonic cleaning is mainly applied in water. The use of other solvents compatible with membranes is possible as these give an enhanced cleaning effect (Li, Sanderson and Jacobs 2002; Kyllönen, Pirkonen and Nyström 2005; Wan *et al.* 2013).

Sponge ball cleaning is a mechanical process which involves the use of sponge balls to wipe the surface of the membrane. This cleaning process is usually applied in tubular membranes with wide diameters. The sponge balls are passed through the membrane module, scrubbing the surface of the membrane and thereby scrapping off the foulants on the membrane surface (Yan-Jun *et al.* 2000).

Chemical cleaning: chemical cleaning is used in cases of irreversible fouling, where foulants are not merely just deposited on the membrane surface but may be within the pores of the membrane. Chemical cleaning is expected to dislodge foulant by loosening and dissolving in the solution. This is done through the interaction of the cleaning chemical with the foulant and the membrane. This makes chemical cleaning very sensitive, as the knowledge of how the fouling particles interact with the membrane material as well as the

cleaning chemicals is very important to avoid damaging the membrane with the cleaning chemical (Siavash Madaeni, Mohamamdi and Kazemi Moghadam 2001; Porcelli and Judd 2010).

Chemicals used in membrane cleaning are mainly classified as acids, bases/alkalis, chelating agents, sequestrants, enzymes, surfactants, or disinfectants. Each of these chemicals play specific roles in removing specific foulants. Acids such as HCl, H_2SO_4, NHO_3 and H_3PO_4 are applied in the removal of inorganic foulants like metal oxides and salts. Bases/alkalis such as NaOH are used in the removal of organic foulants like suspended normal organic matter. Most chemical cleaning processes employ both acid and base/alkali in cleaning of the membrane (Porcelli and Judd 2010; José Miguel, Beatriz and María 2011).

Physico-chemical cleaning methods combine both physical and chemical cleaning processes in membrane cleaning. For example, in chemically enhanced back flushing, chemicals are added to the process to enhance the removal of foulants. Similarly, chemicals can be added to the medium within which an ultrasonic cleaning is performed. All these combine both physical and chemical cleaning to make the cleaning process more efficient (Shorrock and Bird 1998; Maskooki, Mortazavi and Maskooki 2010).

In biological cleaning processes, biological agents like enzymes or enzyme mixtures are employed in the cleaning process. Biological cleaning processes are environmentally friendly and do not damage the membrane material. They are mostly used in cleaning membranes that are used for treating wastewater from the abattoir (Wang *et al.* 2014).

2.10 Concentrate/Brine treatment

As the needs for water keeps growing, it is expected that the trend for all forms of desalination keeps going up. Figure 2-24 shows the trend and projection of desalination across the globe. While wastewater desalination occupies only about 8-10% of all desalination processes (Burn and Gray 2015), the need for proper disposal of the brine generated during the process is of major concern. The aim of brine management is to enhance the proper disposal of brine to reduce the environmental impact it will have.

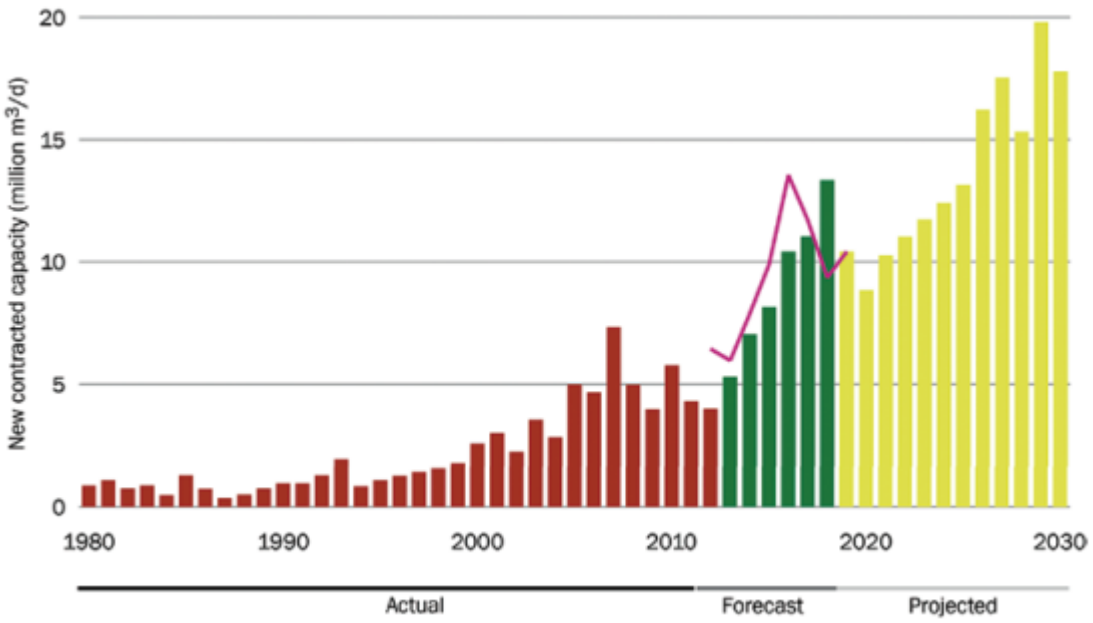

Figure 2-24: Trend of desalination globally (Burn and Gray 2015)

Many options are available depending on the location of the brine producing plant. The most common brine management employed includes deep well injection, evaporation ponds, land applications and zero liquid discharge (ZLD) and disposal into the sea. Desalination plants at coastal areas usually dispose their brine off into the sea ensuring there is proper dispersal. For inland desalination plants, deep well injection, evaporation ponds or land applications are usually employed (Burn and Gray 2015; Singh 2016).

Further concentration of the brine is an option to promote reuse of the salt fraction depending on its purity. This can be achieved through membrane distillation crystallization (MDC). This process combines membrane distillation to recover pure from the brine and crystallization to recover crystals of salt (Ji *et al.* 2010; Creusen *et al.* 2012). Gryta (2002) applied the MDC to recover NaCl crystals of up to 100 kg/m^{2}d from brine and Tun *et al.* (2005) recovered anhydrous Na_2SO_4 crystals from aqueous solution of Na_2SO_4 and NaCl, while maintaining a permeation flux of up to 20 L/m^2 h. The MDC process offers great prospects towards sustainable brine management.

2.11 Experimental design

The experimental design was achieved using the design of experiment (DoE) software (Design Expert software V.11.1.0.1, Stat-Ease Inc., Minneapolis, MA, USA). This statistical design of experiment is a powerful tool that has been used for the optimization of many chemical and biochemical processes (Weissman and Anderson 2015). DoE has

succeeded in replacing the traditional one factor/variable at a time (OFAT or OVAT) due to the significant advantages it offers in statistical analysis and cost saving. Firstly, DoE is able to eliminate bias in an experiment, adequately separating noise within the experiment from its improvements. Again, with DoE, interaction between operating variables can be studied, providing the opportunity of simultaneously varying these variables. Optimization of key process parameters is another great advantage of DoE which is hard to achieve using OFAT/OVAT (Pilipauskas 1999).

Statistical relevance and proper representation of results obtained in DoE are represented using analysis of variance (ANOVA), half normal plots and a host of other model defining tools. Contour plots and response surface plots provide great visual effects to help researchers better appreciate the variations in the process variables and their responses (Xiarchos, Jaworska and Zakrzewska-Trznadel 2008; Weissman and Anderson 2015).

2.11.1 The Box-Behnken Design (BBD)

BBD is one of the response-surface designs that are widely used apart from the central composite design (CCD) in experimental design. The Box-Behnken designs are a class of rotatable or nearly rotatable second order designs based on three-level factorial designs (Ferreira *et al.* 2007). By applying BBD, the number of experimental runs that should be conducted is optimized in a way that it analyses the interactions that are possible among the studied factors and among their possible impact on the response of the process. The BBD has three levels per factor that is -1, 0, +1, which correspond to the lowest, middle and highest points respectively (Tetteh, Rathilal and Robinson 2018).

2.12 Summary

Water scarcity and environmental sustainability continues to be a major challenge to the world. Efforts to conserve water and make potable water accessible to all are still an agenda of all stakeholders within the water sector. As the consumer of nearly 20% of the world's freshwater resources, industrial activities generate large quantities of effluents from which water can be recovered for reuse. Again, proper treatment of these effluents promotes proper and regulated disposal of the toxic constituents of the effluents, thereby protecting our environment.

The oil industry plays a significant role in world economies, through provision of employment, production of valuable products like LPG, and fuels to run many companies.

However, the generation of tons of effluent from this industry continues to pose real threats to the environment. Persistent contaminants like the PAHs, high concentrations of dissolved salts, phenols, carcinogenic materials, etc. in ORE are at the top of the list for toxic contaminants whose removal need attention.

As discharge limits and concerns for water reuse continue to rise as the days go by, effluent treatment plants are faced with the challenge of upgrading their treatment processes as the conventional treatment processes fail to meet the ever-increasing discharge limits. In the ETP of a local waste oil refinery in South Africa, removal of dissolved salts before final discharge of the effluent is a great challenge. The effluent treatment train has conventional ORE treatment processes focused mainly on residual oil recovery and removal of organics. The need for desalination of the effluent is therefore of great importance to the ETP to avoid severe environmental contamination and prevent sanctions from the municipality.

Desalination is generally energy intensive. A major shift from thermal desalination to membrane-based desalination has brought many prospects for energy savings during desalination. This study therefore investigated three membrane-based desalination techniques in desalinating ORE to meet discharge limits. FO, RO and hybrid FO-RO were evaluated on the basis of permeation flux, salt rejection and flux recoverability. Operating parameters like FS flow rate, DS flow rate, DS concentration, operating pressure, feed concentration and time were investigated and their effects on the performance of the above-named processes were presented. The use of the BBD of the RSM was handy in experimental design and optimization of the key process variables.

Chapter 3

METHODOLOGY

3.1 Introduction

This chapter presents the experimental approach adopted in achieving the objectives of this study. It details the procedures in water quality testing and analysis as well as the standard analytical methods applied. All experimental procedures have been well explained. Three processes were investigated on the basis of permeation flux, salt rejection and membrane cleaning and flux recovery. These were FO as a standalone membrane process, RO as a standalone membrane technique and the FO-RO hybrid process.

The main operating parameters on which the FO process was investigated were the FS flow rate (7.5 L/h, 8.4 L/h and 9.4 L/h), DS flow rates (7.5 L/h, 8.4 L/h and 9.4 L/h) and DS concentration (20, 35, and 50 g/L). For RO, feed concentration (298.667, 500, 653.33 mg Cl^-/L; 291.67, 583.33, and 966.67 g SO_4^{2-}/L and 86.33, 200, 390 mg CO_3^{2-}/L), operating pressure (14, 16, and 18 bar) and operating time (4, 5, and 6 hours) were the main process variables. The individual effects and the interactive effects of these variables were investigated and optimized using the Box-Behnken design (BBD) of response surface methodology (RSM) - design expert (DOE) software (Stat-Ease Inc, Minneapolis, USA). Based on the optimum conditions of the individual processes, the FO-RO hybrid process was formulated and conducted.

A significant intervention worth noting is the application of nanofiltration as the recovery method during the hybrid process that is, making it FO-NF instead of FO-RO. NF came in as an alternative when the application of RO could not recover permeate from the diluted DS due to insufficient hydraulic pressure generated by the pump used in this study. Osmotic pressure (26.63 bar) generated by the draw solution (32.6 g/L NaCl) used during the hybrid process was higher than the maximum allowable pressure of the pump (18 bar). After dilution of the DS with the 50% recovered water, the osmotic pressure of the DS reduced by 1.05 bar (calculations are shown in section 4.13). This reduction was, however not enough to bring the osmotic pressure down to the maximum allowable pressure of the pump. A nanofiltration membrane (NF90), being more permeable than the RO membrane was used as an alternative.

3.2 Materials and analytical equipment

3.2.1 Sample collection and storage

Effluent samples were obtained from a local South African oil refinery WWTP located in Durban, in the KwaZulu-Natal province. The feed to the effluent treatment plant (ETP) constitutes about 65% water and 35% oil droplets from a variety of sources such as ships slop, refinery off specs and industrial processes. The sampling point was at the three-phase separator (sewer), which served as the inlet to the municipal sewer system.

Before reaching the sampling point, the effluent had undergone some treatment, mostly primary treatment, which removes residual oils through the oil-water separator, total suspended solids (TSS) and colloidal materials at the coagulation, flocculation and dissolved air floatation (DAF) units. Table 3-1 shows the characteristics of the effluent at the sewer. These values represent the average of one month of characterization of the effluent.

Table 3-1: Characteristics of ORE sampled from the sewer, characterized over a one-month period

Water parameter	Value
pH	9.09 ± 1.34
Conductivity (mS/cm)	18.03 ± 4.38
SO_4^{2-} (mg/L)	855.756 ± 138.23
Cl^- (mg/L)	714.4 ± 332.85
*CO_3^{2-} (mg/L)	206

*as total hardness (Ca^{2+} and Mg^{2+})

3.2.2 Chemicals

Chemicals used in this study are shown in Table 3-2. Two main categories of chemicals were used (membrane cleaning chemicals and chemicals serving as source of the target salts used in the preparation of the synthetic ORE). All chemicals were laboratory grade chemicals and needed no further purification before use.

Table 3-2: Chemicals used in this study

Chemical	purpose	supplier
NaOH	pH correction and chemical cleaning	Sigma Aldrich
HCl	pH correction and chemical cleaning	Sigma Aldrich
NaCl	Preparation of draw solution	Minema Chemicals,
$NaHCO_3$	Source of CO_3^{2-}	Associated Chemical Enterprise (ACE)
$CaCl_2 \cdot 2H_2O$	Source of Cl^-	Radchem Laboratory supplies
$CaSO_4 \cdot 2H_2O$	Source of SO_4^{2-}	Sigma Aldrich

3.2.3 Analytical Equipment

The water quality parameters of interest in this project were mainly the Cl^-, SO_4^{2-} and CO_3^{2-} salt concentrations, pH, and conductivity. Table 3-3 shows the analytical instruments used.

Table 3-3: Analytical instruments used in this study

Water quality parameter	Instrument used	Method
pH	pH paper strip	Standard method
Conductivity	HI98130 pH&EC meter (calibrated with 12.88 mS/cm EC calibration solution)	Standard method
SO_4^{2-}	DR 3900 spectrophotometer	Standard method
Cl^-	DR 3900 spectrophotometer	Standard method
CO_3^{2-}	DR 3900spectrophotometer	Standard method

3.2.4 Procedure for characterization of ORE samples for SO_4^{2-}, CO_3^{2-} and Cl^-

The effluent sample was diluted with DI water in the ratio 1:10. Taking 10 ml of the diluted effluent in a cuvette, reagents for the target salt (whether SO_4^{2-}, CO_3^{2-} or Cl^-) was added and inverted 5 times to ensure a good mixture of the reagent and the sample was achieved. The appropriate testing option was chosen on the spectrophotometer. The cuvette was then placed in the spectrophotometer for analysis. Before each reading, the photometer was blanked using raw samples.

3.2.5 Feed solution preparation

To cater for the 30 runs (15 each for FO and RO) generated by the design expert software, synthetic solution was prepared. This was done by diluting 25 L raw ORE with DI water in the ratio 1:2. Before use, the required volume of feed solution was transferred into a

beaker and spiked with the target salts to mimic the concentration of the real effluent. This made available enough feed solution for all the 30 runs. It is however noteworthy, that the confirmatory runs conducted after the optimization of the two processes and the FO-RO/NF hybrid runs were conducted with raw effluent.

3.3 Experimental apparatus

3.3.1 FO Test apparatus

3.3.1.1 Membrane and draw solutes

The properties of the FO membrane used are shown in Table 3-4. The $FTSH_2O$ FO membrane was supplied by Sterlitech, Kent, WA, USA.

Table 3-4: Properties of FO membranes

Type	Cellulose triacetate (CTA)
Support layer	Polymer mesh
Mean pore size/MWCO	0.307 ± 0.003 nm
pH range	2-11
Thickness	0.0965 mm
Transport properties	
*A	1.4 LMH
*B	0.74×10^{-6} m/s
*S	1020 ± 60 µm

*A = water permeability of active layer, *B = solute permeability and *S = structural parameter of membrane support layer

Two draw solutes (NaCl and $CaCl_2$) were considered based on literature (Ahmed *et al.* 2018; Mogashane *et al.* 2020). The NaCl and $CaCl_2$ draw solutes were both used in separate experiments (Ezugbe *et al.* 2020; Ezugbe *et al.* 2021) which gave the author the basis to choose NaCl as the draw solute for this study. NaCl generated more osmotic pressure compared with $CaCl_2$. In addition, $CaCl_2$ had a higher fouling propensity than NaCl.

3.3.1.2 FS and DS tanks

The feed and draw solution tanks used for the FO experiment are shown in Figure 3-1. The 5 L Duran bottles were labeled to reflect their containments. In all cases, the DS tank label was changed to reflect the changing concentration of the DS used.

Figure 3-1: FO set up showing all components of the process

3.3.1.3 Membrane cell

The membrane test cell (Figure 3-2) comprised of two PVC blocks of dimensions 35 cm x 15 cm x 6 cm, between which was sandwiched the CTA FO membrane. Two rubber seals were installed to avoid leakage of FS and DS during the experimental process. 12 x 8 mm polyurethane rubber tubing was fitted onto nozzles that connected the test cell to the FS and DS tanks and the peristaltic pumps that circulate FS and DS. Four pieces A2 – 70 stainless steel bolts, 12 cm long were used to fasten the entire test cell in place, tightly fitted with nuts.

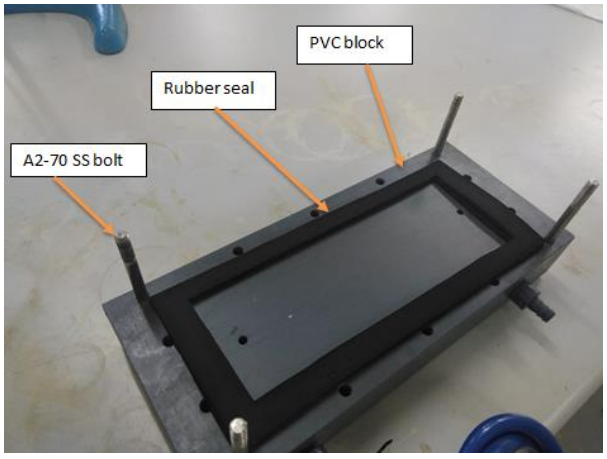

Figure 3-2: Membrane cell, showing rubber seal and stainless-steel bolt

3.3.1.4 Pumps

Peristaltic pumps were used for circulating the FS and DS. Each solution had a dedicated pump for its circulation. A picture of the peristaltic pump (Blue-White Industries,

Huntington Beach, CA, USA) used in this study is shown in Figure 3-1. The maximum flow rate of the pump was 9.4 L/h and maximum pressure was 6.9 bar.

3.3.2 Experimental procedures for FO

3.3.2.1 CTA membrane activation and preservation

The FO membrane came as a square sheet of dimension 30.5 x 30.5 cm packed in 1% sodium Metabisulfite water solution. Before use, the membrane was cut into the required dimension of 9 x 25 cm (effective membrane area = 0.0225 m^2) and thoroughly rinsed with deionized (DI) water (ELGA PURELAB Option-Q water deionizer, UK). It was then soaked in DI water over night and until use. A used membrane is stored in DI water after being thoroughly rinsed with clean water. This storage method is prescribed by the manufacturer, with the intent of keeping the membrane from being deformed or shrunk.

3.3.2.2 Testing of key parameters

Using the pH paper strip, the pH for both the feed and draw solutions were tested before and after each experimental run.

Initial and final concentrations of the individual ions, Cl^-, SO_4^{2-} and CO_3^{2-} in the FS were determined according to the procedure in section 3.2.4.

Initial and final conductivities of the FS were determined using the HI98130 pH&EC meter.

3.3.2.3 Preparation of draw solution

In preparing the draw solution for each run, the following procedure was followed.

Using a chemical balance (HCB 602H, Adam equipment Inc, Oxford, USA), the required mass (20, 35 or 50 g/L) of NaCl was weighed and placed into a beaker. DS concentration was chosen based on previous studies by Nelson and Ghosh (2011) and Bamaga *et al.* (2011) to reflect a wide range of concentrations.

0.25 L of DI water was added to the contents within the beaker and thoroughly stirred until the NaCl dissolved.

The mixture was transferred to the DS tank (5 L) Duran bottle. It was then topped up with DI water to the 1 L mark.

3.3.2.4 Feed solution for FO

The feed solution was stored in a 25 L container and transferred in smaller volumes according to the experimental requirements. Getting the FS ready for the experiment involved the following procedure.

- The required volume (2 L) was transferred into a beaker
- Pre-filtration was carried out using filter paper (Whatman filter paper, retention 10 -15 µm). This takes out slims and macro particles that can easily damage the membrane
- By means of a chemical balance 3 g of $Cacl_2 \cdot 2H_2O$, 3.06 g of $CaSO_4 \cdot 2H_2O$ and 1.2 g of NaHCO were weighed and thoroughly dissolved in the 2 L FS to form a homogeneous mixture.

3.3.2.5 FO process description

Figure 3-3 shows the schematic diagram of the FO process. The feed tank was filled with the feed solution to the 2 L mark. The draw solution tank was filled to the 1 L mark with the DS. The peristaltic pumps were set to the appropriate flow rates (7.5 L/h being 80% pump discharge rate, 8.4 L/h being 90% pump discharge rate or 9.4 L/h being 100% pump discharge rate). The independent magnetic stirrers were regulated to the speed of 800 rpm.

The experiment was conducted in the continuous dilution method, where the draw solution was diluted with water drawn from the feed for the entire duration of the experiment (Ferrari *et al.* 2019). The membrane configuration used was the FO mode, where the active layer of the membrane faced the FS. The direction of flow of the FS and DS was counter current, where the FS and the DS were circulated in opposite direction to each other. This flow configuration is advantageous as higher fluxes can be achieved (Cath *et al.* 2010; Giagnorio *et al.* 2019).

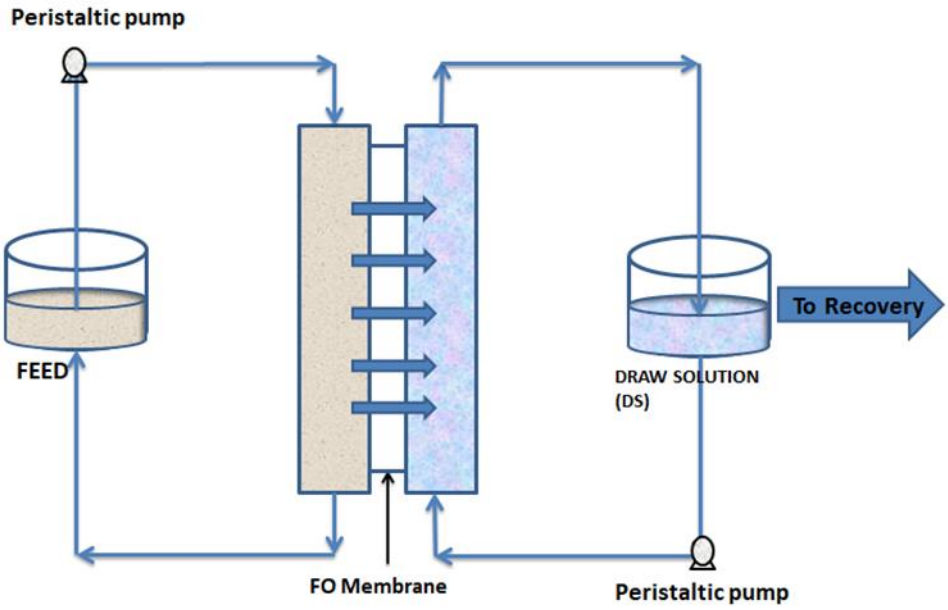

Figure 3-3: Principle of FO. Adapted from (Ezugbe and Rathilal 2020)

3.3.2.6 Determination of Pure water flux (PWF) of virgin CTA membrane

This is the water flux of the virgin membrane. In order to set a basis for comparison of permeation fluxes during the experiments, the water flux of the virgin membrane is first determined. deionized (DI) water was first used as feed solution with 1 L of 1 M NaCl as draw solution under a batch mode for 8 hours (Cath *et al.* 2013). This was done in triplicate. The procedure is as follows.

- The CTA membrane was well fastened onto the test cell
- The feed tank was filled with DI water to the 3 L mark.
- The draw solution (DS) tank was filled with 1 L of 1 M NaCl solution
- Membrane was oriented in the FO mode.
- The process was allowed to run for 8 hours.
- Pure water flux was calculated using equation 3.1
- The process was repeated three times with fresh pieces of membranes

$$J_w = \frac{V_p}{At} \qquad \text{Equation 3.1}$$

Where J_w is the water flux (L/m^{2}h); V_p is the permeate-volume (mL); A is the effective membrane area (m^2) of the membrane and t is the time (h) taken for the experiment.

3.3.2.7 Permeation flux determination

Permeation flux is basically the movement of components across the membrane per unit area (m^2), per unit time (h). The two main components transported during FO are water

and solute. Water molecules move in the direction of the osmotic pressure gradient whereas solutes move in the direction of the chemical potential gradient (Nagy 2019a).

Procedure

i. The FS tank was filled with the feed to the 2L mark.
ii. The DS tank was filled with the DS to the 1 L mark
iii. The volume of permeate was determined by subtracting the final DS volume from the initial DS volume (V_f - V_i). This gives volume of water drawn from the FS into the DS.
iv. Permeation flux was calculated in L/m^2·h according to equation 3.1

3.3.2.8 Salt Rejection

The membrane's ability to reject the salts is determined by measuring the amount of salts that moved from the FS into the DS over the period of the experiment. Particularly, membrane properties such as pore size and charge play a great role in rejection of materials. FO is a dilution process; hence the dilution factor is an integral part of determining the salt rejection (Alturki *et al.* 2013). The salt concentrations were determined in the DS. By comparing the final concentration of the salts (in the DS) to the initial concentration of the salts (in the FS), the percentage rejection was determined (Holloway *et al.* 2007). The procedure is as follows.

i. The dilution factor (D_f) was first determined according to equation 3.2 (Ezugbe *et al.* 2021)

$$D_f = \frac{V_{f,DS}}{V_p} \qquad \text{Equation 3.2}$$

Where, $V_{f,DS}$ = final volume of draw solution (mL), V_p= volume of permeate (mL)

ii. Individual concentrations of carbonates, sulphates and chlorides were determined in DS at the end of each experiment.

iii. Salt rejection was calculated using equation 3.3

$$R\% \ \frac{C_0 - D_f C_f}{C_0} \ x\ 100 \qquad \text{Equation 3.3}$$

Where C_0= concentration (mg/L) of target component in FS, C_f= Concentration (mg/L) of target component in DS and D_f is the dilution factor.

3.3.2.9 FS enrichment with Cl^-

Due to the concentration gradient between the Cl^- in the FS and the DS, it is possible and probable for the Cl^- to move from the DS into the FS. This is characteristic of osmotically driven membrane processes as described in section 2.9.6.1. The chloride enrichment was calculated according to the following equation (Gadallah *et al.* 2014).

$$\text{Reverse solute flux } (J_s) = \frac{C_f V_f - C_0 V_0}{At} \qquad \text{Equation 3.4}$$

Where J_s is the reverse salute flux (g/m^2 h), C_0 and C_f are the initial and final concentrations (mg/L) of Cl^- in the FS respectively, V_0 and V_f are the initial and final volumes (mL) of the FS respectively, A is the effective membrane area (m^2), and t is the time (h). Values of J_s for all runs are shown in table A-2 in appendix A

3.3.2.10 Membrane cleaning and flux recovery for FO process

Membrane cleaning was achieved by both physical cleaning and osmotic backwashing. Physical cleaning was first performed, followed by osmotic backwashing. While physical cleaning was done after every run, a full cleaning program (manual scrubbing and osmotic backwashing) was performed after 30 hours of membrane use. The procedure is as followed.

A. Physical cleaning

Fouled FO membrane (Figure 3-4) was extracted from the test cell and manually scrubbed with the fingers (wearing gloves) under running water. This was done thoroughly to remove dirt and slims that accumulated on the surface of the membrane material.

Figure 3-4: Fouled FO membrane

B. Osmotic backwashing

This was performed to reverse the flow of permeate, in so doing the direction of the osmotic pressure was reversed, thus dislodging particles that may have clogged the membrane pores. The procedure (Holloway *et al.* 2007) is as follows:

i. Both feed and draw solution vessels were filled with DI water to the 3 L mark.
ii. Both sides of the membrane were flushed with the DI water for at least 1 hour.
iii. The flushing solution was drained from the FS and DS tanks. These tanks were then thoroughly rinsed with DI water.
iv. This was followed by filling the feed vessel with 35 g/L NaCl solution to the 1 L mark and the DS vessel was filled with DI water to the 3 L mark
v. Both solutions were circulated for 1 hour.
vi. DI water was used to flush both sides of the membrane for 30 minutes
vii. To ascertain the flux recovery, PWF was determined for the cleaned membrane and compared with the PWF of the virgin membrane.
viii. Water Flux recovery (WFR) was calculated by the formula (Schäfer *et al.* 2004; Ezugbe *et al.* 2021) below.

$$\text{WFR} = \frac{J_c}{J_0} x\ 100 \qquad \text{Equation 3.5}$$

Where J_c= PWF (L/m^{2}h), after cleaning J_0= PWF of virgin membrane.

3.4 Experimental procedure for RO

3.4.1 RO Test rig components

3.4.1.1 Membrane

The thin film composite (TFC) RO membrane was supplied by DOW Filmtec, South Miami USA. The properties are shown in Table 3-5. The flat sheet TFC membrane came as a large sheet of dimensions 30.5 x 30.5 cm. It was cut to the required size of 8 x 3 cm (effective membrane area of 0.0025 m^2) (Figure 3-5 A). The membrane was then soaked in DI water (Figure 3-5B) for 24 hours before use.

Table 3-5: Properties of RO membranes

Type	Thin film composite (TFC) polyamide
Support layer	polysulfone
Mean pore size/MWCO	100 Da
pH range	2 - 11
Contact angle	33º
Thickness	200 µm

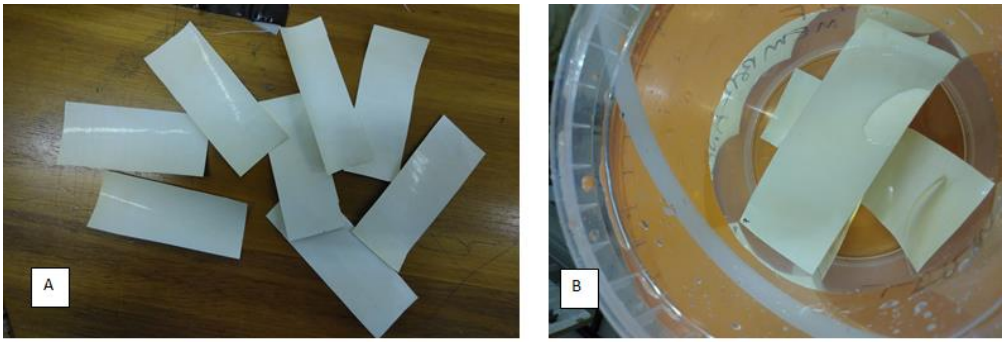

Figure 3-5: A: RO membrane cut into the required size. B: RO membrane soaked in DI water

3.4.1.2 Feed tank

A plastic feed tank with a volume of 20 L was used as shown in Figure 3-6. Cooling coils were immersed into the tank to constantly remove the heat generated by the process.

Figure 3-6: RO experimental set up, showing the major components

3.4.1.3 Membrane cell

The membrane test cell (Figure 3-7) was made of two identical PVC blocks of dimensions 13.5 x 11 x 3.5 cm, between which were sandwiched the RO membrane, tightly fastened together using bolts and nuts with a flat sheet stainless steel plate as additional support. One of the PVC blocks had a porous center, where permeate passes during the filtration process. The RO membrane was placed over the porous area. The neoprene gasket, placed over the membrane served as a seal to avoid leakage.

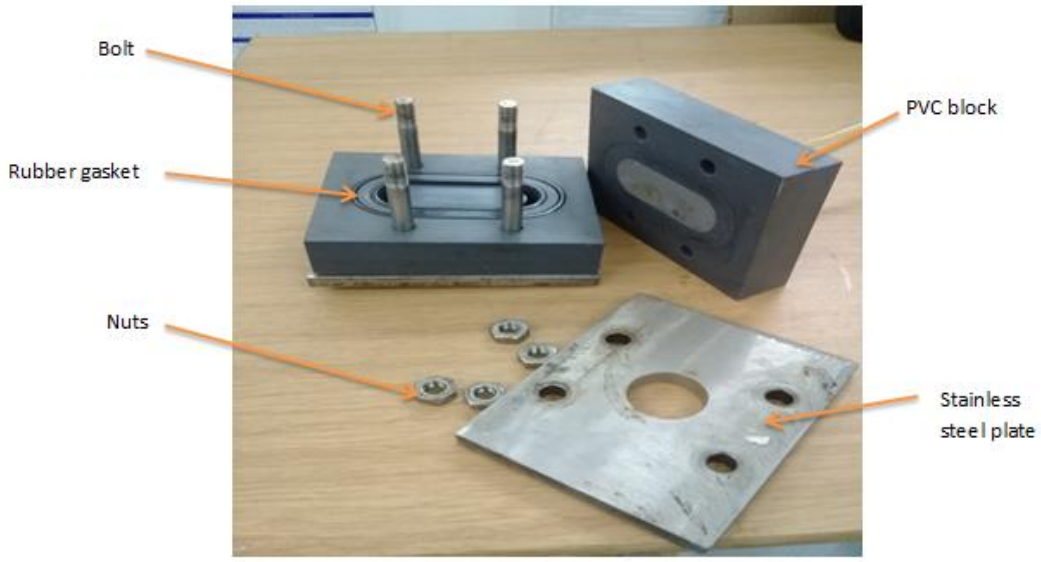

Figure 3-7: RO membrane cell, showing major components

3.4.1.4 Pump

The high-pressure pump used for this experiment was a stainless-steel pump with the highest output pressure of 18 bar. The Fluid-o-Tech magnet drive rotary vane pump, TH series had a maximum speed of 1725 rpm and a working temperature range of 20 – 70℃.

3.4.1.5 Cooling system

To ensure the maintenance of a constant range of temperature (19 – 22℃) during the process, cooling coils were used to remove the heat that is produced during the RO process. Cooling water was pumped from a 50 L cooling tank, furnished with a chiller (2900W Puron carrier NANOCHIL). Cooling water from the cooling tank enters the cooling coil and warm water escapes from the cooling coil outlet into the cooling tank. This was a continuous process.

3.4.1.6 RO process description

The RO process flow diagram is shown in Figure 3-8. V1 is a ball valve, installed at the FS outlet, opened and closed manually to control feed solution flow. V2 is a non-return valve, installed to protect the pump from back pressure build up at elevated pressures. V3 is a needle valve, used to control the pressure of the system. V4, ball valve controlled the cooling water inlet. The brine/retentate is recycled into the feed tank during the process, while the permeate water is collected in the permeate tank for analysis.

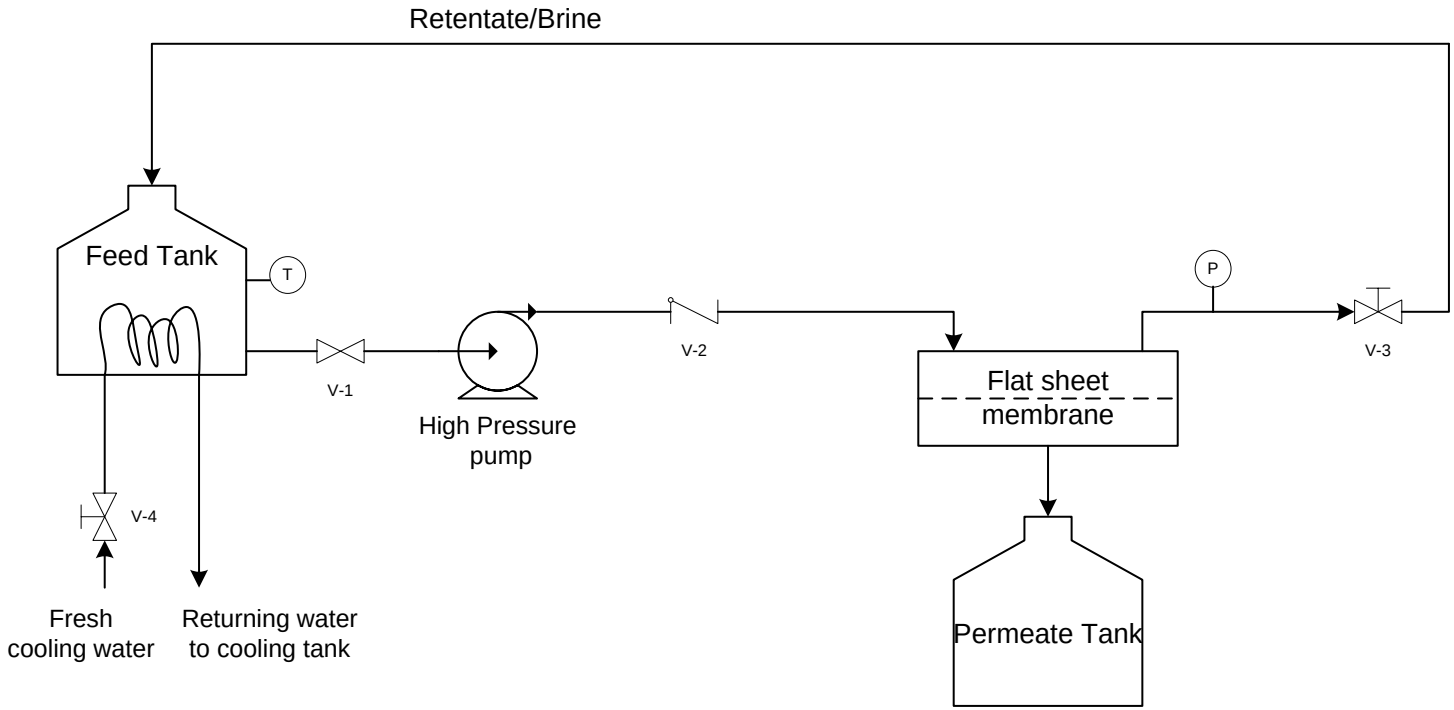

Figure 3-8: RO process flow diagram showing the major components

3.4.1.7 RO start-up procedures

To get the system ready for operation, some basic procedures were carried out. V1, the feed tank outlet valve was fully opened. V3, which controls the back pressure, was fully opened as well. The chiller and the cooling water pump were then started to produce and circulate cooling water through the system.

3.4.1.8 Pure water flux determination of virgin TFC membrane

The water flux of the virgin TFC membrane was first determined to provide a basis of comparison for the process in terms of permeation flux and flux recovery after cleaning. The following procedure was followed.

i. The TFC membrane was well fastened onto the test cell
ii. The feed tank was filled with DI water to the 15 L mark.
iii. The high-pressure pump was started
iv. The needle valve, V3 was used to adjust the pressure to 15 bar.
v. The permeate was channeled into the permeate tank and volume measured, while the retentate was recycled into the feed tank
vi. The setup was allowed to run for 4 hours.
vii. The experiment was repeated three times with fresh pieces of membranes.
viii. The water flux is calculated using equation 3.6

$$J_w = \frac{V}{At} \qquad \text{Equation 3.6}$$

Where J_w is the water flux (L/m^{2}h) through the TFC membrane, V is the permeate volume (mL), A is the effective membrane area (m^2) and t is the experimental time (s).

3.4.1.9 Determination of permeation flux of actual feed

The procedure for determining the permeation flux of the actual feed is similar to that of the PWF, except that the feed was changed to actual feed of volume 7 L and the operating times and pressures were changed accordingly. Permeation flux was measured in L/m^2·h.

3.4.1.10 Salt rejection

Unlike FO, rejection of the target salts was determined directly by calculation using equation 3.7.

$$R\% = \left(1 - \frac{c_p}{c_f}\right) \text{x } 100 \qquad \text{Equation 3.7}$$

Where c_p = concentration (mg/L) of component in permeate, c_f = concentration (mg/L) of component in feed. Analysis of the permeate water was made using the analytical instruments listed in Table 3-3 and according to the procedure spelled out in section 3.2.4.

3.4.1.11 Membrane cleaning and flux recovery for RO process

Physical cleaning by forward flushing and chemical cleaning (using NaOH and HCl) were administered during each cleaning process.

Procedure for forward flushing;

i. The feed tank was filled with DI water to the 15 L mark. The needle valve V3 was almost fully opened to make sure there was little or no restriction, thereby preventing the generation of permeate.
ii. The pump was turned on and allowed to run for at least 30 minutes, after which the flushing liquid was disposed of and refilled with fresh DI water.
iii. The process was repeated once more.

Procedure for chemical cleaning;

i. 0.1 wt% NaOH was prepared and used for alkali cleaning.
ii. The feed tank was filled with the cleaning solution to the 10 L mark. The needle valve V3 was almost fully opened as it was in the forward flushing process.
iii. The cleaning chemical was run through the retentate channel for 30-45 minutes under a pH of 11.
iv. This was followed by flushing of the channel with DI water
v. Acid cleaning then followed using 0.2 wt% HCl, in the same manner as the alkali cleaning but under pH of 1–2.
vi. DI water was used to flush the system twice as described above.
vii. Pure water flux was conducted to ascertain flux recovery.
viii. Water Flux recovery (WFR) was calculated according to equation 3.5.

3.4.1.12 Experimental procedure for FO-RO/NF

Figure 3-9 shows the set up for this process. Operating conditions for this process were the obtained optimum conditions of both FO and RO. These were FS-FR of 7.7 L/h, DS-FR of 9.4 L/h and DS concentration of 32.6 g/L for FO while for RO, operating pressure was 18

bar and run time was 6 hours. Real effluent was used, hence the real effluent concentration was adopted.

Figure 3-9: FO-RO/NF hybrid process

3.4.2 FO-RO/NF Process description

Figure 3.11 shows the process flow diagram employed for the FO-RO/NF hybrid process. The experiment was conducted in batch mode. FO process was allowed to run for extended number of hours until at least 50% of the water was recovered from the FS, after which the RO was applied for DS reconstitution and permeate water recovery. The following procedure was followed.

i. The FS tank of the FO was filled to the 3 L mark.
ii. The DS tank was filled with 32.6 g/L NaCl solution to the 1.5 L mark.
iii. The stirrers were switched on to ensure continuous homogeneity of the solutions.
iv. The peristaltic pumps were switched on and the FS pump flow rate was set to 7.5 L/h while the DS pump flow rate was set to 9.1 L/h.
v. After 50% recovery of water from the feed, the DS became diluted.
vi. The RO process was then applied. The procedure was similar to the RO procedure described in section 3.4, except that in this case, the feed was the DS diluted with permeate from the FO process.
vii. The RO process was allowed to run for 6 hours.

After the 6 hours of RO there was no permeate water. As an alternative, a nanofiltration membrane (NF90, properties shown in Table 3-6) was applied as the recovery method. The

procedure of application was the same as described above, with all process variables unchanged.

Table 3-6: Properties of NF90

supplier	Dow filmtec
Membrane material	polyamide
pH range	1 - 13
Contact angle	27º
MWCO*	150 – 200 Da**

MWCO* = Molecular weight cut off; **Da = Daltons

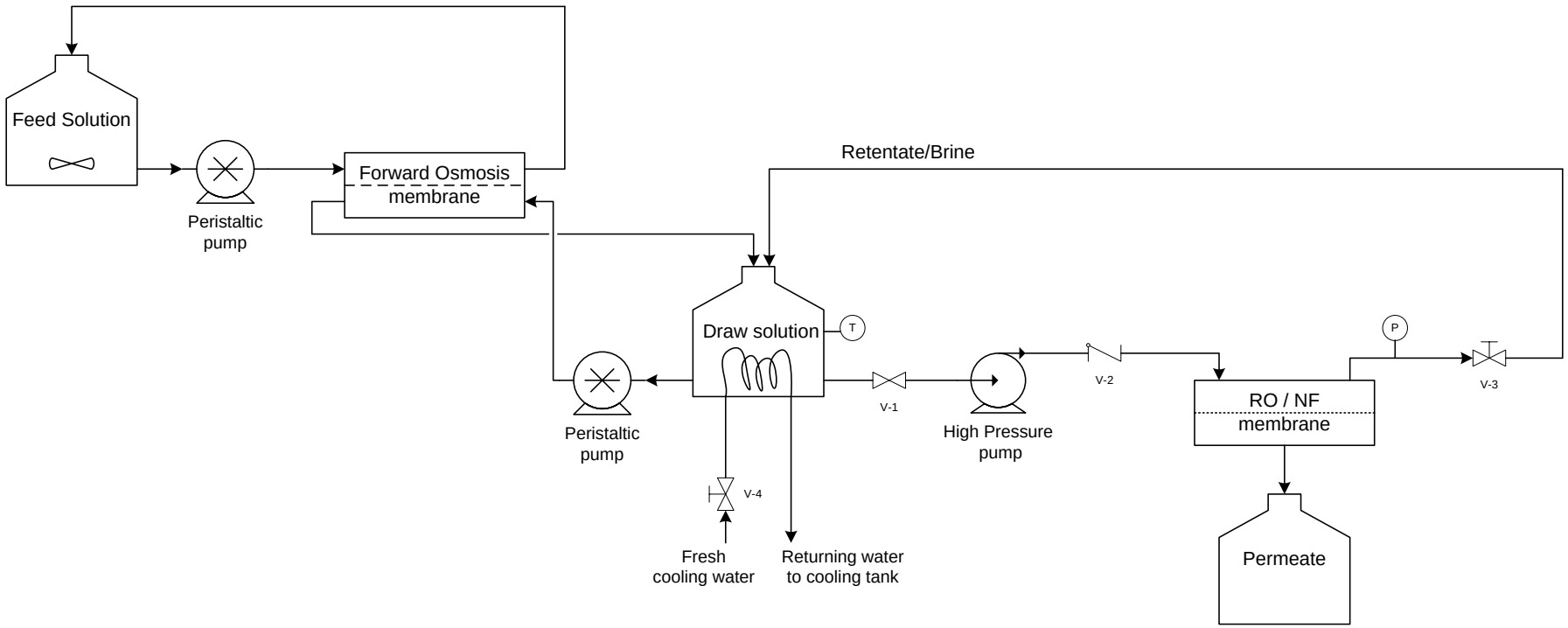

Figure 3-10: Process flow diagram of FO-RO/NF hybrid system

3.4.3 Permeate collection and analysis

After each run, permeate from the process was analyzed immediately. The key parameters tested were pH, Cl^- concentration, SO_4^{2-} concentration, CO_3^{2-} concentration and conductivity. The procedure for analysis was initially outlined in section 3.2.4.

3.4.4 Design of experiment

Design expert software (Design Expert software V.11.1.0.1, Stat-Ease Inc., Minneapolis, MA, USA) was utilized in the experimental design of this study. Using the Box-Behnken design (BBD) of the response surface methodology (RSM), 15 experimental runs each were generated for FO and RO standalone processes. The 15 runs included three replications. The three different normalized central levels were coded as −1, 0, +1, corresponding to the minimum, central point, and maximum for the factors considered. These experimental runs were randomized in order to eliminate bias. The optimum conditions were used for confirmatory runs, made up of three independent runs at the same conditions. Table 3-7 shows the factors for the experimental design using the BBD.

Table 3-7: Factors for experimental design using BBD

Process	Input variables	Coded levels		
		-1	0	1
FO	X_1: Feed solution flow rate (FS-FR) (L/h)	7.5	8.5	9.4
	X_2: Draw solution flow rate (DS-FR) (L/h)	7.5	8.5	9.4
	X_3: Draw solution concentration (DS-C) (g/L)	20	35	50
RO	X_1: Operating Pressure (p) (bar)	14	16	18
	X_2: Feed solution concentration (FS-Con)(mg/L)*	298.667	500	653.33
	Cl^-	291.67	583.33	966.67
	SO_4^{2-}	86.33	200	390
	CO_3^{2-}			
	X_3: Operating time (t) (h)	4	5	6

*composition of feed solution, a mixture of the target salts

Chapter 4

RESULTS AND DISCUSSION

The results of this study are presented and discussed in this chapter. Firstly, the pure water fluxes obtained from virgin membranes are presented. This is followed by the individual and interactive effects of the operating variables on FO and RO performance, in terms of permeation flux and salt rejection, studied using BBD. Again, the results of the optimization and the effectiveness of the various cleaning protocols to enhance permeation flux recovery are presented. Finally, comparison on the bases of permeation flux, salt rejection efficiencies and permeation flux recovery between FO, RO and FO-NF are presented and discussed.

4.1 Pure water flux (PWF) of virgin membranes

Figure 4-1 shows the PWF for the various membranes used in the study. This was the first permeation flux of the membranes after the membranes were activated. This served as the bases of comparison for flux recoverability after membrane cleaning.

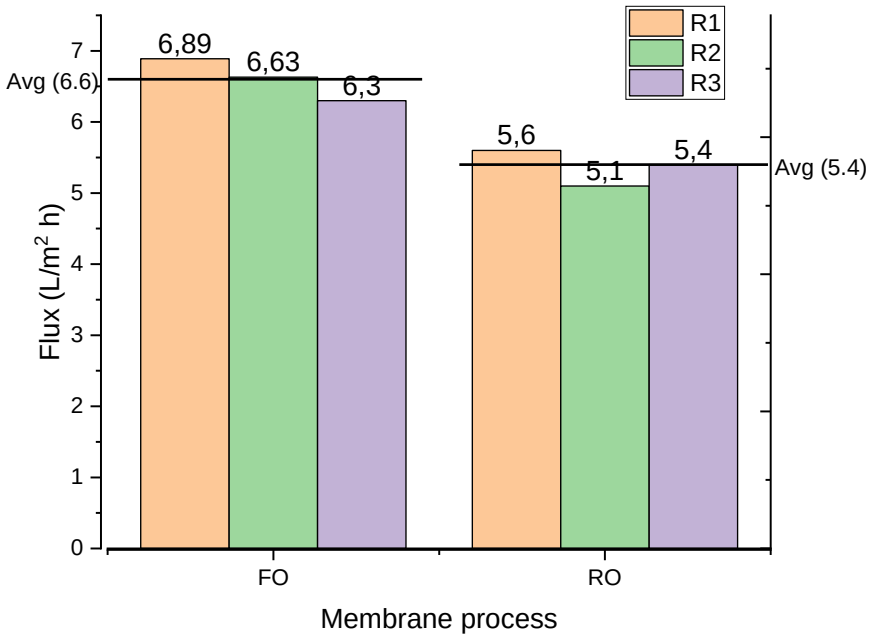

Figure 4-1: PWF of virgin membrane of FO and RO

To ensure the repeatability of results, the test was performed three times at the same conditions. Each test was conducted with a fresh piece of membrane. As can be seen from

figure 4.1, the results of the three independent runs show very little variation. The average of the three runs for FO was 6.60 ± 0.24 L/m^{2}h and for RO, the average was 5.37 ± 0.21 L/m^{2}h. These two values served as the bases for measuring permeation flux and flux recoverability.

4.2 FO BBD design matrix – actual and predicted values

Table 4-1 shows the design matrix and the results obtained after the experimental runs. These include the studied factors, in coded form, the actual results and the model-predicted results of the response factors. The actual values are the measured response data of a specific run while the predicted values are calculated from the model.

Table 4-1: BBD design matrix for FO, showing the actual and predicted values

	F1	**F2**	**F3**	**R1**		**R2**		**R3**		**R4**	
	A:FS-FR	B:DS-FR	C:DS-C	flux, L/m²h		Cl^- Enrich		SO_4^{2-} Rejec		CO_3^{2-} Rejec	
Run	L/h	L/h	g/L	Actual	Predicted	Actual	Predicted	Actual	Predicted	Actual	Predicted
1	1	0	-1	1.72	1.74	4.48	4.32	88.91	89.59	89.23	89.36
2	1	1	0	2.59	2.63	20.29	20.52	87.03	87.17	92.49	92.92
3	0	0	0	3.05	3.21	27.9	27.01	96.94	98.48	95.01	94.95
4	0	1	1	3.03	3.06	52.11	52.74	100	98.33	93.28	93.39
5	-1	0	1	4.01	3.96	39.33	39.98	99.05	98.74	94.03	94.36
6	-1	1	0	4.09	4.1	35.01	33.79	99.96	100.42	96.08	96.23
7	1	-1	0	3.04	3.01	41.08	42.8	99.22	98.39	92.29	92.5
8	1	0	1	2.98	2.9	66.01	65.2	95.97	95.97	93.89	93.12
9	0	-1	1	3.71	3.81	63.09	62.62	100	102.04	97.01	97.34
10	0	-1	-1	1.33	1.34	29.33	27.82	100	98.62	86.89	87.13
11	-1	-1	0	3.19	3.13	31.01	31.27	97.13	96.61	91.73	91.66
12	-1	0	-1	2.23	2.27	29.98	31.28	97.92	98.29	90.99	90.59
13	0	0	0	3.18	3.21	26.22	27.01	99.96	98.48	95.28	94.95
14	0	0	0	3.36	3.21	27.9	27.01	97.91	98.48	95.28	94.95
15	0	1	-1	2.74	2.68	17.58	17.94	94.53	94.92	96.04	96.07

4.3 Model fitting and statistical analysis

Equations 4.1 – 4.4 represent the models generated by the software for the various responses in coded form. These are 2nd order quadratic models in their reduced form, expressed as functions of the input and output variables. Model reduction was necessary in order improve the predictability of the response variables.

$$Flux = 3.21 - 0.3981A + 0.1482B + 0.7133C - 0.337AB - 0.13AC - 0.5217BC - 0.4939C^2$$ equation 4.1

$$Cl^- \text{ enrichment} = 27.01 - 0.4338A - 4.94B + 17.4C - 6.2AB + 13.05AC + 5.08B^2 + 8.19C^2$$ equation 4.2

$$SO_4^{2-} \text{ rejection} = 98.84 - 2.87A - 1.85B + 1.71C - 3.75AB + 1.48AC - 2.83A^2$$ equation 4.3

$$CO_3^{2-} \text{ rejection} = 94.95 - 0.6162A + 1.25B + 1.88C - 1.04AB + 0.405AC - 3.22BC - 1.63A^2 - 1.47C^2$$ equation 4.4

The extents to which terms of the models can affect the response are associated with the positive and negative coefficients of the terms. Negative coefficients depict unfavorable effects of the factors, whereas positive coefficients show that a factor or combination of factors contribute favorably to the contaminant removal. Again, the magnitudes of the coefficients correlate with the degree to which the response variable is affected (Tetteh *et al.* 2020). To this effect, the impact of the model terms of each model in a descending order are as follows; Flux = C > B > AC > AB > A > C^2 > BC; Cl^- enrichment = C > AC > C^2 > B^2 > A > B > AB; SO_4^{2-} rejection = C > AC > B > A^2 > A > AB; CO_3^{2-} rejection = C > B > AC > A > AB > C^2 > BC. A, B and C are the individual factors, AB, AC and BC represent the interactions between the factors while A^2, B^2 and C^2 represent the quadratic effects, where each factor interacts with itself.

The statistical relevance and accuracy of the models were verified by the analysis of variance (ANOVA), which is a powerful statistical tool used to explain the variations in the magnitude of a response variable of interest (Doncaster and Davey 2007). The ANOVA of the quadratic models of the various responses are shown in the tables below.

Table 4-2: ANOVA of reduced quadratic model for permeation flux

Source	Sum of Squares	df	Mean Square	F-value	p-value	
Model	3776.56	7	539.51	300.1	< 0.0001	significant
A-FS-FR	1.51	1	1.51	0.8372	0.3906	
B-DS-FR	195.23	1	195.23	108.6	< 0.0001	
C-DS-C	2421.04	1	2421.04	1346.71	< 0.0001	
AB	153.64	1	153.64	85.46	< 0.0001	
AC	680.69	1	680.69	378.63	< 0.0001	
B^2	95.99	1	95.99	53.39	0.0002	
C^2	248.91	1	248.91	138.45	< 0.0001	
Residual	12.58	7	1.8			
Lack of Fit	10.7	5	2.14	2.28	0.3329	not significant
Pure Error	1.88	2	0.9408			
Cor Total	3789.15	14				
R^2 (0.9967)	Adjusted R^2 (0.9934)	Predicted R^2 (0.9759)	Adeq Precision (62.1769)	Std. Dev. (1.34)	Mean (34.09)	

Table 4-3: ANOVA of reduced quadratic model for Cl^- Enrichment

Source	Sum of Squares	df	Mean Square	F-value	p-value	
Model	3776.56	7	539.51	300.1	< 0.0001	significant
A-FS-FR	1.51	1	1.51	0.8372	0.3906	
B-DS-FR	195.23	1	195.23	108.6	< 0.0001	
C-DS-C	2421.04	1	2421.04	1346.71	< 0.0001	
AB	153.64	1	153.64	85.46	< 0.0001	
AC	680.69	1	680.69	378.63	< 0.0001	
B^2	95.99	1	95.99	53.39	0.0002	
C^2	248.91	1	248.91	138.45	< 0.0001	
Residual	12.58	7	1.8			
Lack of Fit	10.7	5	2.14	2.28	0.3329	not significant
Pure Error	1.88	2	0.9408			
Cor Total	3789.15	14				
R^2 (0.9967)	Adjusted R^2 (0.9934)	Predicted R^2 (0.9759)	Adeq Precision (62.1769)	Std. Dev. (1.34)	Mean (34.09)	

Table 4-4: ANOVA of reduced quadratic model for SO_4^{2-} rejection

Source	Sum of Squares	df	Mean Square	F-value	p-value	
Model	211.6	6	35.27	17.91	0.0003	significant
A-FS-FR	65.72	1	65.72	33.38	0.0004	
B-DS-FR	27.49	1	27.49	13.96	0.0057	
C-DS-C	23.32	1	23.32	11.85	0.0088	
AB	56.4	1	56.4	28.65	0.0007	
AC	8.79	1	8.79	4.47	0.0675	
A^2	29.87	1	29.87	15.17	0.0046	
Residual	15.75	8	1.97			
Lack of Fit	10.99	6	1.83	0.7708	0.6598	not significant
Pure Error	4.75	2	2.38			
Cor Total	227.35	14				
R^2 (0.9307)	Adjusted R^2 (0.8788)	Predicted R^2 (0.8047)	Adeq Precision (15.5084)	Std. Dev. (1.40)	Mean (96.97)	

Table 4-5: ANOVA of reduced quadratic model for CO_3^{2-} Rejection

Source	Sum of Squares	df	Mean Square	F-value	p-value	
Model	106.91	8	13.36	92.36	< 0.0001	significant
A-FS-FR	3.04	1	3.04	21	0.0038	
B-DS-FR	12.43	1	12.43	85.88	< 0.0001	
C-DS-C	28.35	1	28.35	195.94	< 0.0001	
AB	4.31	1	4.31	29.76	0.0016	
AC	0.6561	1	0.6561	4.53	0.0773	
BC	41.47	1	41.47	286.64	< 0.0001	
A^2	9.83	1	9.83	67.92	0.0002	
C^2	8.02	1	8.02	55.4	0.0003	
Residual	0.8681	6	0.1447			
Lack of Fit	0.8195	4	0.2049	8.43	0.1088	not significant
Pure Error	0.0486	2	0.0243			
Cor Total	107.78	14				
R^2 (0.9919)	Adjusted R^2 (0.9812)	Predicted R^2 (0.9329)	Adeq Precision (34.6355)	Std. Dev. (0.3804)	Mean (93.30)	

From Table 4-2 – Table 4-5, it can be seen that the R^2 values of 0.9901, 0.9967, 0.9307 and 0.9919, for permeation flux, Cl^- enrichment, SO_4^{2-} rejection efficiency and CO_3^{2-} rejection efficiency, respectively, are significantly close to 1. These values measure the degree of linear association between the independent and the response variable. As shown in Figure 4-2, the obtained data fits a straight line. This indicates the validity of the generated quadratic models (Tetteh *et al.* 2020). Other diagnostic analytics data, namely normal plot vs. residual and residual vs. predicted are presented in appendix B.

Again, in each case, it can be seen that the adjusted R^2 (0.9802, 0.9934, 0.8788 and 0.9812) and the Predicted R^2 (0.9639, 0.9759, 0.8047 and 0.9329) are in reasonable agreement with each other, that is, having a difference less than 0.2. Furthermore, the adequate precision value for all models is higher than 4. This value measures the signal to noise ratio. Values greater than 4 indicate an adequate model, which can be safely used to navigate the entire design space (Houshmand, Daud and Shafeeyan 2011).

The lack-of-fit (LOF) in all cases were not significant. This is good for the validity of the models as the significance of LOF indicates the inability of the model to sufficiently describe the functional agreements between the experimental factors and the response variables. All other model accuracy indicators like the fisher variation ratio (F-values) and probability (P-values) were all within the limits that indicate the significance of a model (Xiarchos, Jaworska and Zakrzewska-Trznadel 2008).

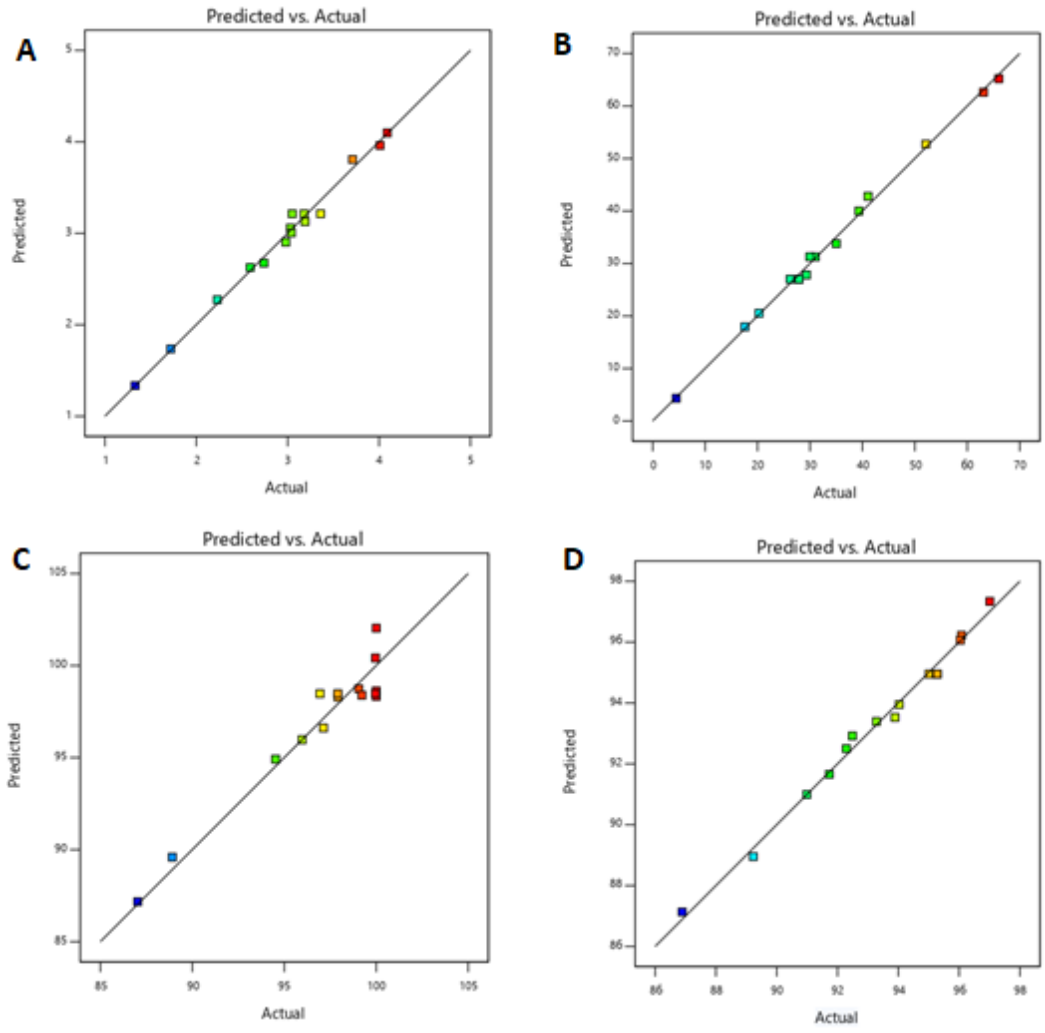

Figure 4-2: Predicted vs actual values for A: permeation flux, B: Cl^- enrichment, C: SO_4^{2-} rejection and D: CO_3^{2-} rejection

4.4 Evaluation of the effects of process variables on FO performance using RSM

The basis of performance of the membrane processes were determined by the permeation flux produced and their ability to reject the target salts. The effects of the chosen process variables – FS-FR, DS-FR and DS-C on the performance of FO were given a critical assessment under this section. To ascertain the individual effects of the various process variables, each process variable was varied while keeping the other two constants at their midpoint values.

4.4.1 Effects of process variables on permeation flux

Figure 4-3 shows the effects of the various process variables on permeation flux. From the figure (Figure 4-3A), the variation of FS-FR with permeation flux is shown. The linear relationship shows a decrease in permeation flux when FS-FR increases. This may be due to the following reason; as FO is a dilution process, there is the need for enough contact between the FS and the DS to enhance the movement of water molecules from the FS to the DS. As FS-FR decreases, the dilution factor becomes high, leading to a high rate of transport of water molecules through the membrane into the DS. Consequently, the net driving force from the DS becomes reduced leading to low fluxes. Similar observations were made by Ezugbe *et al.* (2020) and Seker *et al.* (2017).

From Figure 4-3B, the relationship between permeation flux and DS-C is shown. The linear relationship shows an increase in permeation flux as DS-FR increases. This may be due to the influence of ECP on the DS side of the membrane. Creation of turbulence at the DS-membrane boundary layer at increased DS-FR may have reduced the influence of ECP, thereby allowing more permeate transport (Al-Zuhairi *et al.* 2015).

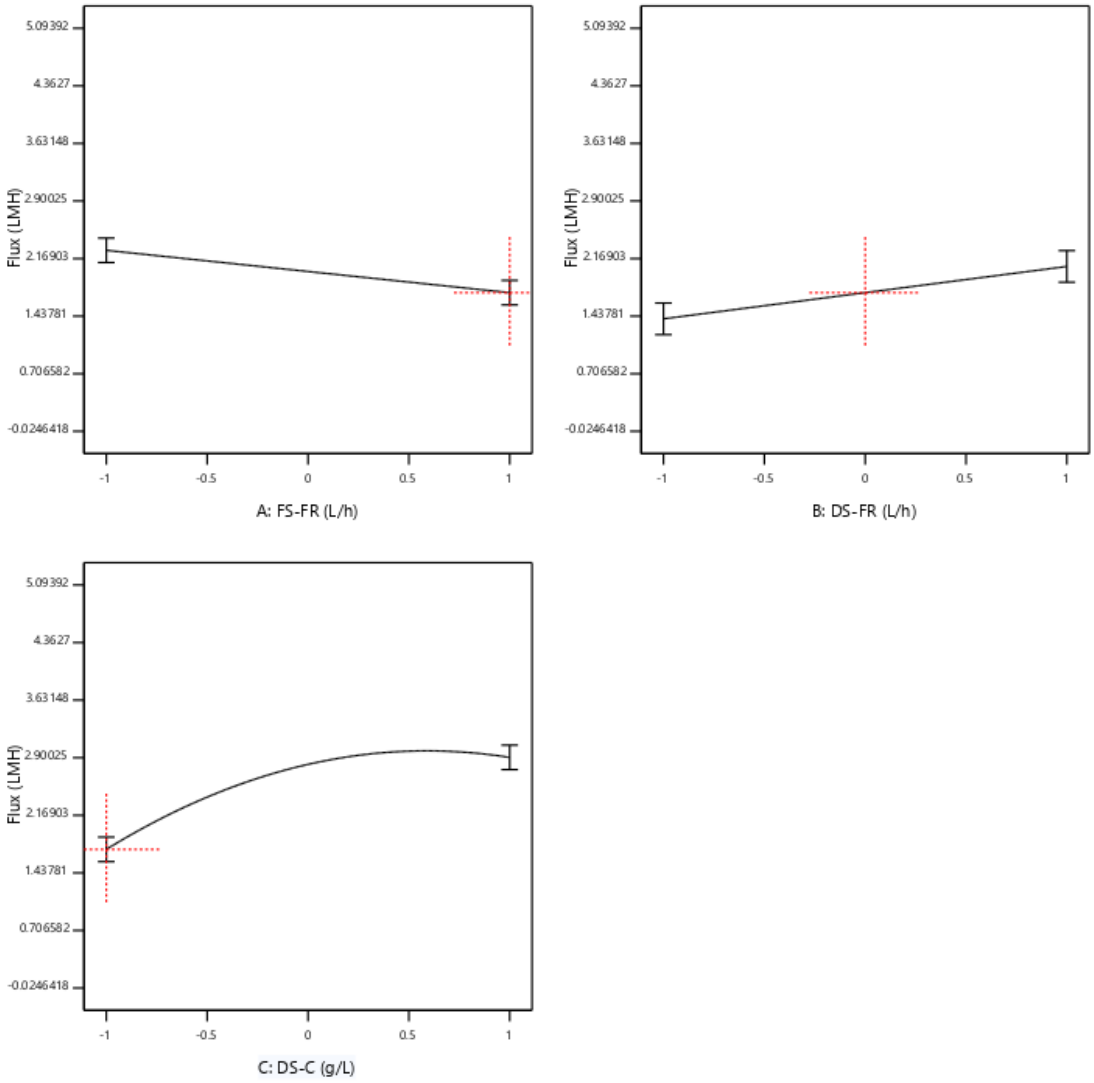

Figure 4-3: Effects of process variables on permeate flux; A: FS-FR; B: DS-FR; C: DS-C

Figure 4-3C shows the effects of DS-C on permeation flux. The relationship is nonlinear, tapering towards a plateau. Increasing DS-C leads to an increase in permeation flux. The DS-C provides the driving force for water transport through the membrane. However, continual increase in DS-C also leads to increased reverse solute flux, which tends to balance the osmotic gradient between the FS and the DS. As the system approaches equilibrium, water transport becomes constant (McCutcheon and Elimelech 2007).

4.4.1.1 Effects of process variables on Cl^- enrichment of FS

The feed solution was enriched with Cl^-. This implies that the Cl^- concentration in the feed increased after the FO process. Cl^- enrichment, described as reverse solute diffusion, results from the backward movement of the Cl^- due to the difference in concentrations of Cl^-

between the FS and the DS. Figure 4-4 shows the effects of the process variables on Cl^- enrichment of the FS.

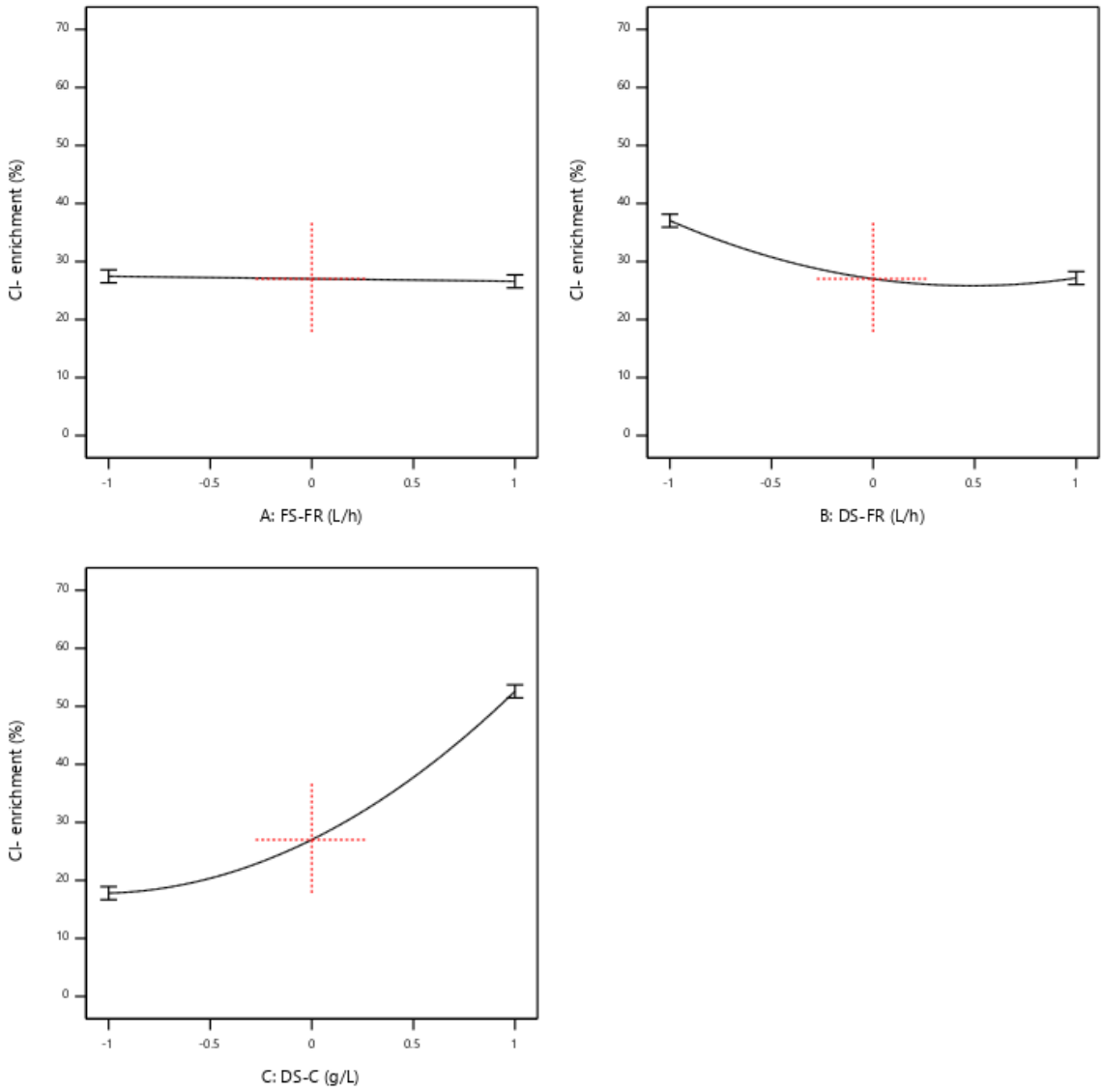

Figure 4-4: Effects of process variables on Cl^- enrichment of FS; A: FS-FR; B: DS-FR; C: DS-C

From Figure 4-4A, the influence of FS-FR is presented. Varying the FS-FR has little influence on Cl^- enrichment of the FS. In Figure 4-4B, the effect of DS-FR is presented. As DS-FR increases, Cl^- enrichment of the FS decreases, but rather weakly. This could be due to the association of high flow rates with the creation of turbulence at the membrane - solution boundary layer. This turbulence sweeps away the accumulated solutes that have the tendency of diffusing through the membrane. Hence, as DS-FR increases, the Cl^- enrichment of the FS reduces (Klyuchnikov *et al.* 2020).

The DS-C by far, showed the most influence on the Cl^- enrichment of the FS. This is shown in Figure 4-4C. The DS-C, being higher in Cl^- concentration than the FS, provides a concentration gradient along which Cl^- move into the FS. The higher the Cl^- concentration of the DS, the more the backwards diffusion of the Cl^- into the FS is. This accounts for the trend shown on Figure 4-4C (Zhang *et al.* 2017).

4.4.2 Effects of process variables on SO_4^{2-} and CO_3^{2-} rejection

Figure 4-5 and Figure 4-6 show the effects of the process variables on SO_4^{2-} and CO_3^{2-} rejection efficiency, respectively. Increase in FS-FR shows an overall decline in SO_4^{2-} and CO_3^{2-} rejection (Figure 4-5A and Figure 4-6A) with SO_4^{2-} rejection showing a steeper decline. In terms of DS-FR, SO_4^{2-} and CO_3^{2-} rejection show opposite trends. As DS-FR increases, SO_4^{2-} rejection decreases while CO_3^{2-} rejection increases (Figure 4-5B and Figure 4-6B). With DS-C, both SO_4^{2-} and CO_3^{2-} rejection show an increasing trend with increase in DS-C (Figure 4-5C and Figure 4-6C), however the relation for SO_4^{2-} rejection is linear while that of CO_3^{2-} rejection increases and tapers to a plateau.

To explain the effects of DS-C on rejection ion (Figure 4-5C and Figure 4-6C), the bidirectional transport of ions through the membrane pores must be considered. Ions move through the same pores as does permeate water. At increased DS-C, more water is drawn through the membrane pores while limiting the movement of the SO_4^{2-} and CO_3^{2-} through the membrane pores. In addition, at increased DS-C, the reverse diffusion of draw solutes becomes more pronounced. This implies that the membrane pores at any point in time will not be easily permeable to the SO_4^{2-} and CO_3^{2-} which happen to be large in size due to their divalent nature.

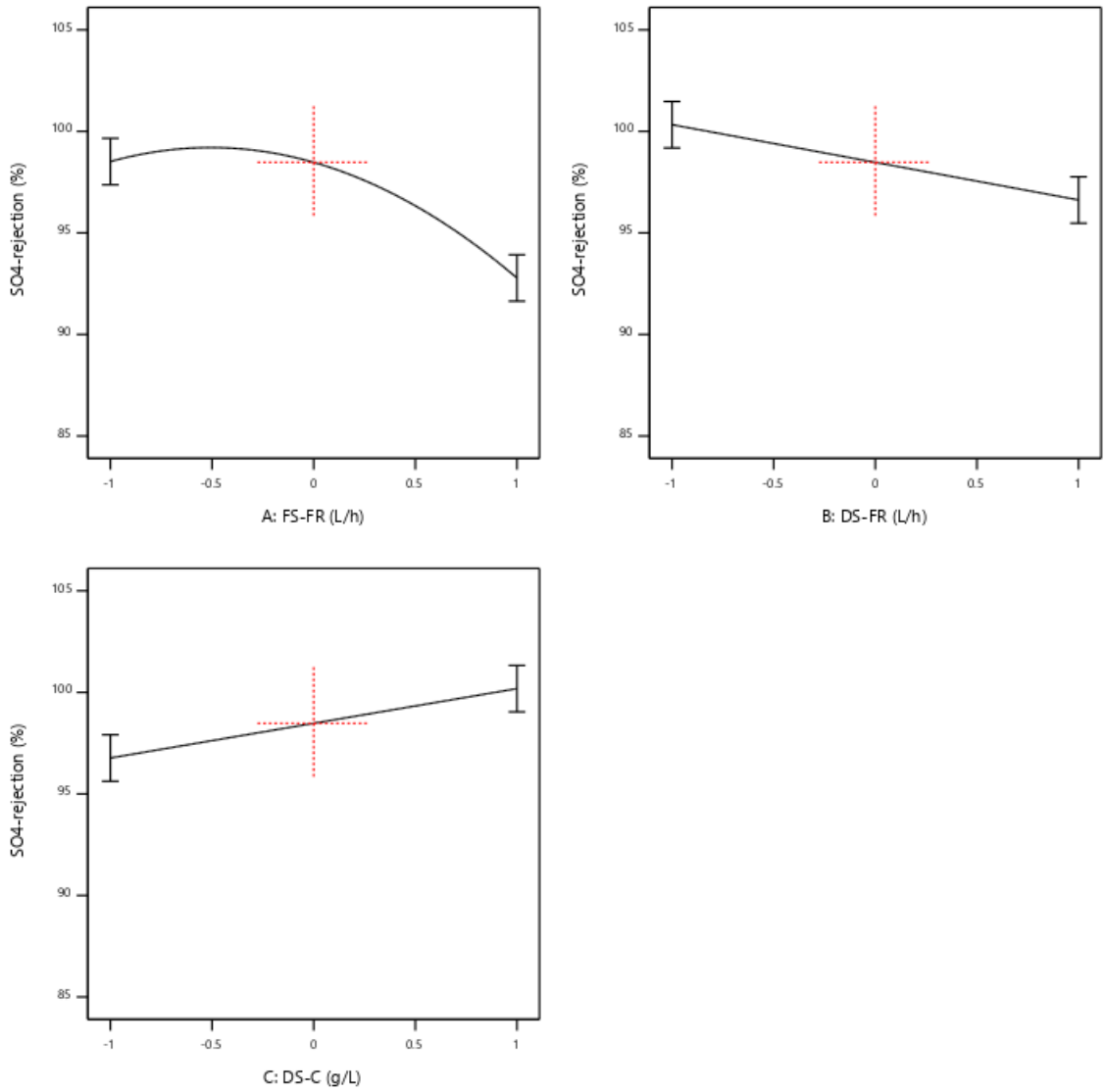

Figure 4-5: Effects of process variables on SO_4^{2-} rejection efficiency; A: FS-FR; B: DS-FR; C: DS-C

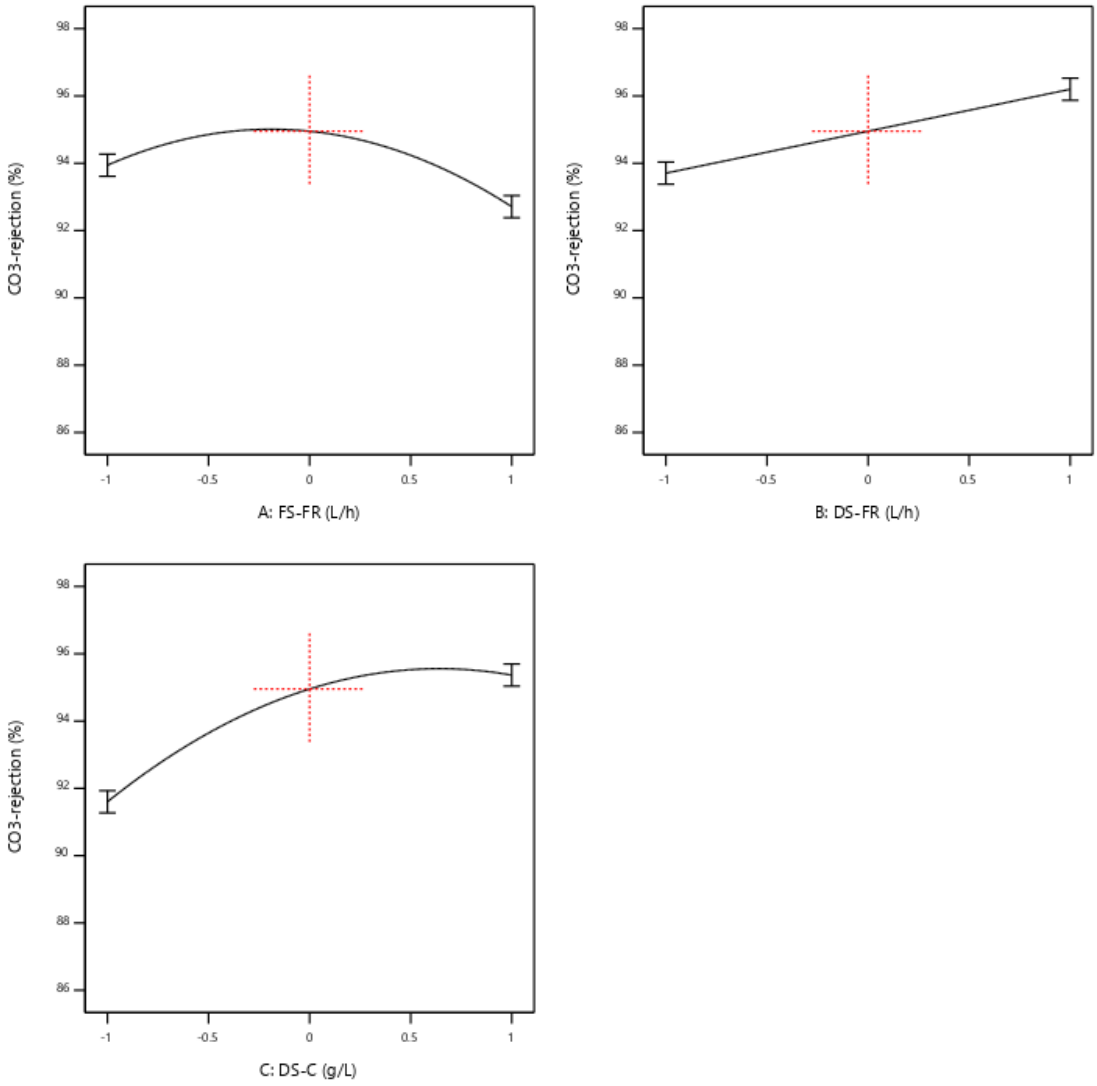

Figure 4-6: Effects of process variables on CO_3^{2-} rejection efficiency A: FS-FR; B: DS-FR; C: DS-C

4.5 FO 3D surface graphs.

The cross-factor interactions presented in Figure 4-7and Figure 4-8 represent the response surface plots for the interactions between the two most significant factors that affected the various responses according to the generated models. The response surface plots are graphical or visual illustrations of how two independent variables related to a response. These two independent variables are plotted on the x and y axes while the response, is plotted on the z-axis.

In Figure 4-7A, the FS-FR and DS-C interaction showed a permeation flux of between 3.5 LMH and 3.9 LMH for FS-FR of between 7.5 L/h and 8.4 L/h (0 to -1 in coded form) and DS-C of 27.5 to 50 g/L (-0.5 to 1 in coded form). As FS-FR further increases (8.4 L/h – 9.4

L/h), DS-C decreases, leading to a corresponding decrease in permeation flux (3.5 – 1.5 L/m^2h). This could be due to the combined effects of the reduction in osmotic pressure gradient and the creation of turbulence by high flow rates at the solution-membrane boundary layer.

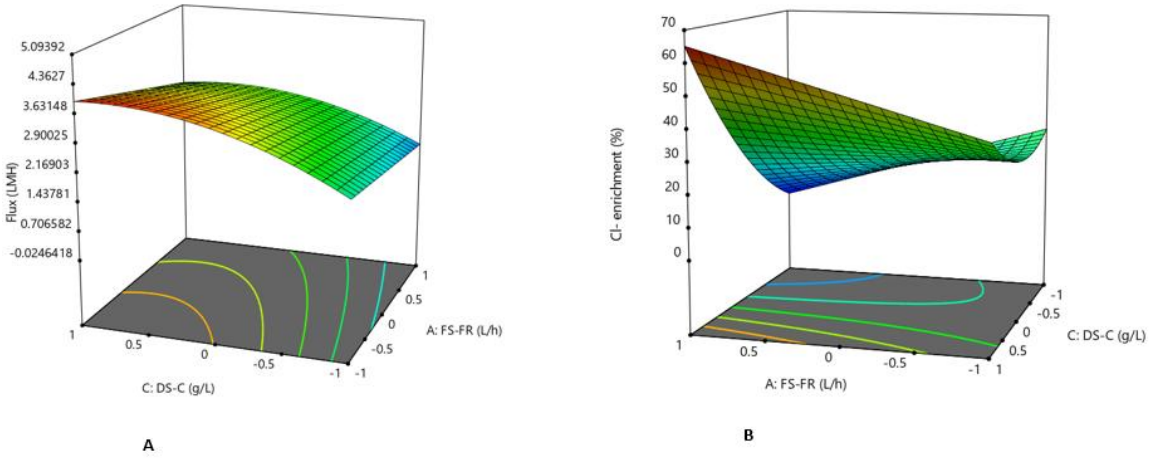

Figure 4-7: Response surface plots showing cross factor interactions of DS-C and FS-FR for A: permeation flux; B: Cl^- rejection.

Figure 4-7B shows the effects of the interaction between FS-FR and DS-C on Cl^- enrichment. The pronouncement of the Cl^- enrichment is seen from a DS-C of 35 – 50 g/L (corresponding to 0 to +1 in coded form) and FS-FR of 8.4 L/h to 9.4 L/h (corresponding to 0 to +1 in coded form). Compared to the FS-FR, a significant reduction in Cl^- enrichment is observed for lower values of DS-C (20 L/h to 27.5 L/h), corresponding to -0.5 to -1 in the codded form. This could be due to the reduction in chemical potential gradient of the Cl^- between the FS and the DS (Nagy 2019a).

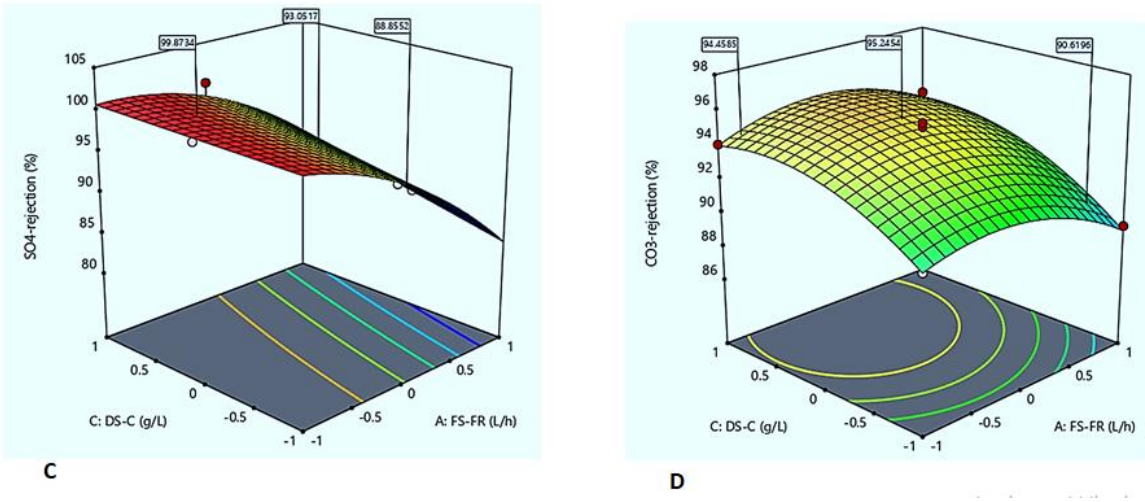

Figure 4-8: Response surface plots showing cross factor interactions of DS-C and FS-FR for C: SO_4^{2-} rejection and D: CO_3^{2-} rejection.

From Figure 4-8C, it can be inferred that the effects of DS-C on SO_4^{2-} rejection efficiency is constant. From the lowest value (coded -1) to the highest value (coded 1), the SO_4^{2-} rejection efficiency is unchanged. This corresponds with the perfect SO_4^{2-} rejection efficiency of 100%. Increasing FS-FR showed a decline in SO_4^{2-} rejection efficiency. This implies that a perfect rejection efficiency of SO_4^{2-} is possible even at low FS-FR and DS-C. In Figure 4-8D maximum CO_3^{2-} rejection efficiency is seen towards the midpoint values of both DS-C and FS-FR. At higher values of the FS-FR, the CO_3^{2-} rejection efficiency gradually declines. In the case of DS-C, higher values show fairly constant rejection efficiency the CO_3^{2-}.

4.6 Optimization of FO process variables

One of the aims of this study was to optimize the operating conditions of the process in order to improve its overall performance and maximize rejection. The numerical optimization approach was employed to optimize the three operating conditions. This technique explores the entire design space on the basis of the designed models to detect the optimum conditions for each factor within the given range. The model equations 4.1 – 4.4 serve as the objective functions with the three independent variables (response variables) serving as the constraints. Table 4-6 gives details of the conditions of optimization. All input variables were within range. Permeation flux, SO_4^{2-} rejection and CO_3^{2-} rejection were maximized whereas Cl^- enrichment was minimized.

Table 4-6: Conditions for optimization of FO process variables

Variable	Lower limit	Higher limit	Goal
FS-FR (L/h)	7.5	9.4	Within range
DS-FR (L/h)	7.5	9.4	Within range
DS-C (g/L)	20	50	Within range
Permeation flux (L/m^{2}h)	1.34	4.10	maximize
Cl^- enrichment (%)	4.48	66.01	minimize
SO_4^{2-} rejection (%)	87.03	100	maximize
CO_3^{2-} rejection (%)	86.89	97.01	maximize

The results of the optimization study are shown in Figure 4-9. The ramp graphs show the optimum operating conditions and the desirability obtained. For a desirability of 81% and FS-FR of 9.2 L/h, DS-FR of 9.4 L/h and DS-C of 32.6 g/L (all corresponding to the coded values in the ramp plot), a permeation flux of 3.9 L/m^{2}h, SO_4^{2-} rejection of 100%, CO_3^{2-} rejection of 97% and Cl^- enrichment of 31% would be achieved. These results were further validated with three confirmatory runs.

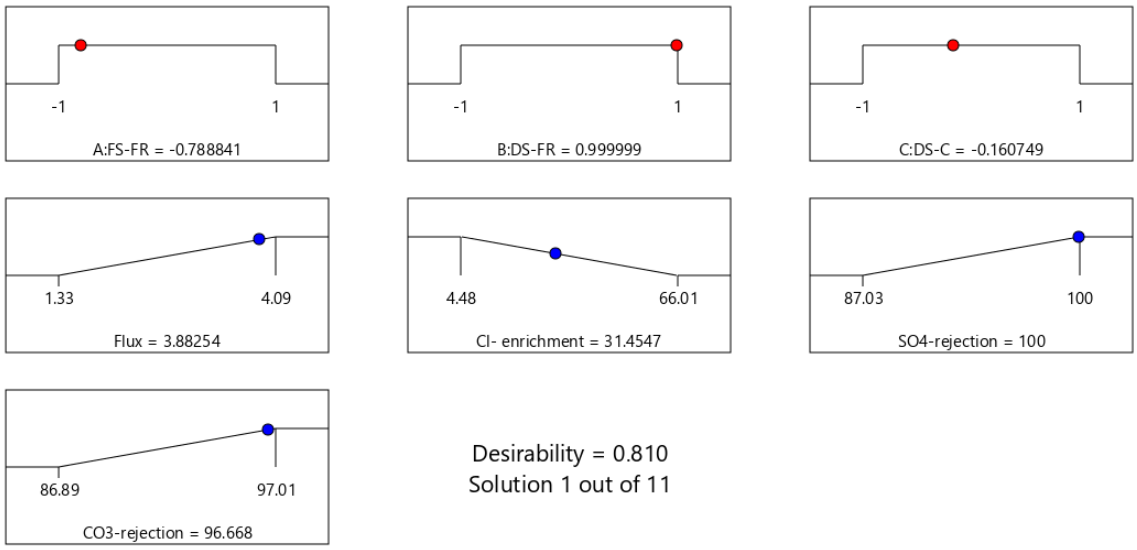

Figure 4-9: Ramp plot showing the optimized conditions of FO process variables at a desirability of 81.0%

4.7 Confirmatory FO runs

Figure 4-10 shows the results of the confirmatory runs. These runs served to further validate the accuracy of the predicted models. On average, apart from the Cl^- enrichment which shows a wide variation (35.5 ± 5.15%), all other responses (flux: 3.64 ± 0.13 l/m^2h; SO_4^{2-} rejection: 100%; CO_3^{2-} rejection: 94.59 ± 0.32%) were in close agreement with the predicted values.

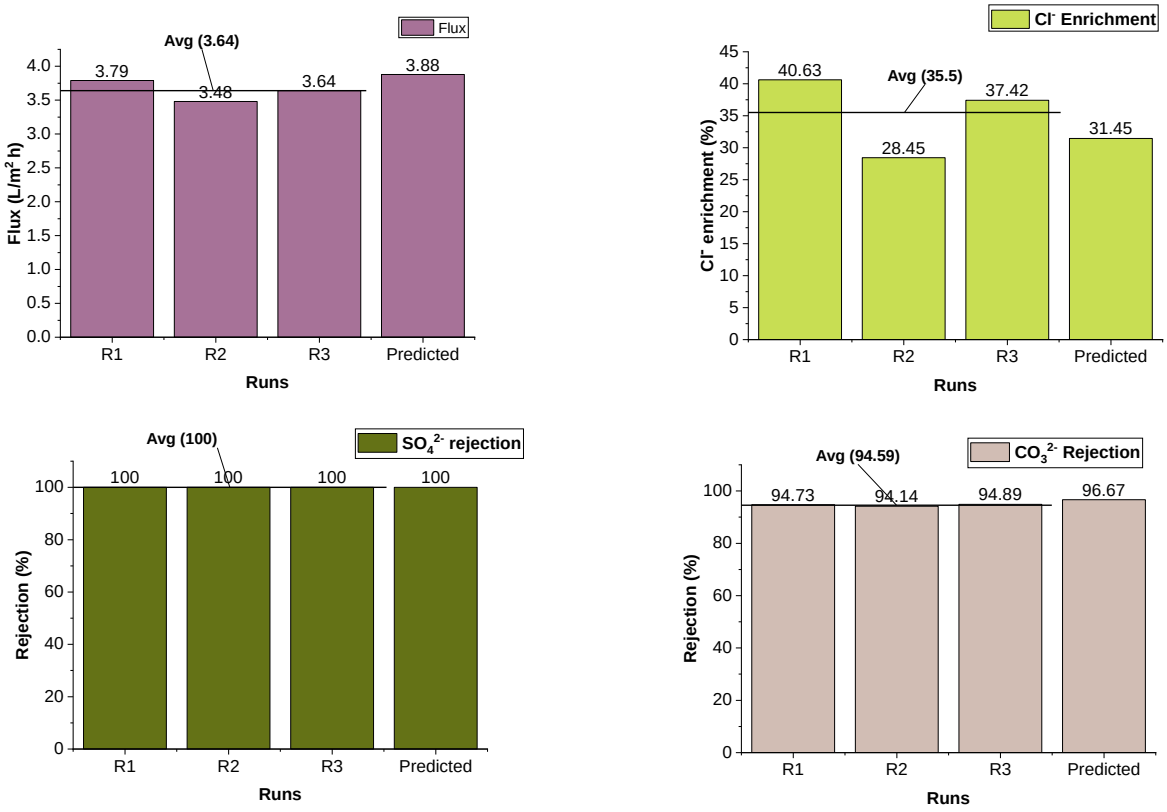

Figure 4-10: Values obtained for confirmatory runs; (A): Permeation flux; (B): Cl^- enrichment; (C): SO_4^{2-} rejection; (D): CO_3^{2-} rejection.

Table 4-7 shows the water chemistry before and after treatment (confirmatory runs) of the raw effluent. The average values of the studied parameters are presented. Apart from Cl^-, the rejection efficiency of the FO process was good. Size exclusion and electrostatic effects play a major role in a membrane's ability to reject ions. This may have accounted for the good rejection of the SO_4^{2-} and CO_3^{2-}, which are divalent ions with negative charges. Above the isoelectric point of the FO membrane (which is at pH of 4), the membrane becomes slightly negatively charged, inducing some resistance to the permeation of SO_4^{2-} and CO_3^{2-} (Xie *et al.* 2012; Alturki *et al.* 2013).

Table 4-7: Water chemistry before and after application of FO

Parameter	Value (avg)	
	raw	treated
pH	9.52 ± 0.37	8.4 ± 0.51
Conductivity (mS/cm)	13.02 ± 0.47	1.31 ± 0.41
Cl^- concentration (mg/L)	719.62 ± 4.38	Limited*
SO_4^{2-} concentration (mg/L)	870 ± 15.52	0
CO_3^{2-} concentration (mg/L)	213 ± 5.6	11.15 ± 0.66

*further explanations given below

There was a total rejection of SO_4^{2-}. This could be due to its large hydration radius (0.379 nm) and low diffusion coefficient of 0.32 x 10^{-5} cm^2/s (Linde and Jönsson 1995; Mondal, Tran and Van der Bruggen 2016), which may have played a part in its rejection.

The rejection of Cl^- is highly limited due to its reverse diffusion from the DS into the FS. It must however, be noted that the CTA membrane has a proven Cl^- rejection efficiency of 90 – 95% (Applied Membrane Inc 2007; Nguyen *et al.* 2013). The reverse salt fluxes for all FO runs are shown in appendix A. A reduction in conductivity buttresses the reduction in the free ions within the system that define electrical conductivity. Water pH within a range of 6.5 – 8.5 is highly desirable. For pH values below or above this range, water becomes corrosive (AECOM 2010).

4.8 FO membrane cleaning efficiency - flux recoverability.

Pure water flux (PWF) of the membrane after cleaning was compared to the PWF of the virgin membrane. Figure 4-11 shows the extent of flux recoverability of the FO membrane. On average, permeation flux recovered was 86.01 ± 2.66%. This shows a fairly good result of membrane cleaning. In FO, since external hydraulic pressure is not applied, membrane cleaning easily recovers the lost flux due to fouling. Other studies have shown a slightly higher value for FO flux recovery (Yu, Lee and Maeng 2016). However, these membranes were used for shorter hours compared to the cumulative hours of 30, as it was the case in this study.

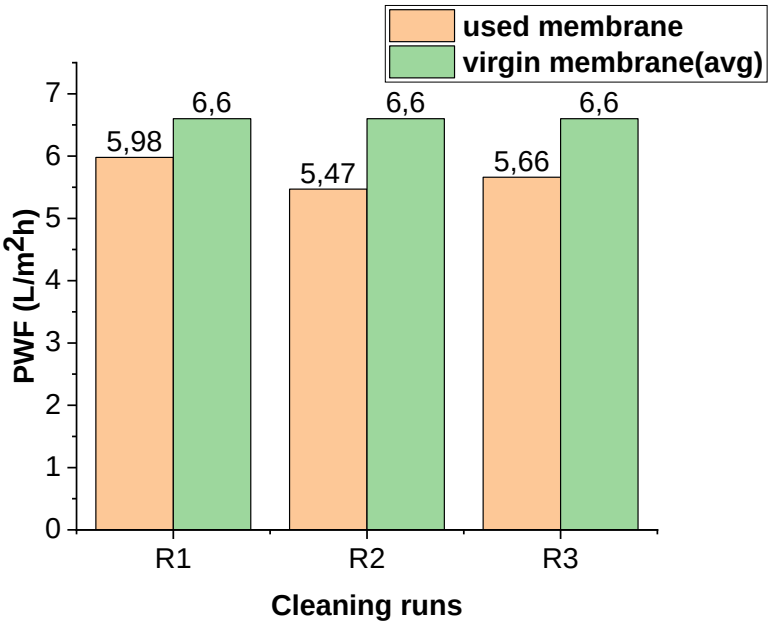

Figure 4-11: FO membrane flux recovery after membrane cleaning

4.9 RO BBD design matrix – actual and predicted values

The BBD design matrix for RO is shown in Table 4-8. This includes the actual values after experimental runs and the model-predicted values.

Table 4-8: BBD design matrix for RO, showing the actual and predicted values

	F1	F2	F3	R1		R2		R3		R4	
	A: Time,	B:Press,	C:F-Con,	flux, L/m²h		Cl^- Rejec		SO_4^{2-} Rejec		CO_3^{2-} Rejec	
Run	h	bar	mg/L	Actual	Predicted	Actual	Predicted	Actual	Predicted	Actual	Predicted
1	-1	-1	0	1.13	1.26	75	74.69	86.4	86.55	98.73	98.83
2	0	-1	-1	0.301	0.0231	90.62	90.56	96.22	96.6	99.38	99.33
3	-1	0	-1	1.25	1.23	89.96	92.56	94.02	93.68	98.84	98.79
4	1	0	1	3.89	4.09	69.12	70.89	83.99	84.71	98.33	98.38
5	0	0	0	1.98	1.89	77.9	76.46	86.92	86.9	93.78	93.84
6	0	1	1	3.81	3.76	67.01	68.62	86.55	86.8	98.33	98.38
7	0	0	0	1.69	1.89	78.8	76.46	87.01	86.9	93.82	93.84
8	1	0	-1	0.98	1.16	97.08	97.28	96.53	97.34	98.84	98.88
9	1	1	0	4.01	3.7	85.01	83.86	93.82	93.04	99.08	98.98
10	0	1	-1	1.5	1.68	94.83	95.01	96.23	96.64	98.63	98.68
11	0	0	0	1.76	1.89	75.6	76.46	88.02	86.9	93.91	93.84
12	0	-1	1	2.2	2.1	62.98	64.17	80.95	81.17	98.16	98.11
13	-1	0	1	2.45	2.46	67.83	66.18	80.98	81.05	97.82	97.78
14	1	-1	0	1.61	1.55	91.4	90.58	96.57	95.82	98.87	98.88
15	-1	1	0	2.55	2.43	90.95	90.31	94.86	94.98	98.35	98.34

4.9.1 Model fitting and statistical analysis

Equations 4.5 - 4.8 represent the quadratic equations generated by the software. The statistical relevance of these models was determined as explained in section 4.3.

$$Flux = 1.89 + 0.3887A + 0.8286B + 1.04C + 0.245AB + 0.4275AC + 0.3422A^2$$

Equation 4.5

$$Cl^- rej = 77.33 + 2.61A + 2.41B - 13.01C - 5.58AB - 0.9575AC + 5.17A^2 + 3.09B^2 - 1.50C^2$$

Equation 4.6

$$SO_4^{2-} rej = 86.9 + 1.83A + 1.41B - 6.32C - 2.8AB + 1.4BC + 2.3A^2 + 3.4B^2$$

Equation 4.7

$$CO_3^{2-} rej = 93.84 + 0.1725A - 0.0938B - 0.3813C + 0.23BC + 2.38A^2 + 2.54B^2 + 2.24C^2$$

Equation 4.8

The level of impact of the model terms on the response variable in descending order as flows:

Flux: C > B > A C > A > A^2 > AB

Cl^-: A^2 > B^2 > A > B > AC > AB > C

SO_4^{2-}: B^2 > A^2 > A > C > BC > AB > C

CO_3^{2-}: B^2 > A^2 > C^2 > A > BC > B > C

4.9.2 ANOVA for RO model equations

ANOVA for the generated models are presented in the following tables (4-9 to 4-12).

Table 4-9: ANOVA of the reduced model for permeation flux

Source	Sum of Squares	df	Mean Square	F-value	p-value	
Model	16.43	6	2.74	64.50	< 0.0001	significant
A-Time	1.36	1	1.36	32.06	0.0005	
B-Pressure	5.49	1	5.49	129.37	< 0.0001	
C-Feed Conc	8.26	1	8.26	194.54	< 0.0001	
AB	0.2401	1	0.2401	5.65	0.0447	
AC	0.5776	1	0.5776	13.60	0.0061	
A^2	0.4999	1	0.4999	11.77	0.0089	
Residual	0.3397	8	0.0425			
Lack of Fit	0.2939	6	0.0490	2.14	0.3524	not significant
Pure Error	0.0458	2	0.0229			
Cor Total	16.77	14				
R^2 (0.980)	Adjusted R^2 (0.965)	Predicted R^2 (0.912)	Adeq Precision (28.5539)	Std. Dev. (0.206)	Mean (2.09)	

Table 4-10: ANOVA of the reduced model for Cl^- rejection

Source	Sum of Squares	df	Mean Square	F-value	p-value	
Model	1721.24	7	245.89	284.48	< 0.0001	significant
A-Time	54.44	1	54.44	62.99	< 0.0001	
B-Pressure	46.51	1	46.51	53.81	0.0002	
C-Feed Conc	1353.56	1	1353.56	1565.99	< 0.0001	
AB	124.77	1	124.77	144.35	< 0.0001	
A^2	98.66	1	98.66	114.14	< 0.0001	
B^2	35.35	1	35.35	40.90	0.0004	
C^2	8.29	1	8.29	9.59	0.0174	
Residual	6.05	7	0.8643			
Lack of Fit	5.55	5	1.11	4.48	0.1926	not significant
Pure Error	0.4963	2	0.2481			
Cor Total	1727.29	14				
R^2 (0.997)	Adjusted R^2 (0.993)	Predicted R^2 (0.987)	Adeq Precision (48.766)	Std. Dev. (0.93)	Mean (80.93)	

Table 4-11: ANOVA of the reduced model for SO_4^{2-} rejection

Source	Sum of Squares	df	Mean Square	F-value	p-value	
Model	460.01	7	65.72	109.53	< 0.0001	significant
A-Time	26.83	1	26.83	44.71	0.0003	
B-Pressure	16.02	1	16.02	26.7	0.0013	
C-Feed Conc	319.16	1	319.16	531.94	< 0.0001	
AB	31.42	1	31.42	52.36	0.0002	
BC	7.81	1	7.81	13.02	0.0086	
A^2	19.59	1	19.59	32.65	0.0007	
B^2	43.04	1	43.04	71.73	< 0.0001	
Residual	4.2	7	0.6			
Lack of Fit	3.45	5	0.6908	1.85	0.3867	not significant
Pure Error	0.7461	2	0.373			
Cor Total	464.21	14				
R^2 (0.991)	Adjusted R^2 (0.982)	Predicted R^2 (0.949)	Adeq Precision (28.806)	Std. Dev. (0.775)	Mean (89.94)	

Table 4-12: ANOVA of the reduced model for CO_3^{2-} rejection

Source	Sum of Squares	df	Mean Square	F-value	p-value	
Model	56.62	7	8.09	285.77	< 0.0001	significant
A-Time	0.238	1	0.238	8.41	0.023	
B-Pressure	0.0703	1	0.0703	2.48	0.159	
C-Feed Conc	1.16	1	1.16	41.08	0.0004	
BC	0.2116	1	0.2116	7.48	0.0292	
A^2	20.86	1	20.86	736.81	< 0.0001	
B^2	23.9	1	23.9	844.33	< 0.0001	
C^2	18.6	1	18.6	656.95	< 0.0001	
Residual	0.1981	7	0.0283			
Lack of Fit	0.1893	5	0.0379	8.54	0.1081	not significant
Pure Error	0.0089	2	0.0044			
Cor Total	56.82	14				
R^2 (0.997)	Adjusted R^2 (0.993)	Predicted R^2 (0.984)	Adeq Precision (44.709)	Std. Dev. (0.168)	Mean (97.66)	

From Table 4-9 - Table 4-12 it can be seen that all the model-significance indicators fall within the expected range that point to the accuracy of the models generated. These are R^2 values (0.977, 0.984, 0.99 and 0.997), adjusted R^2 (0.959, 0.973, 0.982 and 0.993), Predicted R^2 (0.891, 0.946, 0.94 and 0.984) and Adequate precision (28.55, 48.77, 28.81 and 44.71).

LOF for all models are not significant and the p-values are significantly low. This indicates the validity and accuracy of the generated models.

The plot of predicted values vs. actual values is shown in Figure 4-12. From the figure, it can be seen that there is a good agreement between the actual values and the model-predicted ones. The Normal plot vs. residual and residual vs. predicted plots, which represent other forms of diagnostic analytics of the generated models are presented in Appendix B.

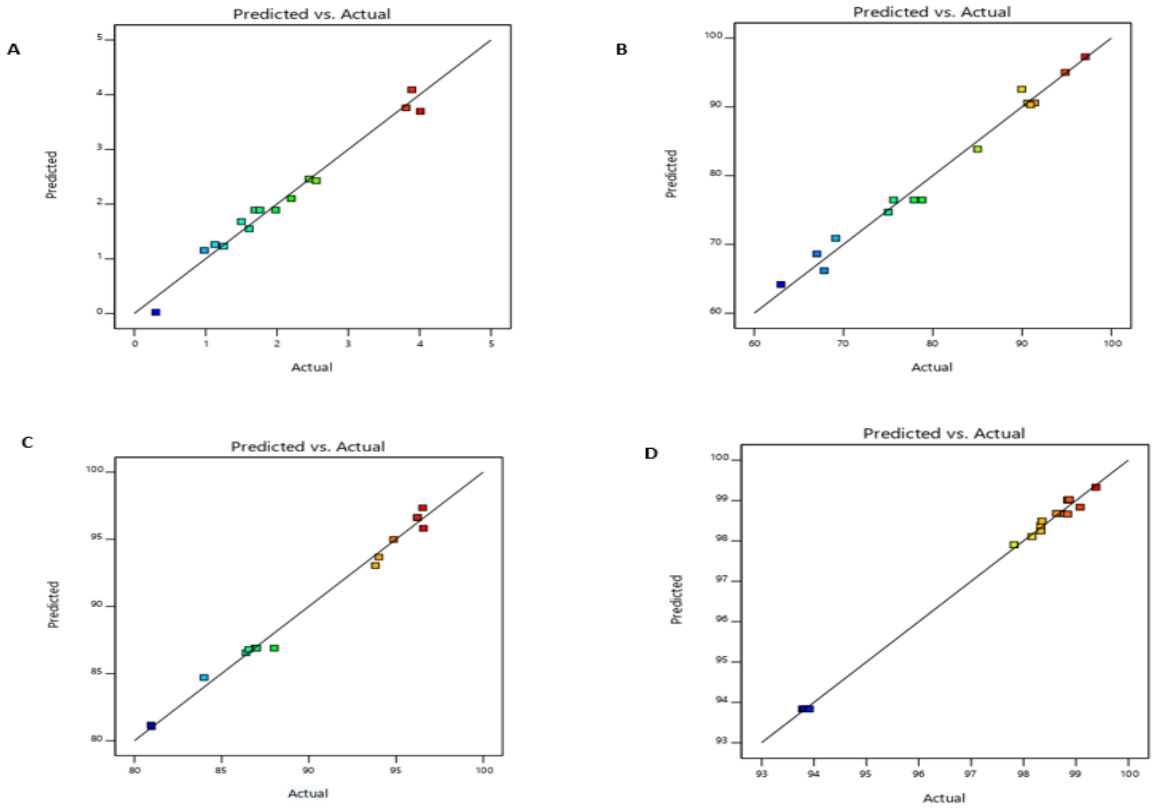

Figure 4-12: Plot of predicted values vs actual values for all responses; A: permeation flux; B: Cl^- rejection efficiency; C: SO_4^{2-} rejection efficiency; D: CO_3^{2-} rejection efficiency

4.10 Evaluation of the effects of process variables on RO performance using RSM

The effects of the studied process variables (Time (h), pressure (bar) and Feed concentration (mg/L)) on the performance of RO are presented here. Their individual effects as well as their interactive effects are given a critical analysis. To ascertain the individual effects of the various process variables, each process variable was varied while keeping the other two constants at their midpoint values.

4.10.1 Effects of process variables on permeation flux

The influence of the process variables on permeation flux are shown in Figure 4-13. Operating time (Figure 4-13A) shows a slight nonlinear variation with permeation flux. The longer the time of operation, the more the permeation flux. The effect of operating time on flux is minimal compared to operating pressure and feed concentration.

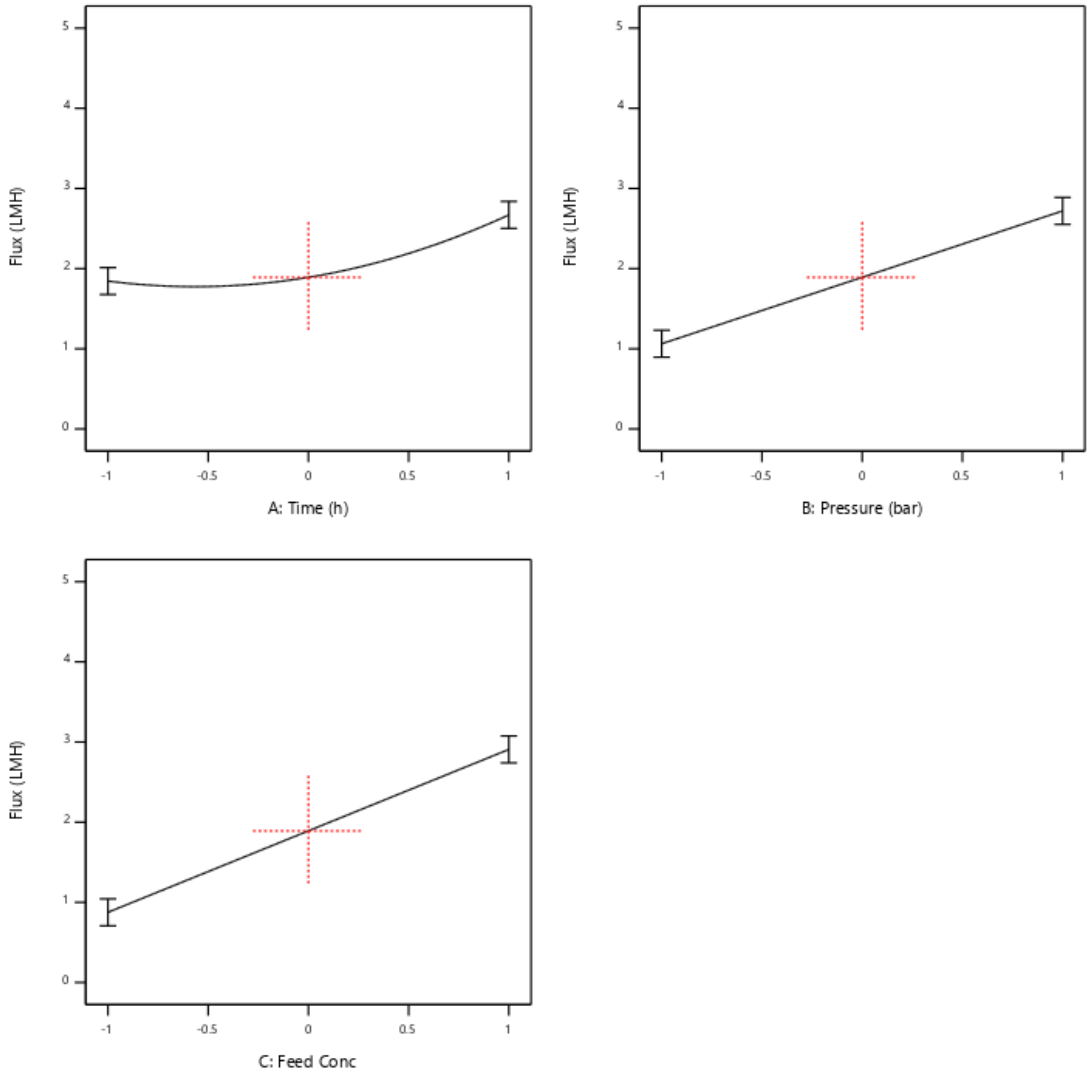

Figure 4-13: Effects of process variables on permeation flux; A: time; B: operating pressure; C: feed concentration

Operating pressure (Figure 4-13B) is the principal driving force of permeation flux in pressure driven membrane processes. This variable has a linear relationship with the response. As the applied pressure increases, there is increase in permeation flux. As the applied pressure increases, the intrinsic osmotic pressure of the feed reduces. This makes more water molecules move across the membrane. For this reason, to achieve high

recoveries in RO, high pressures are required (Mohammed, Abbas and Sabry 2014). In Figure 4-13C, the influence of feed concentration on permeation flux is shown. The trend shows a linear increase in permeation flux as feed concentration increases. Feed concentration affects the net driving pressure of the RO process. At constant operating pressure, increase in feed concentration leads to decrease in permeation flux.

4.10.2 Effects of process variables on Cl^- rejection efficiency

The impact of the process variables on Cl^- rejection efficiency is shown in Figure 4-14. Operating time (Figure 4-14A) and operating pressure (Figure 4-14B) show a nonlinear trend of increasing Cl^- rejection efficiency as they increase. The effect of operating time could be due to the permeation of more water across the membrane as operating time increases. As more water moves across the membrane, less space is made for movement of ions. Consequently, the ion rejection increases. Similarly, as operating pressure increases, osmotic pressure of the feed is reduced and more water is forced through the membrane. As this happens, less pores are made available for movement of the ions, making their rejection high (Al-Mutaz and Al-Ghunaimi 2001; DOW Water 2010).

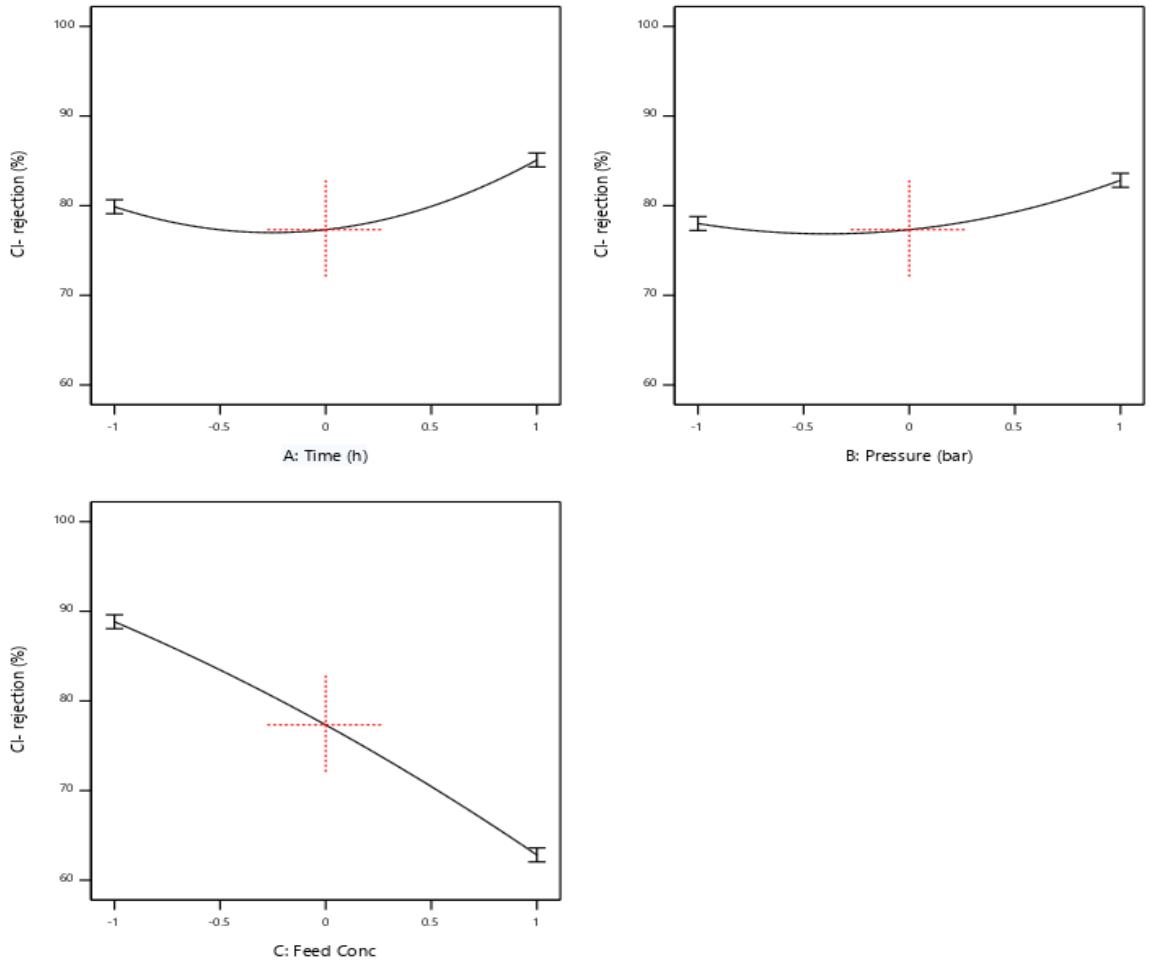

Figure 4-14: Effects of process variables on Cl^- rejection efficiency; A: time; B: operating pressure; C: feed concentration

In Figure 4-14C, the influence of feed concentration on Cl^- rejection is presented. Clearly, high feed concentrations of Cl^- leads to low Cl^- rejection. Rightly so, at high concentrations, more of the salt passes through the membrane to the permeate side under the influence of osmosis. This affects the rejection of the Cl^- or any other ion for that matter (Bartels *et al.* 2005).

4.10.3 Effects of process variables on SO_4^{2-} rejection efficiency

SO_4^{2-} rejection and how it is affected by the process variables is shown in Figure 4-15. This follows the same trend as the Cl^- rejection. Increase in operating time (Figure 4-15A) and pressure (Figure 4-15B) show slight increase in SO_4^{2-} rejection for the same reason as explained for Cl^- rejection efficiency.

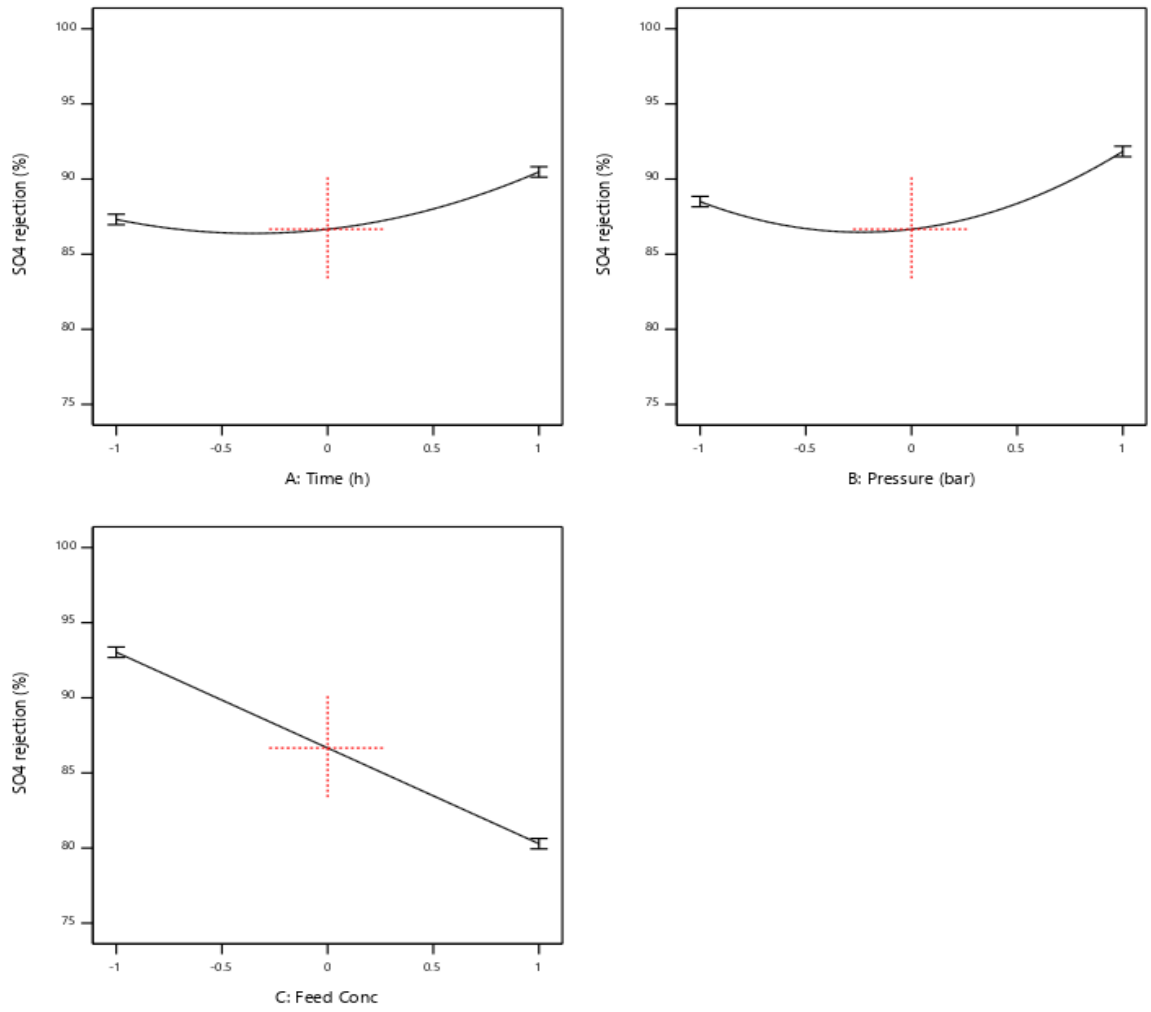

Figure 4-15: Effects of process variables on SO_4^{2-} rejection efficiency; A: time; B: operating pressure; C: feed concentration

In terms of how feed concentration (Figure 4-15C) influences rejection of SO_4^{2-}, an increase in feed concentration linearly reduces the rejection of the SO_4^{2-}. This may be explained as passage of more SO_4^{2-} through the membrane to the permeate side due to the large concentration difference between the feed side and the permeate side. Consequently, rejection efficiency of the SO_4^{2-} reduces (Bartels *et al.* 2005; DOW Water 2010).

4.10.4 Effects of process variables on CO_3^{2-} rejection efficiency

Rejection efficiency of CO_3^{2-} (Figure 4-16) shows almost the same quadratic trend for all process variables. There was a gradual reduction in rejection efficiency as the process variables increased (-1 to 0 in coded form). From the midpoint values of the process variable to the highest value (0 to 1), the rejection efficiency gradually increased.

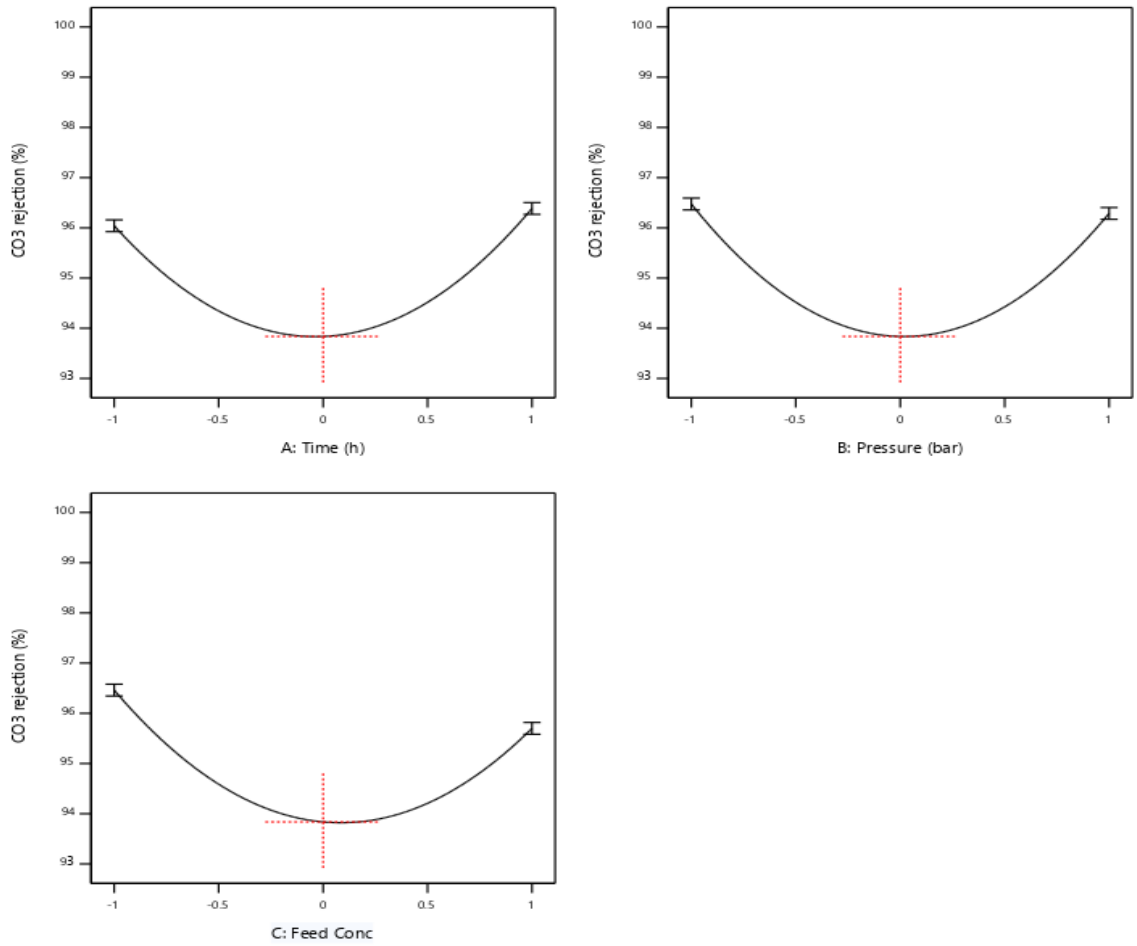

Figure 4-16: Effects of process variables on CO_3^{2-} rejection efficiency; A: time; B: operating pressure; C: feed concentration

4.10.5 RO 3D surface graphs.

The graphical representation of the regression equations is shown in Figure 4-17. The response surface plots give a visual effect of the two input variables, their interactions and the effects of their interactions on the various responses. In all cases, the interactive effects of operating pressure and experimental time on the various responses are presented. From Figure 4-17A, increasing both variables (time and pressure) lead to a corresponding increase in permeation flux. From Figure 4-17B and Figure 4-18A, maximum Cl^- and SO_4^{2-} rejection efficiency is achieved when operating pressure is at its highest within a short operating time. From Figure 4-18B, a quadratic relationship between operating pressure and experimental time on CO_3^{2-} rejection efficiency is presented. Increase in operating pressure and experimental time leads to increase in CO_3^{2-} rejection efficiency until the midpoint where the rejection efficiency reduces to the minimum and then increases again as the operating pressure and experimental time increased.

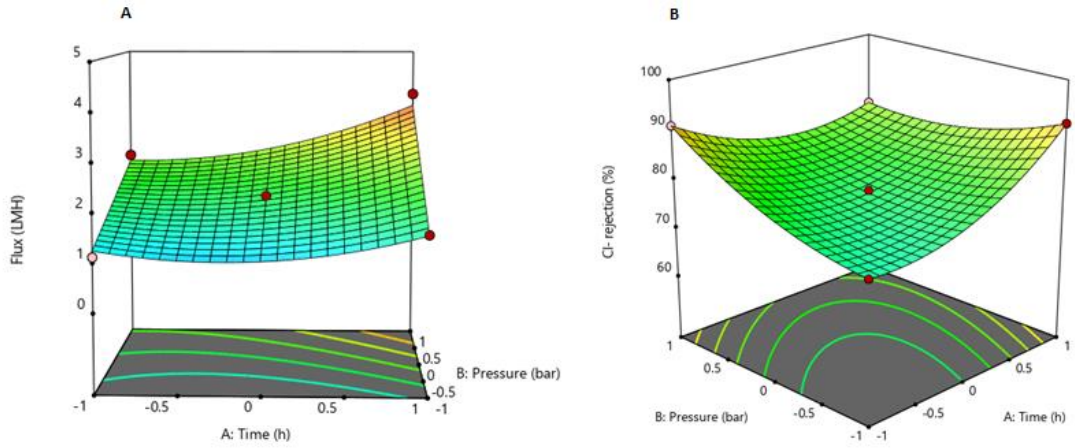

Figure 4-17: Response surface plots showing cross factor interactions of operating pressure and time for; A: permeation flux; B: Cl^- rejection efficiency.

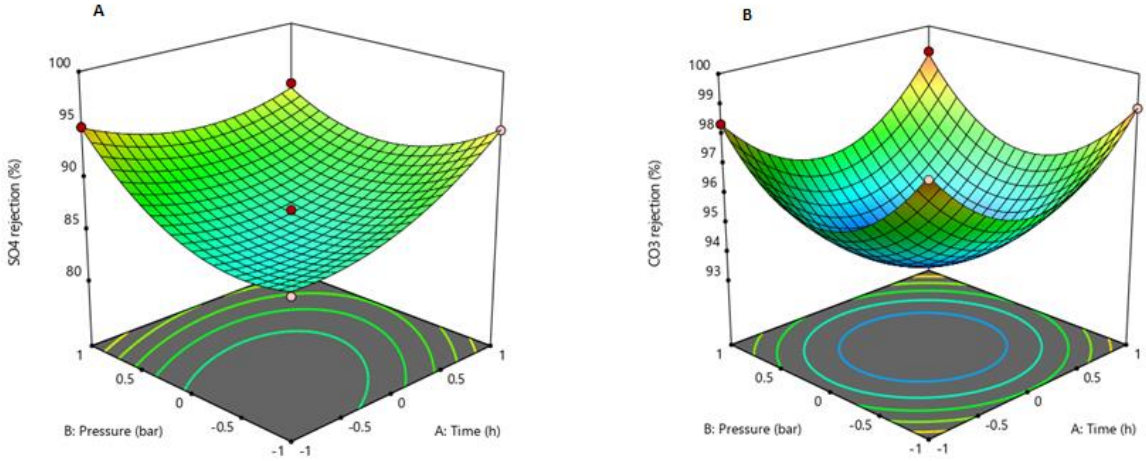

Figure 4-18: Response surface plots showing cross factor interactions of operating pressure and time for: A: SO_4^{2-} rejection efficiency; B: CO_3^{2-} rejection efficiency.

4.10.6 Optimization of RO variables

The numerical optimization tool under RSM was utilized to optimize the three RO operating variables. Table 4-13 gives details of the conditions of optimization. All input variables were within range. The response variables, viz permeation flux, Cl^- rejection, SO_4^{2-} rejection and CO_3^{2-} rejection were maximized.

Table 4-13: Conditions of optimization of RO process variables

Variable	Lower limit	Higher limit	Goal
Time (h)	4	6	Within range
Pressure (bar)	14	18	Within range
Permeation flux (L/m^2 h)	0.30	4.01	maximize
Cl^- rejection (%)	62.98	97.08	maximize
SO_4^{2-} rejection (%)	80.98	98	maximize
CO_3^{2-} rejection (%)	93.78	99.38	maximize

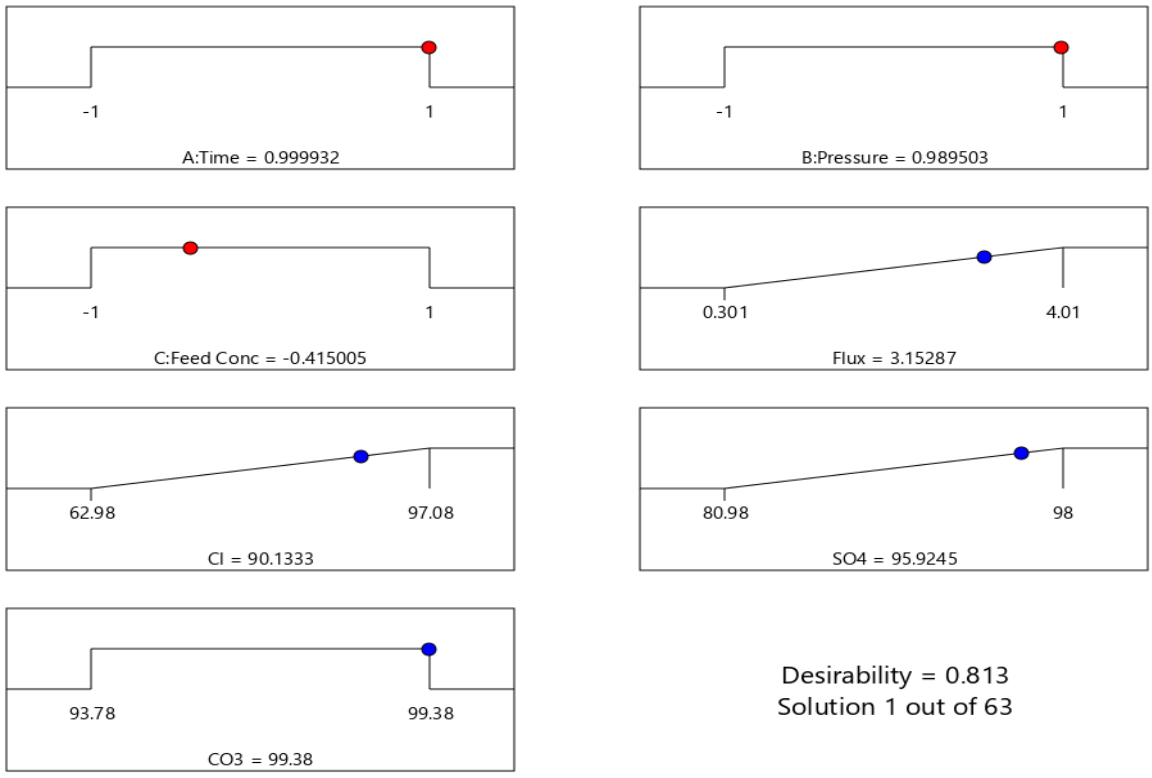

Figure 4-189: Ramp plot showing the optimized conditions of RO process variables at a desirability of 81.3%

The result of the optimization is shown in Figure 4-189. The ramp graphs show the optimum operating conditions and the desirability obtained. For a desirability of 81.3% and operating time of 6 hours, operating pressure of 18 bar and feed concentration of (383.22 mg Cl^-/L, 414.17 mg SO_4^{2-}/L and 134.07 mg CO_3^{2-}/L), (all corresponding to the coded values in the ramp plot), a permeation flux of 3.15 L/m^2h, Cl^- rejection efficiency of 90.1%, SO_4^{2-}

rejection of 96%, CO_3^{2-} rejection of 99% would be achieved. These results were further validated with three confirmatory runs.

4.11 Confirmatory RO runs

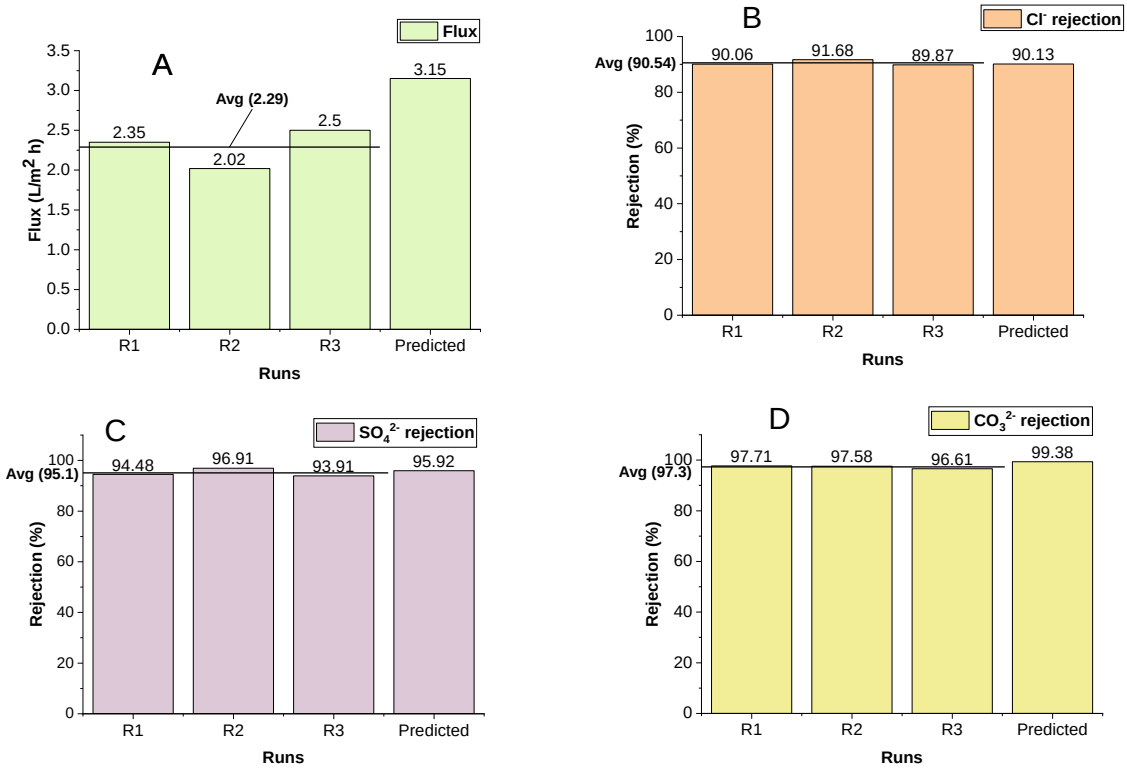

Figure 4-2019: Confirmatory RO runs using raw effluent; A: permeation flux; B: Cl^- rejection efficiency; C: SO_4^{2-} rejection efficiency; D: CO_3^{2-} rejection efficiency

Results of the confirmatory runs are shown in Figure 4-201920. All responses were relatively in good agreement with the predicted values (Cl^- rejection = 90.54 ± 0.81%; SO_4^{2-} rejection = 95.1 ± 1.3%; CO_3^{2-} = 97.3 ± 0.49%). Only the permeation flux showed a slight difference (flux = 2.29 ± 0.2 L/m^2h).

Table 4-14 shows the water chemistry before and after RO confirmatory runs. RO provides an excellent rejection for all types of ions including univalent ions. With the tight and non-porous nature of the membrane, movement of ions across the membrane is highly limited.

Table 4-14: Water chemistry before and after RO treatment

Parameter	Value (avg)	
	raw	treated
pH	9.52 ± 0.37	7 ± 0.05
Conductivity (mS/cm)	13.02 ± 0.47	1.07 ± 0.25
Cl^- concentration (mg/L)	719.62 ± 4.38	67.56 ± 5.80
SO_4^{2-} concentration (mg/L)	870 ± 15.52	40.91 ± 10.73
CO_3^{2-} concentration (mg/L)	213 ± 5.6	5.56 ± 1.0

4.12 RO membrane cleaning efficiency – Flux recoverability

Pure water flux (PWF) of the membrane after cleaning was compared to the PWF of the virgin membrane. Figure 4-201 shows the extent of flux recoverability of the RO membrane.

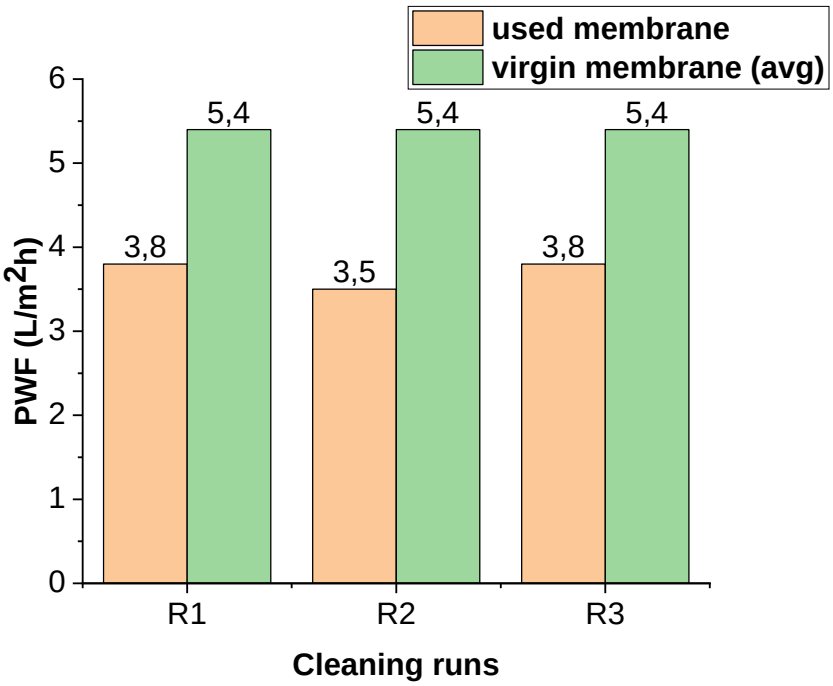

Figure 4-201: RO Flux recovery after membrane cleaning.

Fouling in RO is usually very pronounced due to the application of hydraulic pressure. Physical cleaning alone hardly recovers any flux when conducted. As shown in the figure, an average of 62.52 ± 2.62% of flux was recovered after combined physical and chemical cleaning.

4.13 FO-RO/NF Hybrid process

To study the hybrid process, NF was used as the recovery method. This came as an intervention when the RO process proved more pressure demanding than can be provided by the filtration unit used. During the hybrid process, the DS (32 g/L NaCl) generated higher osmotic pressure (26.63 bar) than the maximum pressure of the filtration unit (18 bar). After dilution of the DS by the water drawn from the FS (1.5 L) during the FO process, the osmotic pressure reduced by 1.05 bar. This was estimated based on the fact that for every 1 L of permeate drawn from the FS during FO, 1.5 g of salt is lost (Bamaga *et al.* 2011). Based on the osmotic pressure model for NaCl by Mogashane *et al.* (2020) and DOW water solutions (2010), the final osmotic pressure of the DS was estimated as follows.

Osmotic pressure of NaCl = 0.843 x Con (g/L) – 0.848

Initial DS osmotic pressure = 0.843 x 32.6 – 0.848 = 26.63 bar

50% water recovery = 1.5 L water recovered from FS into DS. This corresponds to 2.25 g of NaCl lost.

Osmotic pressure of 2.25 g of NaCl lost = 0.843 x 2.25 – 0.848 = 1.05 bar

Final osmotic pressure of DS = 26.63 bar – 1.05 bar = 25.58 bar. This value is higher than the maximum allowable pressure of the existing experimental filtration unit (18 bar).

The NF membrane was used as an alternative since it is more ‘loose’ than the RO membrane. Figure 4-212 shows the results for the permeation flux for the hybrid FO-NF process.

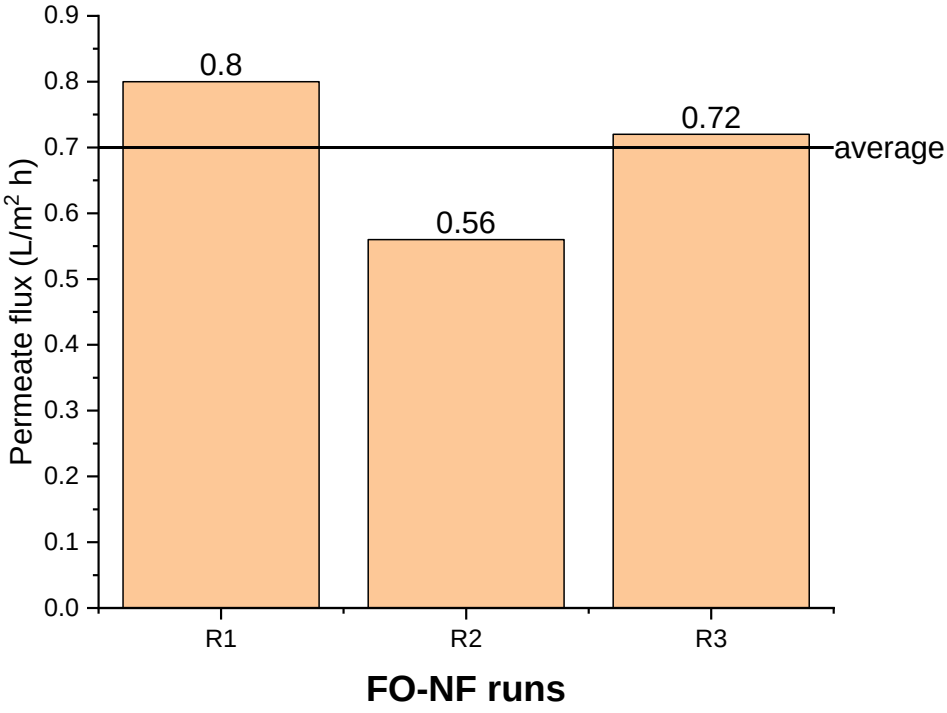

Figure 4-212: Permeation flux of FO-NF hybrid process

The permeation flux of the hybrid FO-NF process was very low as shown in the figure above. The process lacked the needed hydraulic pressure to achieve the needed separation. The permeate water achieved by the process was too low for any analysis to be conducted. It is however worthy to note that previous studies have shown that under the appropriate conditions of pressure and water recovery, FO-RO/NF hybrid processes produce good quality permeate with high rejections of ions (Thompson and Nicoll 2011; Choi *et al.* 2017).

In addition, FO-RO/NF hybrid systems are more advantageous in maintaining high permeation fluxes, utilizing energy and controlling fouling compared to the individual processes. At low hydraulic pressures, fouling in RO/NF membranes will be low. Due to the osmotic dilution that takes place during the FO-RO/NF hybrid process, the resultant pressure required by RO/NF is low and hence leads to low fouling. In the same vein as fouling control, osmotic dilution also has a bearing on energy of desalination. The net energy required for the hybrid process is less compared to RO/NF as a standalone (Choi, Kim and Hong 2016; Choi *et al.* 2016; Choi *et al.* 2017).

4.14 Performance comparison between membrane processes

As afore mentioned, the basis of comparison of the performance of the membrane processes is permeation flux, salt rejection and flux recoverability. The comparison is based on the confirmatory runs, which provides a common ground for the three membrane separation processes. These are presented below.

4.14.1 Permeation flux

Permeation flux is the volume of water that flows through the membrane per m^2 per unit time. Figure 4-223 shows the permeation flux of the three membrane processes. It can be seen that flux for the FO separation process was the highest having an average of 3.64 ± 0.13 L/m^2h. This was followed by RO permeation flux with an average of 2.29 ± 0.2 L/m^2h and then the hybrid FO-NF separation process having an average of 0.69 ± 0.10 L/m^2/h. Even though FO does not depend on hydraulic pressure, with enough osmotic pressure from the DS, good permeation flux was achieved. To achieve higher permeation flux for RO, higher pressures will be required. In the same vein, to increase the permeation flux for FO, larger membrane areas would be required.

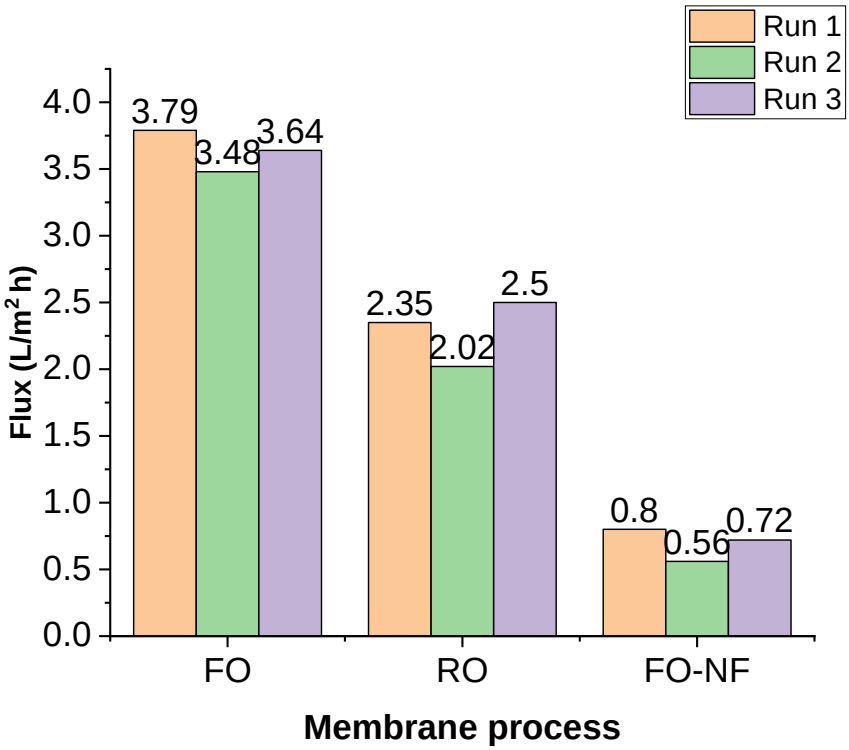

Figure 4-223: Comparison of permeation flux for FO, RO and FO-NF membrane processes

4.14.2 Cl^- rejection and enrichment efficiency of RO and FO

Cl^- rejection efficiency is the ability of the membrane to prevent the Cl^- from passing through the membrane into the permeate side. Figure 4-234A shows the Cl^- rejection efficiency for RO. An average of 90.54 ± 0.81% rejection efficiency was achieved.

With Figure 4-234B, the Cl^- enrichment of the FS is shown. The average Cl^- enrichment value obtained was 35.5 ± 5.15%. This represents the increase in Cl^- concentration in the FS. Consequently, Cl^- rejection is not determined. With the FO mode adopted for the experiment, the porous support layer of the membrane faces the DS. The 32.6 g NaCl/L DS makes available more Cl^- in solution than was in the FS. While FO membranes have the ability to reject Cl^- in solution, the situation of RSD in this study makes the process handicapped in determining the Cl^- rejection efficiency of the FO.

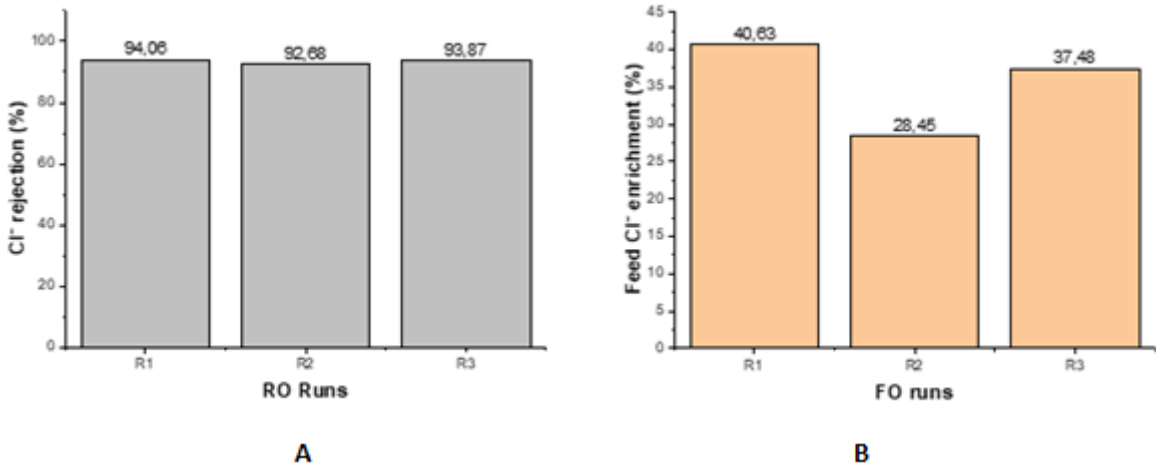

Figure 4-234: A: Cl^- rejection efficiency by RO and B: Cl^- enrichment of the FS by FO

4.14.3 SO_4^{2-} and CO_3^{2-} rejection efficiencies

The SO_4^{2-} and CO_3^{2-} rejection efficiency of FO and RO are shown in Figure 4-245A. For all runs, the SO_4^{2-} rejection efficiency of the FO process was 100%. For the RO process, the SO_4^{2-} rejection efficiency was 95.1 ± 1.3%. The FO showed better rejection of SO_4^{2-} than RO. CO_3^{2-} rejection efficiencies of FO and RO are shown in Figure 4-245B. For all runs, the RO process with average CO_3^{2-} rejection efficiency of 97.3 ± 0.49% out-performed the FO process, having an average CO_3^{2-} rejection efficiency of 94.59 ± 0.32%. The differences in rejection efficiencies of the two membrane processes could be due to their membrane surface chemistries namely charge, contact angle and hydrophobicity.

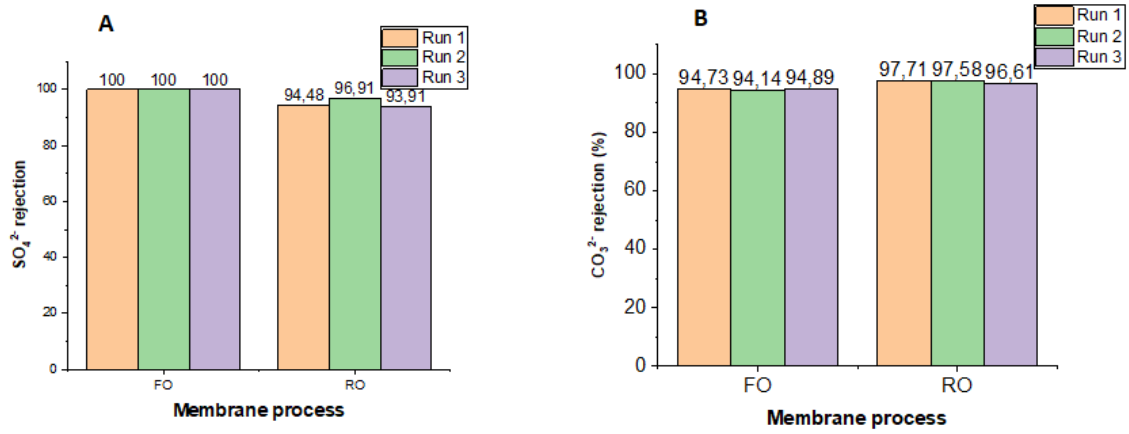

Figure 4-245: Comparison between FO and RO for; A: SO_4^{2-} rejection efficiency; B: CO_3^{2-} rejection efficiency

4.14.4 Permeation flux recoverability

Comparison between permeation flux recovery of FO and RO is presented in Figure 4-256. For all recovery runs, the FO process out-performed the RO process. Unlike in FO, where no external pressure is used, due to the application of hydraulic pressure in RO, fouling reversal is usually a challenge. The applied pressure forces foulants into membrane pores, clogging the pores and building resistance to permeate flow. In FO, foulants merely deposit at the membrane surface or loosely within the pores of the membrane. These are easily removed by physical cleaning (Lee *et al.* 2010).

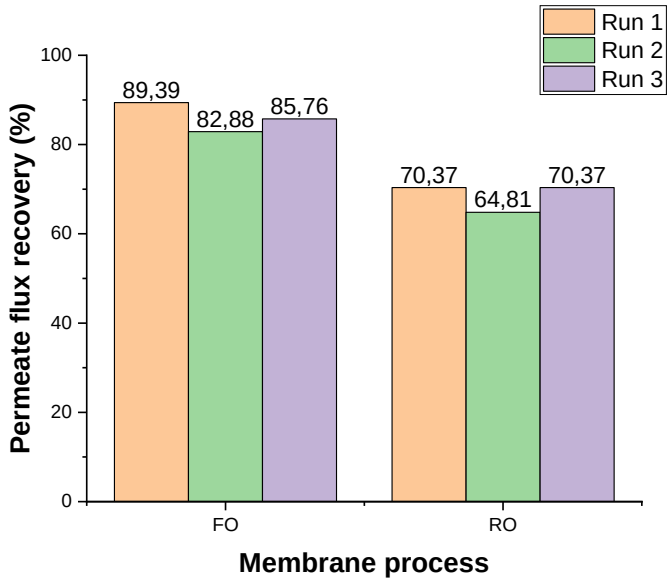

Figure 4-256: Comparison between FO and RO for permeate flux recovery

4.15 Summary

Using the BBD of RSM proved useful in optimizing both FO and RO separation processes. Of all the process variables involved in FO application, the draw solution concentration was critical in the efficiency of the process, affecting the permeation flux and the RSD. The ion rejection efficiency of the FO membrane was > 90% for SO_4^{2-} and CO_3^{2-} while Cl^- enrichment of the FS was found to be as high as 35%, a situation that is highly undesirable. Manual scrubbing of the membrane and osmotic backwash recovered at least 82% of the permeation flux.

For RO, the operating pressure and feed concentration proved fundamental in the efficiency of the separation process. Ion rejection was above 90% for all ions. Both physical and chemical cleaning recovered at least 65% of the permeation flux.

The FO-RO/NF hybrid process was inapplicable due to constraints of the filtration unit. Using NF membrane as an alternative recovery process equally proved unsatisfactory, as the permeation fluxes obtained were extremely low.

In comparison, the results point to the RO process as more advantageous in desalinating this effluent stream than FO and FO-RO/NF.

Chapter 5

CONCLUSIONS AND RECOMMENDATIONS

This study investigated three membrane separation processes viz FO, RO and hybrid FO-RO/NF in desalinating a local waste oil refinery effluent to meet discharge limits. Key operating variables were optimized using the Box-Behnken design (BBD) of response surface methodology (RSM). Comparison of permeation flux, salt rejection and flux recovery at optimum conditions was made. This chapter summarizes the significant findings and deductions of the study. Again, recommendations towards decision making and future research are made.

The specific objectives were;

i. To determine the optimum operating conditions for each process using Design Expert Software.
ii. To evaluate the permeation flux of FO, RO and hybrid FO-RO/NF system based on optimum conditions.
iii. To evaluate and compare salt rejection of the three membrane processes at optimum conditions.
iv. To evaluate flux recoverability of the three processes after membrane cleaning.

5.1 Conclusions

- The Box-Benhken Design was successful in optimizing forward osmosis (FO) and reverse osmosis (RO) as standalone processes towards the ORE desalination. The optimum conditions for FO were feed solution flowrate (FS-FR) of 9.2 g/L, draw solution flowrate (DS-FR) of 9.4 g/L and draw solution concentration (DS-C) of 32.6 g. The DS-C had the highest impact on the process, followed by the FS-FR and then DS-FR. In the case of RO, the obtained optimum conditions were operating time of 6 hours and operating pressure of 18 bar. Operating pressure showed the greatest impact on permeation flux while feed concentration had the most impact on salt rejection. The hybrid process was conducted at the optimum conditions achieved during the standalone processes.

- At optimum conditions, the permeation flux was 3.64 ± 0.13 L/m^2 h for FO, being the highest permeation flux of the three processes, followed by 2.29 ± 0.2 L/m^2 h being the permeation flux for RO and finally 0.69 ± 0.10 L/m^2 h being the permeation flux for the hybrid process.
- Based on the optimum conditions, FO achieved a perfect rejection efficiency (100%) of SO_4^{2-} ions while rejection of CO_3^{2-} was 94.59 ± 0.32%. There was however severe reverse Cl^- diffusion of up to 35%, which is highly undesirable as it leads to loss of draw solutes and contamination of the FS.
- For RO at optimum conditions, SO_4^{2-} rejection efficiency was 95.1 ± 1.3%, CO_3^{2-} rejection efficiency was 97.3 ± 0.49% and Cl^- rejection efficiency was 90.54 ± 0.81% making all target ions well rejected below their discharge limits.
- Permeate volume obtained for the hybrid process was consistently too low (<10 mL) to be used for analysis and hence salt rejection analysis was limited to FO and RO.
- Permeate flux for FO was easily recovered by physical cleaning – average of 86.01 ± 2.66% permeate flux was recovered after 30 hours of continuous use of the FO membrane. The RO membrane however required both physical and chemical cleaning to achieve and average of 62.52 ± 2.62% flux recovery.
- Application of FO-RO/NF was unsuccessful due to operational inefficiencies in the filtration unit used in this study. The maximum allowable pressure (18 bar) for the filtration unit used as the recovery was too low to recover permeate from the diluted DS, having an osmotic pressure of 25.58 bar.
- Overall, RO desalination of the ORE proved more applicable based on the following;
    - ❖ All ions were well rejected to below the discharge limits
    - ❖ Permeation water needs no post treatment, in case treated water is to be re-used compared to FO which will require post treatment of permeate.
    - ❖ There was no contamination of FS as seen in FO.
    - ❖ Considering the range of operating pressure (14 – 18 bar), and the permeation flux obtained, the RO process qualifies as low-pressure RO desalination which is capable of producing quality permeate at low cost.

5.2 Recommendations for future studies

- FO units should consider other membrane modules such as spiral wound module to provide larger membrane surface area, which will enhance high water recovery rates.

- Other forms of draw solutes should be considered to reduce the effects of reverse solute diffusion
- FO should be conducted at higher flow rates, therefore, the pump with a higher range should be used
- An analytical balance should be placed under the draw solution tank for accurate determination of permeate flux
- The RO system should be upgraded to handle higher pressures to enhance higher water recoveries
- Membrane modules with higher effective area should be used
- FO-RO prefabricated units should be procured for an in-depth study of the process.
- Ion chromatography should be conducted on both the FS and DS before and after FO runs, to determine more accurately the forward and backward flow of ions across the membrane.
- Detailed economic analysis should be done to ascertain the cost effectiveness of the processes.

References

Abadi, S. R. H., Sebzari, M. R., Hemati, M., Rekabdar, F. and Mohammadi, T. 2011. Ceramic membrane performance in microfiltration of oily wastewater. *Desalination*, 265 (1): 222-228.

Achilli, A. and Hickenbottom, K. L. 2016. 3 - Pressure retarded osmosis: Applications. In: Cipollina, A. and Micale, G. eds. *Sustainable Energy from Salinity Gradients*. Woodhead Publishing, 55-75. Available: https://www.sciencedirect.com/science/article/pii/B9780081003121000031 (Accessed 11 March 2021).

Adin, A. 2003. Slow granular filtration for water reuse. *Water Supply* 3(4): 123-130. Available: https://doi.org/10.2166/ws.2003.0053 (Accessed 2/19/2021).

AECOM. 2010. Petroleum refining water/wastewater use and management Available: https://www.ipieca.org/resources/good-practice/petroleum-refining-water-wastewater-use-and-management/ (Accessed 27 February 2021).

Ahmed, M., Kumar, R., Al-Wazzan, Y., Garudachari, B. and Thomas, J. P. 2018. Assessment of performance of inorganic draw solutions tested in forward osmosis process for desalinating arabian gulf seawater. *Arabian Journal for Science and Engineering*, 43 (11): 6171-6180.

Akhter, M., Habib, G. and Qamar, S. U. 2018. Application of electrodialysis in waste water treatment and impact of fouling on process performance. *Membr Sci Technol* 8(2): 1-8

Akther, N., Sodiq, A., Giwa, A., Daer, S., Arafat, H. A. and Hasan, S. W. 2015. Recent advancements in forward osmosis desalination: a review. *Chemical Engineering Journal*, 281: 502-522.

Al-Amoudi, A. and Lovitt, R. W. 2007. Fouling strategies and the cleaning system of NF membranes and factors affecting cleaning efficiency. *Journal of Membrane Science* 303(1): 4-28. Available: http://www.sciencedirect.com/science/article/pii/S0376738807003845 (Accessed 29 December 2020).

Al-Amshawee, S., Yunus, M. Y. B. M., Azoddein, A. A. M., Hassell, D. G., Dakhil, I. H. and Hasan, H. A. 2020. Electrodialysis desalination for water and wastewater: A review. *Chemical Engineering Journal* 380: 122231. Available: https://www.sciencedirect.com/science/article/pii/S1385894719316250 (Accessed 23 February 2021).

Al-Mutaz, I. S. and Al-Ghunaimi, M. A. 2001. Performance of reverse osmosis units at high temperatures. In: Proceedings of *The IDA World Congress on Desalination and Water Reuse, Bahrain: IDA*.

Al-Shamrani, A. A., James, A. and Xiao, H. 2002. Separation of oil from water by dissolved air flotation. *Colloids and Surfaces A: Physicochemical and Engineering Aspects* 209(1): 15-26. Available: https://www.sciencedirect.com/science/article/pii/S092777570200208X (Accessed 18 February 2021).

Al-Zuhairi, A., Merdaw, A. A., Al-Aibi, S., Hamdan, M., Nicoll, P., Monjezi, A. A., Al-Aswad, S., Mahood, H. B., Aryafar, M. and Sharif, A. O. 2015. Forward osmosis desalination from laboratory to market. *Water Supply*, 15 (4): 834-844.

Al Zarooni, M. and Elshorbagy, W. 2006. Characterization and assessment of Al Ruwais refinery wastewater. *Journal of Harzadous Materials* 136(3): 398-405. Available: https://www.sciencedirect.com/science/article/pii/S030438940500645X (Accessed 22 March 2019).

Alejo, T., Arruebo, M., Carcelen, V., Monsalvo, V. M. and Sebastian, V. 2017. Advances in draw solutes for forward osmosis: Hybrid organic-inorganic nanoparticles and conventional solutes. *Chemical Engineering Journal* 309: 738-752. Available: http://www.sciencedirect.com/science/article/pii/S1385894716314899 (Accessed 03 September 2019).

Alijuboury, D. A., Palaniandy, P., Abdul Aziz, H. B. and Feroz, S. 2017. Treatment of petroleum wastewater by conventional and new technologies - A review. *Global nest Journal* 19(3): 439-452 (Accessed 22 March 2019).

Aliyu, U. M., Rathilal, S. and Isa, Y. M. 2018. Membrane desalination technologies in water treatment: A review. *Water Practice Technology* 13(4): 738-752. Available: https://iwaponline.com/wpt/article/13/4/738/65108/Membrane-desalination-technologies-in-water (Accessed 18 November 2019).

Alkhudhiri, A., Darwish, N. and Hilal, N. 2012. Membrane distillation: A comprehensive review. *Desalination* 287: 2-18. Available: http://www.sciencedirect.com/science/article/pii/S0011916411007284 (Accessed 16 March 2019).

Alkhudhiri, A., Darwish, N. and Hilal, N. 2013. Produced water treatment: Application of Air Gap Membrane Distillation. *Desalination* 309: 46-51. Available: http://www.sciencedirect.com/science/article/pii/S0011916412005218 (Accessed 05 February 2020).

Alon Yeshayahu, K. 2019. Membrane Fouling – Mechanisms, Modeling, and Mitigation. Doctor of Philosophy, The University of Texas at Austin.

Alturki, A. A., McDonald, J. A., Khan, S. J., Price, W. E., Nghiem, L. D. and Elimelech, M. 2013. Removal of trace organic contaminants by the forward osmosis process. *Separation and Purification Technology* 103: 258-266. Available: http://www.sciencedirect.com/science/article/pii/S1383586612005692 (Accessed 29 September 2020).

Amy, G. 2008. Fundamental understanding of organic matter fouling of membranes. *Desalination*, 231 (1): 44-51.

An, Y. 2010. Post-treatment of upflow anaerobic sludge blanket effluent by combining the membrane filtration process: fouling control by intermittent permeation and air sparging. *Water and environment journal : WEJ* 24(1). Available: https://onlinelibrary.wiley.com/doi/full/10.1111/j.1747-6593.2008.00152.x (Accessed 09 January 2020).

Advanced oxidation processes (AOP) for water purification and recovery. 1999. Available: http://www.sciencedirect.com/science/article/pii/S0920586199001029 (Accessed 29 August 2019).

Ang, W. S., Lee, S. and Elimelech, M. 2006. Chemical and physical aspects of cleaning of organic-fouled reverse osmosis membranes. *Journal of Membrane Science* 272(1): 198-210. Available: http://www.sciencedirect.com/science/article/pii/S0376738805005806 (Accessed 08 January 2020).

Applied Membrane Inc. 2007. Technical Database for the water Treatment Industry. Available: https://watertreatmentguide.com/Membrane_Rejection.htm (Accessed 07 April 2021).

Ashoor, B. B., Mansour, S., Giwa, A., Dufour, V. and Hasan, S. W. 2016. Principles and applications of direct contact membrane distillation (DCMD): a comprehensive review. *Desalination* 398: 222-246. Available: https://www.sciencedirect.com/science/article/pii/S0011916416309699 (Accessed 22 March 2019).

Aslan, Ş. 2005. Combined removal of pesticides and nitrates in drinking waters using biodenitrification and sand filter system. *Process Biochemistry* 40(1): 417-424. Available: https://www.sciencedirect.com/science/article/pii/S0032959204000524 (Accessed 19 February 2021).

Baker, R. W. 2012. *Membrane technology and applications*. Wiley Online Library.

Balster, J. 2016. Hollow Fiber Membrane Module. In: Drioli, E. and Giorno, L. eds. *Encyclopedia of Membranes*. Berlin, Heidelberg: Springer Berlin Heidelberg, 955-957. Available: https://doi.org/10.1007/978-3-662-44324-8_1583 (Accessed 06 February 2020).

Bamaga, O. A., Yokochi, A. and Beaudry, E. G. 2009. Application of forward osmosis in pretreatment of seawater for small reverse osmosis desalination units. *Desalination and Water Treatment*, 5 (1-3): 183-191.

Bamaga, O. A., Yokochi, A., Zabara, B. and Babaqi, A. S. 2011. Hybrid FO/RO desalination system: Preliminary assessment of osmotic energy recovery and designs of new FO membrane module configurations. *Desalination* 268(1): 163-169. Available: http://www.sciencedirect.com/science/article/pii/S0011916410007289 (Accessed 25 April 2019).

Bartels, C., Franks, R., Rybar, S., Schierach, M. and Wilf, M. 2005. The effect of feed ionic strength on salt passage through reverse osmosis membranes. *Desalination*, 184 (1): 185-195.

Barthe, P., Chaugny, M., Roudier, S. and Delgado Sancho, L. 2015. Best available techniques (BAT) reference document for the refining of mineral oil and gas. *JRC Science and Policy Report EUR 27140EN*,

Belessiotis, V., Kalogirou, S. and Delyannis, E. 2016. Chapter Four - Membrane Distillation. In: Belessiotis, V., Kalogirou, S. and Delyannis, E. eds. *Thermal Solar Desalination*. Academic Press, 191-251. Available: https://www.sciencedirect.com/science/article/pii/B9780128096567000040 (Accessed 02 April 2021).

Bui, N.-N., Arena, J. T. and McCutcheon, J. R. 2015. Proper accounting of mass transfer resistances in forward osmosis: Improving the accuracy of model predictions of structural parameter. *Journal of Membrane Science*, 492: 289-302.

Burn, S. and Gray, S. 2015. *Efficient Desalination by Reverse Osmosis: A guide to RO practice*. IWA Publishing.

Cai, Y. and Hu, X. M. 2016. A critical review on draw solutes development for forward osmosis. *Desalination* 391: 16-29. Available: http://www.sciencedirect.com/science/article/pii/S0011916416301357 (Accessed 03 September 2019).

Campione, A., Gurreri, L., Ciofalo, M., Micale, G., Tamburini, A. and Cipollina, A. 2018. Electrodialysis for water desalination: A critical assessment of recent developments on process fundamentals, models and applications. *Desalination* 434: 121-160. Available: https://www.sciencedirect.com/science/article/pii/S0011916417321604 (Accessed 22 March 2019).

Cartinella, J. L., Cath, T. Y., Flynn, M. T., Miller, G. C., Hunter, K. W. and Childress, A. E. 2006. Removal of Natural Steroid Hormones from Wastewater Using Membrane Contactor Processes. *Environmental Science & Technology*, 40 (23): 7381-7386.

Cath, T. Y., Childress, A. E. and Elimelech, M. 2006. Forward osmosis: Principles, applications, and recent developments. *Journal of Membrane Science* 281(1): 70-87. Available: http://www.sciencedirect.com/science/article/pii/S0376738806003838 (Accessed 9 May 2019).

Cath, T. Y., Drewes, J. E. and Lundin, C. D. 2009. *A novel hybrid forward osmosis process for drinking water augmentation using impaired water and saline water sources*. USA: Las Cruces NM. Available: http://www.waterrf.org/PublicReportLibrary/4150.pdf (Accessed 9 June 2019).

Cath, T. Y., Elimelech, M., McCutcheon, J. R., McGinnis, R. L., Achilli, A., Anastasio, D., Brady, A. R., Childress, A. E., Farr, I. V., Hancock, N. T., Lampi, J., Nghiem, L. D., Xie, M. and Yip, N. Y. 2013. Standard Methodology for Evaluating Membrane Performance in Osmotically Driven Membrane Processes. *Desalination* 312: 31-38. Available: http://www.sciencedirect.com/science/article/pii/S0011916412003657 (Accessed 11 October 2020).

Cath, T. Y., Gormly, S., Beaudry, E. G., Flynn, M. T., Adams, V. D. and Childress, A. E. 2005. Membrane contactor processes for wastewater reclamation in space: Part I. Direct osmotic concentration as pretreatment for reverse osmosis. *Journal of Membrane Science* 257(1): 85-98. Available: http://www.sciencedirect.com/science/article/pii/S0376738804008439 (Accessed 9 May 2019).

Cath, T. Y., Hancock, N. T., Lundin, C. D., Hoppe-Jones, C. and Drewes, J. E. 2010. A multi-barrier osmotic dilution process for simultaneous desalination and purification of impaired water. *Journal of Membrane Science* 362(1): 417-426. Available: http://www.sciencedirect.com/science/article/pii/S0376738810005235 (Accessed 9 May 2019).

Chang, Y.-R., Lee, Y.-J. and Lee, D.-J. 2019. Membrane fouling during water or wastewater treatments: Current research updated. *Journal of the Taiwan Institute of Chemical Engineers* 94: 88-96. Available: http://www.sciencedirect.com/science/article/pii/S1876107017306600 (Accessed 18 April 2020).

Chao, Y.-M. and Liang, T. M. 2008. A feasibility study of industrial wastewater recovery using electrodialysis reversal. *Desalination* 221(1): 433-439. Available: http://www.sciencedirect.com/science/article/pii/S0011916407007254 (Accessed 05 February 2020).

Chekli, L., Phuntsho, S., Shon, H. K., Vigneswaran, S., Kandasamy, J. and Chanan, A. 2012. A review of draw solutes in forward osmosis process and their use in modern applications. *Desalination and Water Treatment* 43(1-3): 167-184. Available: https://doi.org/10.1080/19443994.2012.672168 (Accessed 05 February 2020).

Choi, B. G., Kim, D. I. and Hong, S. 2016. Fouling evaluation and mechanisms in a FO-RO hybrid process for direct potable reuse. *Journal of Membrane Science* 520: 89-98. Available: https://www.sciencedirect.com/science/article/pii/S0376738816310298 (Accessed 8 April 2019).

Choi, B. G., Zhan, M., Shin, K., Lee, S. and Hong, S. 2017. Pilot-scale evaluation of FO-RO osmotic dilution process for treating wastewater from coal-fired power plant integrated with seawater desalination. *Journal of Membrane Science* 540: 78-87. Available: http://www.sciencedirect.com/science/article/pii/S0376738817300911 (Accessed 8 April 2019).

Choi, Y., Cho, H., Shin, Y., Jang, Y. and Lee, S. 2016. Economic Evaluation of a Hybrid Desalination System Combining Forward and Reverse Osmosis. *Membranes*, 6 (1): 3.

Chollom, M., Rathilal, S. and Pillay, V. L. 2014. Treatment and reuse of reactive dye effluent from textile industry using membrane technology. Master of Engineering, Durban University of Technology.

Chollom, M. N. 2014. Treatment and reuse of reactive dye effluent from textile industry using membrane technology. Master of Technology in Engineering, Durban University of Technology.

Civan, F. 2016. Chapter 12 - Cake Filtration: Mechanism, Parameters and Modeling**Parts of this chapter have been reprinted with permission of the American Institute of Chemical Engineers and the Society of Petroleum Engineers from Civan (©1998b,c AIChE, and ©1999b,c SPE). In: Civan, F. ed. *Reservoir Formation Damage (Third Edition)*. Boston: Gulf Professional Publishing, 295-341. Available:

https://www.sciencedirect.com/science/article/pii/B9780128018989000126 (Accessed 03 April 2021).

Coelho, A., Castro, A. V., Dezotti, M. and Sant'Anna, G. L. 2006. Treatment of petroleum refinery sourwater by advanced oxidation processes. *Journal of Hazardous Materials*, 137 (1): 178-184.

Creusen, R. J. M., van Medevoort, J., Roelands, C. P. M. and Duivenbode, J. A. D. v. R. v. 2012. Brine Treatment by a Membrane Distillation-crystallization (MDC) Process. *Procedia Engineering*, 44: 1756-1759.

Cui, Z. F., Jiang, Y. and Field, R. W. 2010. Chapter 1 - Fundamentals of Pressure-Driven Membrane Separation Processes. In: Cui, Z. F. and Muralidhara, H. S. eds. *Membrane Technology*. Oxford: Butterworth-Heinemann, 1-18. Available: https://www.sciencedirect.com/science/article/pii/B978185617632300001X (Accessed 11 March 2021).

da Cruz, G. F., dos Santos Neto, E. V. and Marsaioli, A. J. 2008. Petroleum degradation by aerobic microbiota from the Pampo Sul Oil Field, Campos Basin, Brazil. *Organic Geochemistry* 39(8): 1204-1209. Available: https://www.sciencedirect.com/science/article/pii/S0146638008001204 (Accessed 19 February 2021).

Diya'uddeen, B. H., Daud, W. M. A. W. and Abdul Aziz, A. R. 2011. Treatment technologies for petroleum refinery effluents: A review. *Process Safety and Environmental Protection* 89(2): 95-105. Available: http://www.sciencedirect.com/science/article/pii/S0957582010001126 (Accessed 29 August 2019).

Doncaster, C. P. and Davey, A. J. 2007. *Analysis of variance and covariance: how to choose and construct models for the life sciences*. Cambridge University Press.

Doran, P. M. 2013. Chapter 11 - Unit Operations. In: Doran, P. M. ed. *Bioprocess Engineering Principles (Second Edition)*. London: Academic Press, 445-595. Available: https://www.sciencedirect.com/science/article/pii/B9780122208515000113 (Accessed 03 April 2021).

Dow, N., Gray, S., Li, J.-d., Zhang, J., Ostarcevic, E., Liubinas, A., Atherton, P., Roeszler, G., Gibbs, A. and Duke, M. 2016. Pilot trial of membrane distillation driven by low grade waste heat: Membrane fouling and energy assessment. *Desalination* 391: 30-42. Available: http://www.sciencedirect.com/science/article/pii/S0011916416300224 (Accessed 4 June 2019).

DOW Water, S. 2010. Filmtec™ Reverse Osmosis Membranes. *Technical Manual, Form*, 399 (609-00071): 1-180.

DOW water solutions. 2010. Technical Manual on water and process solutions Available: https://www.filterwater.com/docs/filmtec/dow-filmtec-ro-membranes-technical-manual-609416.pdf (Accessed 01 April 2021).

Elsaid, K., Sayed, E. T., Abdelkareem, M. A., Mahmoud, M. S., Ramadan, M. and Olabi, A. 2020. Environmental impact of emerging desalination technologies: A preliminary evaluation. *Journal of Environmental Chemical Engineering* 8(5): 104099. Available: https://www.sciencedirect.com/science/article/pii/S2213343720304474?casa_token=2AlzqhN7PSIAAAAA:0wnKCldOMqvYSCWC_eRL4pe9QGunOh5Sl3jogKpf0XQWDq2rX6bRmYt

Emami, P., Fallahianbijan, F., Dinse, E., Motevalian, S. P., Conde, B. C., Reilly, K. and Zydney, A. L. 2020. Modified intermediate pore blockage model describes fouling behavior during sterile filtration of glycoconjugate vaccines. *Journal of Membrane Science*, 613: 118495.

EPA. 2015. Table 4. Water-quality criteria, standards, or recommended limits for selected properties and constituents. Available: https://www.scribd.com/document/373256706/Water-Quality-atandard-mainbodyofreport-3-pdf (Accessed 02 April 2021).

Essien, D. I. E. 2010. Recommendation on a suitable desalination process for the South African Environment. Master of Engineering, North West University.

Ezugbe, E. O., Kweinor Tetteh, E., Rathilal, S., Asante-Sackey, D. and Amo-Duodu, G. 2021. Desalination of Municipal Wastewater Using Forward Osmosis. *Membranes* 11(2): 119. Available: https://www.mdpi.com/2077-0375/11/2/119 (Accessed 8 February 2021).

Ezugbe, E. O. and Rathilal, S. 2020. Membrane Technologies in Wastewater Treatment: A Review. 10(5): 89. Available: https://www.mdpi.com/2077-0375/10/5/89 (Accessed 01 May 2020).

Ezugbe, E. O., Rathilal, S., Ishwarlall, S. and Kweinor, T. E. 2020. Removal of Cl^-, SO_4^{2-} and CO_3^{2-} Salts from Oil Refinery Effluent Using Forward Osmosis. Paper presented at the *18th JOHANNESBURG International Conference on Science, Engineering, Technology and Waste Management (SETWM-20)*. Johannesburg, South Africa, 16 - 18 November 2020. Eminent Association of Researchers in Engineering & Technology (EARET) under Eminent Association of Pioneers (EAP), 193-196. Available: http://earet.org/proceedingspdf.php?id=404 (Accessed 17 January 2021).

Fane, A. T., Wang, R. and Jia, Y. 2011. Membrane technology: past, present and future. In: *Membrane and Desalination Technologies*. Springer, 1-45.

Farajnezhad, H. and Gharbani, P. 2012. Coagulation treatment of wastewater in petroleum industry using poly aluminum chloride and ferric chloride. *International Journal of Research and Reviews in Applied Sciences*, 13 (1): 306-310.

Ferrari, F., Pijuan, M., Rodriguez-Roda, I. and Blandin, G. 2019. Exploring Submerged Forward Osmosis for Water Recovery and Pre-Concentration of Wastewater before Anaerobic Digestion: A Pilot Scale Study. 9(8): 97. Available: https://www.mdpi.com/2077-0375/9/8/97 (Accessed 16 April 2020).

Ferreira, S. L. C., Bruns, R. E., Ferreira, H. S., Matos, G. D., David, J. M., Brandão, G. C., da Silva, E. G. P., Portugal, L. A., dos Reis, P. S., Souza, A. S. and dos Santos, W. N. L. 2007. Box-Behnken design: An alternative for the optimization of analytical methods. *Analytica Chimica Acta* 597(2): 179-186. Available: http://www.sciencedirect.com/science/article/pii/S0003267007011671 (Accessed 18 January 2021).

Gadallah, H., Ali, H. M., Ali, S. S., Sabry, R. and Gadallah, A. 2014. Application of forward/reverse osmosis hybrid system for brackish water desalination using El-Salam Canal Water, Sinai, Egypt, Part (1): FO Performance. In: Proceedings of *4th International conference on environment science and engineering IPCBEE*. 2.29 December 2020).

Galama, A. H., Saakes, M., Bruning, H., Rijnaarts, H. H. M. and Post, J. W. 2014. Seawater predesalination with electrodialysis. *Desalination* 342: 61-69. Available: http://www.sciencedirect.com/science/article/pii/S0011916413003342 (Accessed 21 March 2019).

Garrido-Cardenas, J. A., Esteban-García, B., Agüera, A., Sánchez-Pérez, J. A. and Manzano-Agugliaro, F. 2020. Wastewater Treatment by Advanced Oxidation Process and Their Worldwide Research Trends. *International Journal of Environmental Research and Public Health*, 17 (1): 170.

Ge, Q., Su, J., Amy, G. L. and Chung, T.-S. 2012. Exploration of polyelectrolytes as draw solutes in forward osmosis processes. *Water Research*, 46 (4): 1318-1326.

Giacobbo, A., Moura Bernardes, A., Filipe Rosa, M. J. and De Pinho, M. N. 2018. Concentration Polarization in Ultrafiltration/Nanofiltration for the Recovery of Polyphenols from Winery Wastewaters. 8(3): 46. Available: https://www.mdpi.com/2077-0375/8/3/46 (Accessed 16 April 2020).

Giagnorio, M., Ricceri, F., Tagliabue, M., Zaninetta, L. and Tiraferri, A. 2019. Hybrid Forward Osmosis–Nanofiltration for Wastewater Reuse: System Design. *Membranes*, 9 (5): 61.

González, D., Amigo, J. and Suárez, F. 2017. Membrane distillation: Perspectives for sustainable and improved desalination. *Renewable and Sustainable Energy Reviews* 80: 238-259. Available: https://www.sciencedirect.com/science/article/pii/S1364032117307086 (Accessed 22 March 2019).

Gray, G. T., McCutcheon, J. R. and Elimelech, M. 2006. Internal concentration polarization in forward osmosis: role of membrane orientation. *Desalination* 197(1): 1-8. Available: http://www.sciencedirect.com/science/article/pii/S0011916406010605 (Accessed 27 April 2020).

Greenlee, L. F., Lawler, D. F., Freeman, B. D., Marrot, B. and Moulin, P. 2009. Reverse osmosis desalination: Water sources, technology, and today's challenges. *Water Research* 43(9): 2317-2348. Available: http://www.sciencedirect.com/science/article/pii/S0043135409001547 (Accessed 8 March 2019).

Gryta, M. 2002. Concentration of Nacl Solution by Membrane Distillation Integrated with Crystallization. *Separation Science and Technology*, 37 (15): 3535-3558.

Guo, W., Ngo, H.-H. and Li, J. 2012. A mini-review on membrane fouling. *Bioresource technology* 122: 27-34. Available: https://www.sciencedirect.com/science/article/pii/S0960852412007134 (Accessed 26 February 2021).

Gwak, G. and Hong, S. 2018. Chapter 3 - Draw Solute Selection. In: Sarp, S. and Hilal, N. eds. *Membrane-Based Salinity Gradient Processes for Water Treatment and Power Generation*. Elsevier, 87-122. Available: https://www.sciencedirect.com/science/article/pii/B9780444639615000031 (Accessed 11 March 2021).

Hanafy, M. and Nabih, H. I. 2007. Treatment of Oily Wastewater Using Dissolved Air Flotation Technique. *Energy Sources, Part A: Recovery, Utilization, and Environmental Effects* 29(2): 143-159. Available: https://doi.org/10.1080/009083190948711 (Accessed 18 February 2021).

Hancock, N. T. and Cath, T. Y. 2009. Solute Coupled Diffusion in Osmotically Driven Membrane Processes. *Environmental Science & Technology* 43(17): 6769-6775. Available: https://doi.org/10.1021/es901132x (Accessed 16 May 2020).

Hannah, R. 2020. Energy mix. Available: https://ourworldindata.org/energy-mix?country=#energy-mix-what-sources-do-we-get-our-energy-from (Accessed 18 December 2020).

Hausmann, A., Sanciolo, P., Vasiljevic, T., Ponnampalam, E., Quispe-Chavez, N., Weeks, M. and Duke, M. 2011. Direct Contact Membrane Distillation of Dairy Process Streams. 1(1): 48-58. Available: https://www.mdpi.com/2077-0375/1/1/48 (Accessed 21 April 2020).

Holloway, R. W., Childress, A. E., Dennett, K. E. and Cath, T. Y. 2007. Forward osmosis for concentration of anaerobic digester centrate. *Water Research* 41(17): 4005-4014. Available: http://www.sciencedirect.com/science/article/pii/S0043135407003454 (Accessed 8 May 2019).

Houshmand, A., Daud, W. M. A. W. and Shafeeyan, M. S. 2011. Tailoring the surface chemistry of activated carbon by nitric acid: study using response surface method. *Bulletin of the Chemical Society of Japan* 84(11): 1251-1260. Available: https://www.journal.csj.jp/doi/abs/10.1246/bcsj.20110145 (Accessed 19 August 2019).

Huisman, I. H. 2000. MEMBRANE SEPARATIONS | Microfiltration. In: Wilson, I. D. ed. *Encyclopedia of Separation Science*. Oxford: Academic Press, 1764-1777. Available: https://www.sciencedirect.com/science/article/pii/B0122267702052510 (Accessed 18 March 2021).

Iskander, S. M., Zou, S., Brazil, B., Novak, J. T. and He, Z. 2017. Energy consumption by forward osmosis treatment of landfill leachate for water recovery. *Waste Management*, 63: 284-291.

Ismail, A. and Yuliwati, E. 2000. Membrane Science and Technology for wastewater reclamation. *Membrane Processes* 3(1). Available: https://www.researchgate.net/profile/Ahmad-Ismail-18/publication/265890027_MEMBRANE_SCIENCE_AND_TECHNOLOGY_FOR_WASTEWATER_RECLAMATION/links/5678886108ae125516ee8735/MEMBRANE-SCIENCE-AND-TECHNOLOGY-FOR-WASTEWATER-RECLAMATION.pdf

Jagannadh, S. N. and Muralidhara, H. S. 1996. Electrokinetics Methods To Control Membrane Fouling. *Industrial & Engineering Chemistry Research* 35(4): 1133-1140. Available: https://doi.org/10.1021/ie9503712 (Accessed 08 January 2020).

Jamaly, S., Giwa, A. and Hasan, S. W. 2015. Recent improvements in oily wastewater treatment: Progress, challenges, and future opportunities. *Journal of Environmental Sciences* 37: 15-30. Available: https://www.sciencedirect.com/science/article/pii/S1001074215002570 (Accessed 19 February 2021).

Ji, X., Curcio, E., Al Obaidani, S., Di Profio, G., Fontananova, E. and Drioli, E. 2010. Membrane distillation-crystallization of seawater reverse osmosis brines. *Separation and Purification Technology*, 71 (1): 76-82.

Johnson, D. J., Suwaileh, W. A., Mohammed, A. W. and Hilal, N. 2018. Osmotic's potential: An overview of draw solutes for forward osmosis. *Desalination*, 434: 100-120.

José Miguel, A., Beatriz, G.-F. and María, S. 2011. Membrane cleaning. In: Ning, R. Y. ed. *Expanding Issues on Desalination*. Spain: IntechOpen. Available: https://www.intechopen.com/books/expanding-issues-in-desalination/membrane-cleaning (Accessed 09 January 2020).

Ju, C. and Kang, H. 2017. Zwitterionic polymers showing upper critical solution temperature behavior as draw solutes for forward osmosis. *RSC advances*, 7 (89): 56426-56432.

Khayet, M. and Matsuura, T. 2011. *Membrane distillation: principles and applications*. Elsevier.

Klyuchnikov, A., Ovsyannikov, V. Y., Lobacheva, N., Berestovoy, A. and Klyuchnikova, D. 2020. Hydrodynamic methods for reducing concentration polarization during beer processing by membranes. In: Proceedings of *IOP Conference Series: Earth and Environmental Science*. IOP Publishing, 022006. Available: https://iopscience.iop.org/article/10.1088/1755-1315/421/2/022006/meta (Accessed 16 April 2020).

Koyuncu, I., Sengur, R., Turken, T., Guclu, S. and Pasaoglu, M. E. 2015. 3 - Advances in water treatment by microfiltration, ultrafiltration, and nanofiltration. In: Basile, A., Cassano, A. and Rastogi, N. K. eds. *Advances in Membrane Technologies for Water Treatment*. Oxford: Woodhead Publishing, 83-128. Available: https://www.sciencedirect.com/science/article/pii/B9781782421214000034 (Accessed 03 April 2021).

Kriipsalu, M., Marques, M. and Maastik, A. 2008. Characterization of oily sludge from a wastewater treatment plant flocculation-flotation unit in a petroleum refinery and its treatment implications. *Journal of Material Cycles and Waste Management* 10(1): 79-86. Available: https://link.springer.com/article/10.1007/s10163-007-0188-7 (Accessed 22 March 2019).

Kucera, J. 2015. *Reverse Osmosis: Industrial Processes and Applications*. John Wiley & Sons.

Kuyukina, M. S., Krivoruchko, A. V. and Ivshina, I. B. 2020. Advanced Bioreactor Treatments of Hydrocarbon-Containing Wastewater. *Applied Sciences*, 10 (3): 831.

Kyllönen, H. M., Pirkonen, P. and Nyström, M. 2005. Membrane filtration enhanced by ultrasound: a review. *Desalination* 181(1): 319-335. Available: http://www.sciencedirect.com/science/article/pii/S0011916405004030 (Accessed 09 January 2020).

Lampi, K. and Shethji, J. 2014. Forward osmosis industial wastewater treatment: Landfill leachate and oil and gas porduced waters. *International Forward Osmosis Association World Summit*,

Langerak, R. W., Koehler, P. B. and Tonelli, F. A.Google Patents. 1993. *Tubular membrane module*. United States patent, US 5,227,063.

Leaper, S., Abdel-Karim, A., Gad-Allah, T. A. and Gorgojo, P. 2019. Air-gap membrane distillation as a one-step process for textile wastewater treatment. *Chemical Engineering Journal* 360: 1330-1340. Available: http://www.sciencedirect.com/science/article/pii/S1385894718321697 (Accessed 21 April 2020).

Lee, E. K. and Koros, W. J. 2003. Membranes, Synthetic, Applications. In: Meyers, R. A. ed. *Encyclopedia of Physical Science and Technology (Third Edition)*. New York: Academic Press, 279-344. Available: https://www.sciencedirect.com/science/article/pii/B0122274105004191 (Accessed 02 April 2021).

Lee, K. P., Arnot, T. C. and Mattia, D. 2011. A review of reverse osmosis membrane materials for desalination—Development to date and future potential. *Journal of Membrane Science* 370(1): 1-22. Available: http://www.sciencedirect.com/science/article/pii/S0376738810010045 (Accessed 8 March 2019).

Lee, S., Boo, C., Elimelech, M. and Hong, S. 2010. Comparison of fouling behavior in forward osmosis (FO) and reverse osmosis (RO). *Journal of Membrane Science*, 365 (1): 34-39.

Li, J., Sanderson, R. D. and Jacobs, E. P. 2002. Ultrasonic cleaning of nylon microfiltration membranes fouled by Kraft paper mill effluent. *Journal of Membrane Science* 205(1): 247-257. Available:

http://www.sciencedirect.com/science/article/pii/S0376738802001217 (Accessed 09 January 2020).

Li, L., Shi, W. and Yu, S. 2020. Research on Forward Osmosis Membrane Technology Still Needs Improvement in Water Recovery and Wastewater Treatment. 12(1): 107. Available: https://www.mdpi.com/2073-4441/12/1/107 (Accessed 16 April 2020).

Li, Q. and Elimelech, M. 2004. Organic Fouling and Chemical Cleaning of Nanofiltration Membranes: Measurements and Mechanisms. *Environmental Science & Technology*, 38 (17): 4683-4693.

Lin, J. C.-T., Lee, D.-J. and Huang, C. 2010. Membrane Fouling Mitigation: Membrane Cleaning. *Separation Science and Technology* 45(7): 858-872. Available: https://doi.org/10.1080/01496391003666940 (Accessed 08 January 2020).

Linares, R. V., Li, Z., Sarp, S., Bucs, S. S., Amy, G. and Vrouwenvelder, J. S. 2014. Forward osmosis niches in seawater desalination and wastewater reuse. *Water Research* 66: 122-139. Available: https://www.sciencedirect.com/science/article/pii/S0043135414005880 (Accessed 8 April 2019).

Linde, K. and Jönsson, A.-S. 1995. Nanofiltration of salt solutions and landfill leachate. *Desalination* 103(3): 223-232. Available: http://www.sciencedirect.com/science/article/pii/0011916495000755 (Accessed 18 January 2021).

Luo, H., Wang, Q., Zhang, T. C., Tao, T., Zhou, A., Chen, L. and Bie, X. 2014. A review on the recovery methods of draw solutes in forward osmosis. *Journal of Water Process Engineering*, 4: 212-223.

Luo, W., Hai, F. I., Price, W. E., Elimelech, M. and Nghiem, L. D. 2016. Evaluating ionic organic draw solutes in osmotic membrane bioreactors for water reuse. *Journal of Membrane Science*, 514: 636-645.

Maskooki, A., Mortazavi, S. A. and Maskooki, A. 2010. Cleaning of spiralwound ultrafiltration membranes using ultrasound and alkaline solution of EDTA. *Desalination* 264(1): 63-69. Available:

http://www.sciencedirect.com/science/article/pii/S0011916410005035 (Accessed 31 January 2020).

McCutcheon, J. R. and Elimelech, M. 2007. Modeling water flux in forward osmosis: implications for improved membrane design. *AIChE journal* 53(7): 1736-1744. Available: https://aiche.onlinelibrary.wiley.com/doi/epdf/10.1002/aic.11197 (Accessed 13 February 2021).

McKeen, L. W. 2017. 4 - Markets and Applications for Films, Containers, and Membranes. In: McKeen, L. W. ed. *Permeability Properties of Plastics and Elastomers (Fourth Edition)*. William Andrew Publishing, 61-82. Available: https://www.sciencedirect.com/science/article/pii/B978032350859900004X (Accessed 03 April 2021).

Mehta, G. D. and Loeb, S. 1978. Performance of permasep B-9 and B-10 membranes in various osmotic regions and at high osmotic pressures. *Journal of Membrane Science* 4: 335-349. Available: https://www.sciencedirect.com/science/article/pii/S0376738800833128 (Accessed 13 February 2021).

Membrane Solutions LLC. 2020. *Membrane Solutions* 2020. Available: https://www.membrane-solutions.com/spiral_membrane.htm (Accessed 14 February 2020).

Merten, U., Lonsdale, H. K. and Riley, R. L. 1964. Boundary-Layer Effects in Reverse Osmosis. *Industrial & Engineering Chemistry Fundamentals* 3(3): 210-213. Available: https://doi.org/10.1021/i160011a006 (Accessed 11 February 2021).

Mikulášek, P. 1994. Methods to reduce concentration polarization and fouling in membrane filtration. *Collection of Czechoslovak chemical communications*, 59 (4): 737-755.

Mogashane, T., Maree, J., Nyamutswa, N., Vogel, J., Mujuru, M. and Mphahlele-Makgwane, M. 2020. Evaluation of Forward Osmosis for Treatment of Sodium sulphate Rich Brine. In: Fosso-Kankeu, P. D. E., Waanders, P. D. F. and Bulsara, P. D. H. K. P. eds. Proceedings of *18th JOHANNESBURG Int'l Conference on Science, Engineering, Technology & Waste Management (SETWM-20)*. Johannesburg, South Africa, 16-17 November 2020

Available: http://www.eares.org/siteadmin/upload/4371EAP1120243.pdf (Accessed 29 December 2020).

Mohammadifakhr, M., de Grooth, J., Roesink, H. D. W. and Kemperman, A. J. B. 2020. Forward Osmosis: A Critical Review. 8(4): 404. Available: https://www.mdpi.com/2227-9717/8/4/404 (Accessed 22 April 2020).

Mohammed, S. A., Abbas, A. D. and Sabry, L. S. 2014. Effect of operating conditions on reverse osmosis (RO) membrane performance. *J Eng*, 20: 61-70.

Mondal, P., Tran, A. and Van der Bruggen, B. 2016. Effect of competing and coexisting solutes on As (V) removal by forward osmosis. In: Proceedings of *Arsenic Research and Global Sustainability-Proceedings of the 6th International Congress on Arsenic in the Environment, AS 2016*. 552-553. Available: https://lirias.kuleuven.be/1564442?limo=0 (Accessed 17 January 2021).

Muro, C., Riera, F. and del Carmen Díaz, M. 2012. Membrane separation process in wastewater treatment of food industry. In: *Food industrial processes–methods and equipment*. InTech, Rijeka, 253-280.

Nagy, E. 2012. 10 - Nanofiltration. In: Nagy, E. ed. *Basic Equations of the Mass Transport through a Membrane Layer*. Oxford: Elsevier, 249-266. Available: https://www.sciencedirect.com/science/article/pii/B9780124160255000107 (Accessed 09 March 2021).

Nagy, E. 2019a. Chapter 17 - Forward Osmosis. In: Nagy, E. ed. *Basic Equations of Mass Transport Through a Membrane Layer (Second Edition)*. Elsevier, 447-456. Available: http://www.sciencedirect.com/science/article/pii/B9780128137222000170 (Accessed 05 Jauary 2021).

Nagy, E. 2019b. Chapter 19 - Membrane Distillation. In: Nagy, E. ed. *Basic Equations of Mass Transport Through a Membrane Layer (Second Edition)*. Amsterdam, The Netherlands: Elsevier, 483-496. Available: http://www.sciencedirect.com/science/article/pii/B9780128137222000194 (Accessed 21 March 2021).

Nanda, D., Tung, K.-L., Li, Y.-L., Lin, N.-J. and Chuang, C.-J. 2010. Effect of pH on membrane morphology, fouling potential, and filtration performance of nanofiltration membrane for water softening. *Journal of Membrane Science*, 349 (1): 411-420.

Nelson, C. and Ghosh, A. 2011. *Membrane technology for produced water in Lea County*. Available: https://www.osti.gov/biblio/1062985 (Accessed 28 August 2019).

Nguyen, T. P. N., Yun, E.-T., Kim, I.-C. and Kwon, Y.-N. 2013. Preparation of cellulose triacetate/cellulose acetate (CTA/CA)-based membranes for forward osmosis. *Journal of Membrane Science*, 433: 49-59.

Nicoll, P. 2013a. Forward Osmosis–Ignore It At your Peril. *International Desalination Association*, 22

Nicoll, P. 2013b. Forward osmosis as a pre-treatment to reverse osmosis. In: Proceedings of *Proceedings of the International Desalination Association World Congress on Desalination and Water Reuse, Tianjin, China*. 20-25.

Noble, R. and Stern, S. A. 1995. *Membrane Separations Technology: Principles and Applications*. Denver, Colorado, USA: Elsevier Science & Technology.

Norouzbahari, S., Roostaazad, R. and Hesampour, M. 2009. Crude oil desalter effluent treatment by a hybrid UF/RO membrane separation process. *Desalination*, 238 (1-3): 174-182.

Noshadi, I., Salahi, A., Hemmati, M., Rekabdar, F. and Mohammadi, T. 2013. Experimental and ANFIS modeling for fouling analysis of oily wastewater treatment using ultrafiltration. *Asia-Pacific Journal of Chemical Engineering*, 8 (4): 527-538.

Orme, C. J. and Wilson, A. D. 2015. 1-Cyclohexylpiperidine as a thermolytic draw solute for osmotically driven membrane processes. *Desalination*, 371: 126-133.

Palaniandy, P. and Feroz, S. 2019. Advanced Oxidation Processes (AOPs) to Treat the Petroleum Wastewater. In: *Advanced Oxidation Processes (AOPs) in Water and Wastewater Treatment*. IGI Global, 99-122. Available: https://www.igi-global.com/chapter/advanced-oxidation-processes-aops-to-treat-the-petroleum-wastewater/209302 (Accessed 15 November 2020).

Park, C., Lee, Y. H., Lee, S. and Hong, S. 2008. Effect of cake layer structure on colloidal fouling in reverse osmosis membranes. *Desalination* 220(1): 335-344. Available: https://www.sciencedirect.com/science/article/pii/S0011916407006315 (Accessed 26 February 2021).

Pathak, C. and Mandalia, H. C. 2012. Petroleum industries: Environmental pollution effects, management and treatment methods. *International Journal of Separation for Environmental Sciences* 1(1): 55 (Accessed 11 June 2020).

Peinemann, K.-V. and Nunes, S. P. 2010. *Membranes for water treatment*. John Wiley & Sons.

Pendashteh, A. R., Fakhru'l-Razi, A., Madaeni, S. S., Abdullah, L. C., Abidin, Z. Z. and Biak, D. R. A. 2011. Membrane foulants characterization in a membrane bioreactor (MBR) treating hypersaline oily wastewater. *Chemical Engineering Journal* 168(1): 140-150. Available: https://www.sciencedirect.com/science/article/pii/S1385894710012878 (Accessed 31 July 2019).

Pereira, J., Velasquez, I., Blanco, R., Sanchez, M., Pernalete, C. and Canelón, C. 2015. *Crude oil desalting process*. IntechOpen.

Pilipauskas, D. R. 1999. *Using Factorial Experiments in the Development of Process Chemistry*. Dekker: New York.

Porcelli, N. and Judd, S. 2010. Chemical cleaning of potable water membranes: A review. *Separation and Purification Technology*, 71 (2): 137-143.

Quist-Jensen, C. A., Macedonio, F. and Drioli, E. 2015. Membrane technology for water production in agriculture: desalination and wastewater reuse. *Desalination* 364: 17-32. Available: https://www.sciencedirect.com/science/article/pii/S001191641500140X (Accessed 14 April 2019).

Rackley, S. A. 2017. 8 - Membrane separation systems. In: Rackley, S. A. ed. *Carbon Capture and Storage (Second Edition)*. Boston: Butterworth-Heinemann, 187-225. Available: https://www.sciencedirect.com/science/article/pii/B9780128120415000088 (Accessed 03 April 2021).

Radelyuk, I., Tussupova, K., Zhapargazinova, K., Yelubay, M. and Persson, M. 2019. Pitfalls of Wastewater Treatment in Oil Refinery Enterprises in Kazakhstan—A System Approach. *Sustainability*, 11 (6): 1618.

Rahimpour, A., Rajaeian, B., Hosienzadeh, A., Madaeni, S. S. and Ghoreishi, F. 2011. Treatment of oily wastewater produced by washing of gasoline reserving tanks using self-made and commercial nanofiltration membranes. *Desalination*, 265 (1): 190-198.

Rastogi, N. K. and Nayak, C. A. 2011. 21 - Membranes for forward osmosis in industrial applications. In: Basile, A. and Nunes, S. P. eds. *Advanced Membrane Science and Technology for Sustainable Energy and Environmental Applications*. Woodhead Publishing, 680-717. Available: http://www.sciencedirect.com/science/article/pii/B9781845699697500217 (Accessed 30 November 2020).

Roest, D. 2017. Characterization and performance evaluation of commercially available membranes in forward osmosis. MASTER, Eindhoven University of Technology. 10 October 2020).

Sablani, S. S., Goosen, M. F. A., Al-Belushi, R. and Wilf, M. 2001. Concentration polarization in ultrafiltration and reverse osmosis: a critical review. *Desalination*, 141 (3): 269-289.

Salahi, A., Badrnezhad, R., Abbasi, M., Mohammadi, T. and Rekabdar, F. 2011. Oily wastewater treatment using a hybrid UF/RO system. *Desalination and Water Treatment* 28(1-3): 75-82. Available: https://doi.org/10.5004/dwt.2011.2204 (Accessed 06 February 2020).

Salahi, A., Mohammadi, T. and Rekabdar, F. 2010. Reverse osmosis of refinery oily wastewater effluents. *Journal of Environmental Science and Engineering* 7(5): 413-422. Available: http://ijehse.tums.ac.ir/index.php/jehse/article/view/275 (Accessed 27 March 2019).

Sanmartino, J. A., Khayet, M., García-Payo, M. C., Hankins, N. P. and Singh, R. 2016. Desalination by membrane distillation. In. 77-109. 22 March 2019).

SAPIA. 2021. *South African Petroleum Industry Association Annual Report*. Available: https://www.sapia.org.za/overview/south-african-fuel-industry (Accessed 02 April 2021).

Schäfer, A., Andritsos, N., Karabelas, A. J., Hoek, E., Schneider, R. and Nyström, M. 2004. Fouling in nanofiltration. In. Elsevier. Available: https://era.ed.ac.uk/handle/1842/4271 (Accessed 29 December 2020).

Seker, M., Buyuksari, E., Topcu, S., Sesli, D., Celebi, D., Keskinler, B. and Aydiner, C. 2017. Effect of process parameters on flux for whey concentration with NH3/CO2 in forward osmosis. *Food and Bioproducts Processing*, 105: 64-76.

Shaffer, D. L., Werber, J. R., Jaramillo, H., Lin, S. and Elimelech, M. 2015. Forward osmosis: where are we now? *Desalination* 356: 271-284. Available: https://www.sciencedirect.com/science/article/pii/S0011916414005542 (Accessed 22 March 2019).

She, Q., Jin, X., Li, Q. and Tang, C. Y. 2012. Relating reverse and forward solute diffusion to membrane fouling in osmotically driven membrane processes. *Water Research* 46(7): 2478-2486. Available: http://www.sciencedirect.com/science/article/pii/S0043135412001273 (Accessed 23 October 2020).

Shen, L.-C., Hankins and Nicholas, P. 2016. Forward Osmosis for Sustainable Water Treatment. In: *Emerging Membrane Technology for Sustainable Water Treatment*. Elsevier, 55-76.

Shirazi, S., Lin, C.-J. and Chen, D. 2010. Inorganic fouling of pressure-driven membrane processes — A critical review. *Desalination*, 250 (1): 236-248.

Shokrollahzadeh, S., Azizmohseni, F., Golmohammad, F., Shokouhi, H. and Khademhaghighat, F. 2008. Biodegradation potential and bacterial diversity of a petrochemical wastewater treatment plant in Iran. *Bioresource technology* 99(14): 6127-6133. Available: https://www.sciencedirect.com/science/article/pii/S0960852407010589 (Accessed 19 February 2021).

Shorrock, C. J. and Bird, M. R. 1998. Membrane Cleaning: Chemically Enhanced Removal of Deposits Formed During Yeast Cell Harvesting. *Food and Bioproducts Processing* 76(1): 30-38. Available:

http://www.sciencedirect.com/science/article/pii/S0960308598700884 (Accessed 10 January 2020).

Siavash Madaeni, S., Mohamamdi, T. and Kazemi Moghadam, M. 2001. Chemical cleaning of reverse osmosis membranes. *Desalination*, 134 (1): 77-82.

Singh, R. 2016. Desalination and On-site Energy for Groundwater Treatment in Developing Countries Using Fuel Cells. In: *Emerging Membrane Technology for Sustainable Water Treatment*. Elsevier Boston, 135-162.

Singh, R. and Hankins, N. 2016a. *Emerging membrane technology for sustainable water treatment*. Elsevier.

Singh, R. and Hankins, N. P. 2016b. Introduction to membrane processes for water treatment. In: *Emerging Membrane Technology for Sustainable Water Treatment*. Elsevier, 15-52.

Song, L. and Elimelech, M. 1995. Theory of concentration polarization in crossflow filtration. *Journal of the Chemical Society, Faraday Transactions*, 91 (19): 3389-3398.

South Africa Yearbook. 2018. *South Africa Yearbook*. South Africa: Government Communication and Information System. Available: https://www.gcis.gov.za/content/resourcecentre/sa-info/south-africa-yearbook-201718 (Accessed 11/03/2019).

Souza, B. M., Cerqueira, A. C., Sant'Anna, G. L. and Dezotti, M. 2011. Oil-Refinery Wastewater Treatment Aiming Reuse by Advanced Oxidation Processes (AOPs) Combined with Biological Activated Carbon (BAC). *Ozone: Science & Engineering*, 33 (5): 403-409.

Speth, T. F., Summers, R. S. and Gusses, A. M. 1998. Nanofiltration Foulants from a Treated Surface Water. *Environmental Science & Technology*, 32 (22): 3612-3617.

Spivakov, B. and Shkinev, V. 2005. MEMBRANE TECHNIQUES | Ultrafiltration. In: Worsfold, P., Townshend, A. and Poole, C. eds. *Encyclopedia of Analytical Science (Second Edition)*. Oxford: Elsevier, 524-530. Available: https://www.sciencedirect.com/science/article/pii/B012369397700368X (Accessed 21 November 2020).

Stepnowski, P., Siedlecka, E. M., Behrend, P. and Jastorff, B. 2002. Enhanced photo-degradation of contaminants in petroleum refinery wastewater. *Water Research* 36(9): 2167-2172. Available: http://www.sciencedirect.com/science/article/pii/S004313540100450X (Accessed 1 September 2019).

Sterlitech. 2018. How Does Temperature Affect Membrane Performance? Available: https://www.sterlitech.com/blog/post/how-does-temperature-affect-membrane-performance (Accessed 31 March 2021).

Strathmann, H. 2010. Electrodialysis, a mature technology with a multitude of new applications. *Desalination* 264(3): 268-288. Available: http://www.sciencedirect.com/science/article/pii/S0011916410002985 (Accessed 21 April 2020).

Subramani, A. and Jacangelo, J. G. 2015. Emerging desalination technologies for water treatment: a critical review. *Water Research* 75: 164-187. Available: https://www.sciencedirect.com/science/article/pii/S0043135415001050 (Accessed 20 March 2019).

Teixeira, C. A. and Ghisi, E. 2019. Comparative Analysis of Granular and Membrane Filters for Rainwater Treatment. *Water* 11(5): 1004. Available: https://www.mdpi.com/2073-4441/11/5/1004 (Accessed 19 February 2021).

Tetteh, E. K., Ezugbe, E. O., Rathilal, S. and Asante-Sackey, D. 2020. Removal of COD and SO42− from Oil Refinery Wastewater Using a Photo-Catalytic System—Comparing TiO2 and Zeolite Efficiencies. *Water* 12(1): 214. Available: https://www.mdpi.com/2073-4441/12/1/214 (Accessed 03 February 2020).

Tetteh, E. K., Rathilal, S. and Robinson, K. 2018. Optimisation of dissolved air floatation for separating industrial mineral oil from water. Master in Engineering, Durban University of Technology.

Thompson, N. A. and Nicoll, P. G. 2011. Forward osmosis desalination: a commercial reality. In: Proceedings of *IDA World Congress–Perth Convention and Exhibition Centre (PCEC), Perth, Western Australia September*. 4-9.

Tian, X., Song, Y., Shen, Z., Zhou, Y., Wang, K., Jin, X., Han, Z. and Liu, T. 2020. A comprehensive review on toxic petrochemical wastewater pretreatment and advanced treatment. *Journal of Cleaner Production* 245: 118692. Available: https://www.sciencedirect.com/science/article/pii/S0959652619335620 (Accessed 18 February 2021).

Tiraferri, A., Yip, N. Y., Straub, A. P., Romero-Vargas Castrillon, S. and Elimelech, M. 2013. A method for the simultaneous determination of transport and structural parameters of forward osmosis membranes. *Journal of Membrane Science* 444: 523-538. Available: https://www.sciencedirect.com/science/article/pii/S0376738813004109 (Accessed 11 Febraury 2021).

Tomaszewska, M., Orecki, A. and Karakulski, K. 2005. Treatment of bilge water using a combination of ultrafiltration and reverse osmosis. *Desalination*, 185 (1): 203-212.

Tony, M. A., Purcell, P. J. and Zhao, Y. 2012. Oil refinery wastewater treatment using physicochemical, Fenton and Photo-Fenton oxidation processes. *Journal of Environmental Science and Health, Part A*, 47 (3): 435-440.

Tun, C. M., Fane, A. G., Matheickal, J. T. and Sheikholeslami, R. 2005. Membrane distillation crystallization of concentrated salts—flux and crystal formation. *Journal of Membrane Science*, 257 (1): 144-155.

UN Water. 2019. *World water day - factsheet*. United Nations. Available: http://www.waterwise.co.za/site/water/environment/situation.html (Accessed 27/03/2019).

Varjani, S., Joshi, R., Srivastava, V. K., Ngo, H. H. and Guo, W. 2020. Treatment of wastewater from petroleum industry: current practices and perspectives. *Environmental Science and Pollution Research* 27(22): 27172-27180. Available: https://doi.org/10.1007/s11356-019-04725-x (Accessed 18 February 2021).

Varjani, S. J. and Upasani, V. N. 2017. A new look on factors affecting microbial degradation of petroleum hydrocarbon pollutants. *International Biodeterioration & Biodegradation* 120: 71-83. Available: https://www.sciencedirect.com/science/article/pii/S0964830516308113 (Accessed 18 February 2021).

Vela, M. C. V., Blanco, S. Á., García, J. L. and Rodríguez, E. B. 2008. Analysis of membrane pore blocking models applied to the ultrafiltration of PEG. *Separation and Purification Technology*, 62 (3): 489-498.

Verma, S., Daverey, A. and Sharma, A. 2017. Slow sand filtration for water and wastewater treatment – a review. *Environmental Technology Reviews* 6(1): 47-58. Available: https://doi.org/10.1080/21622515.2016.1278278 (Accessed 19 February 2021).

Volpin, F., Fons, E., Chekli, L., Kim, J. E., Jang, A. and Shon, H. K. 2018. Hybrid forward osmosis-reverse osmosis for wastewater reuse and seawater desalination: Understanding the optimal feed solution to minimise fouling. *Process Safety and Environmental Protection* 117: 523-532. Available: http://www.sciencedirect.com/science/article/pii/S0957582018301587 (Accessed 18 April 2019).

Wan, M.-W., Reguyal, F., Futalan, C., Yang, H.-L. and Kan, C.-C. 2013. Ultrasound irradiation combined with hydraulic cleaning on fouled polyethersulfone and polyvinylidene fluoride membranes. *Environmental Technology* 34(21): 2929-2937. Available: https://doi.org/10.1080/09593330.2012.701235 (Accessed 09 January 2020).

Wang, F. and Tarabara, V. V. 2008. Pore blocking mechanisms during early stages of membrane fouling by colloids. *Journal of colloid and interface science* 328(2): 464-469. Available: https://www.sciencedirect.com/science/article/pii/S0021979708011521 (Accessed 28 February 2021).

Wang, L. K., Chen, J. P., Hung, Y.-T. and Shammas, N. K. 2008. *Membrane and desalination technologies*. Springer.

Wang, X.-M. and Waite, T. D. 2008. Gel layer formation and hollow fiber membrane filterability of polysaccharide dispersions. *Journal of Membrane Science* 322(1): 204-213. Available: https://www.sciencedirect.com/science/article/pii/S0376738808004791 (Accessed 28 February 2021).

Wang, Y.-N., Goh, K., Li, X., Setiawan, L. and Wang, R. 2018. Membranes and processes for forward osmosis-based desalination: Recent advances and future prospects. *Desalination* 434: 81-99. Available:

http://www.sciencedirect.com/science/article/pii/S001191641731189X (Accessed 11 March 2019).

Wang, Y., Wicaksana, F., Tang, C. Y. and Fane, A. G. 2010. Direct Microscopic Observation of Forward Osmosis Membrane Fouling. *Environmental Science & Technology*, 44 (18): 7102-7109.

Wang, Z., Ma, J., Tang, C. Y., Kimura, K., Wang, Q. and Han, X. 2014. Membrane cleaning in membrane bioreactors: A review. *Journal of Membrane Science* 468: 276-307. Available: http://www.sciencedirect.com/science/article/pii/S037673881400444X (Accessed 09 January 2020).

Wei, J., She, Q. and Liu, X. 2021. Insights into the Influence of Membrane Permeability and Structure on Osmotically-Driven Membrane Processes. *Membranes*, 11 (2): 153.

Weissman, S. A. and Anderson, N. G. 2015. Design of Experiments (DoE) and Process Optimization. A Review of Recent Publications. *Organic Process Research & Development*, 19 (11): 1605-1633.

Wijmans, J. G. and Baker, R. W. 1995. The solution-diffusion model: a review. *Journal of Membrane Science* 107(1): 1-21. Available: http://www.sciencedirect.com/science/article/pii/037673889500102I (Accessed 04 October 2020).

Williams, C. and Wakeman, R. 2000. Membrane fouling and alternative techniques for its alleviation. *Membrane Technology* 2000(124): 4-10. Available: http://www.sciencedirect.com/science/article/pii/S0958211800800178 (Accessed 08 January 2020).

Wolff, S., Weber, F., Kerpen, J., Winklhofer, M., Engelhart, M. and Barkmann, L. 2021. Elimination of Microplastics by Downstream Sand Filters in Wastewater Treatment. *Water* 13(1): 33. Available: https://www.mdpi.com/2073-4441/13/1/33 (Accessed 19 February 2021).

Wu, L., Wang, H., Xu, T. W. and Xu, Z. L. 2017. Chapter 12 - Polymeric Membranes. In: Jiang, L. Y. and Li, N. eds. *Membrane-Based Separations in Metallurgy*. Amsterdam: Elsevier, 297-334. Available:

https://www.sciencedirect.com/science/article/pii/B9780128034101000128 (Accessed 09 March 2021).

Xiarchos, I., Jaworska, A. and Zakrzewska-Trznadel, G. 2008. Response surface methodology for the modelling of copper removal from aqueous solutions using micellar-enhanced ultrafiltration. *Journal of Membrane Science* 321(2): 222-231. Available: http://www.sciencedirect.com/science/article/pii/S0376738808004195

Xie, M., Nghiem, L. D., Price, W. E. and Elimelech, M. 2012. Comparison of the removal of hydrophobic trace organic contaminants by forward osmosis and reverse osmosis. *Water Research* 46(8): 2683-2692. Available: http://www.sciencedirect.com/science/article/pii/S0043135412001261 (Accessed 30 September 2020).

Xie, P., Cath, T. Y. and Ladner, D. A. 2021. Mass Transport in Osmotically Driven Membrane Processes. *Membranes*, 11 (1): 29.

Xie, W., Zhong, L. and Chen, J. 2007. Treatment of slightly polluted wastewater in an oil refinery using a biological aerated filter process. *Wuhan University Journal of Natural Sciences*, 12 (6): 1094-1098.

Xue, Y. L., Zhang, R., Cao, B. and Li, P. 2021. Chapter 20 - Tubular membranes and modules. In: Chung, T.-S. and Feng, Y. eds. *Hollow Fiber Membranes*. Elsevier, 431-448. Available: https://www.sciencedirect.com/science/article/pii/B9780128218761000111 (Accessed 03 April 2021).

Yan-Jun, Z., Kai-fen, W., Zheng-jun, W., Liang, Z. and Shu-shen, L. J. E. S. 2000. Fouling and cleaning of membrane–a literature review. 12(2): 241-251. Available: http://www.jesc.ac.cn/jesc_En/ch/reader/create_pdf.aspx?file_no=20000220&year_id=2000&quarter_id=2&falg=1 (Accessed 08 January 2020).

Yasukawa, M., Suzuki, T. and Higa, M. 2018. Chapter 1 - Salinity Gradient Processes: Thermodynamics, Applications, and Future Prospects. In: Sarp, S. and Hilal, N. eds. *Membrane-Based Salinity Gradient Processes for Water Treatment and Power Generation*. Elsevier, 3-56. Available: https://www.sciencedirect.com/science/article/pii/B9780444639615000018 (Accessed 03 April 2021).

Yong, J. S., Phillip, W. A. and Elimelech, M. 2012. Coupled reverse draw solute permeation and water flux in forward osmosis with neutral draw solutes. *Journal of Membrane Science* 392-393: 9-17. Available: http://www.sciencedirect.com/science/article/pii/S0376738811008453 (Accessed 23 October 2020).

York, R., Thiel, R. and Beaudry, E. 1999. Full-scale experience of direct osmosis concentration applied to leachate management. In: Proceedings of *Proceedings of the Seventh International Waste Management and Landfill Symposium (Sardinia'99), S. Margherita di Pula, Cagliari, Sardinia, Italy*. 4-8.

Yu, L., Han, M. and He, F. 2017. A review of treating oily wastewater. *Arabian Journal of Chemistry* 10: S1913-S1922. Available: http://www.sciencedirect.com/science/article/pii/S1878535213002207 (Accessed 1 April 2019).

Yu, Y., Lee, S. and Maeng, S. K. 2016. Forward osmosis membrane fouling and cleaning for wastewater reuse. *Journal of Water Reuse and Desalination*, 7 (2): 111-120.

Zhang, M., She, Q., Yan, X. and Tang, C. Y. 2017. Effect of reverse solute diffusion on scaling in forward osmosis: A new control strategy by tailoring draw solution chemistry. *Desalination*, 401: 230-237.

Zhao, P., Yue, Q., Gao, B., Kong, J., Rong, H., Liu, P., Shon, H. K. and Li, Q. 2014. Influence of different ion types and membrane orientations on the forward osmosis performance. *Desalination*, 344: 123-128.

Zhao, S., Zou, L. and Mulcahy, D. 2011. Effects of membrane orientation on process performance in forward osmosis applications. *Journal of Membrane Science*, 382 (1): 308-315.

Zhao, S., Zou, L., Tang, C. Y. and Mulcahy, D. 2012. Recent developments in forward osmosis: Opportunities and challenges. *Journal of Membrane Science* 396: 1-21. Available: https://www.sciencedirect.com/science/article/pii/S0376738811009215 (Accessed 09 February 2021).

Zhao, X., Wang, Y., Ye, Z., Borthwick, A. G. and Ni, J. 2006. Oil field wastewater treatment in biological aerated filter by immobilized microorganisms. *Process Biochemistry* 41(7): 1475-1483. Available: https://www.sciencedirect.com/science/article/pii/S135951130600064X (Accessed 02 August 2019).

Zou, S. and He, Z. 2016. Enhancing wastewater reuse by forward osmosis with self-diluted commercial fertilizers as draw solutes. *Water Research*, 99: 235-243.

Appendix A

SAMPLE CALCULATIONS AND GRAPHS

This section summarizes the major calculations for the preparation of feed solutions for FO and RO. It also presents calculations on FO dilution factors and the reverse solute flux. A graph of variation in FS conductivity is also presented.

Table A - 1: Molecular weight of elements

Components	MOLAR MASS (g/mol)
Hydrogen	1.00
Carbon	12.01
Oxygen	16.00
Sodium	22.99
Sulphur	32.06
Chlorine	35.45
Calcium	40.08

FORWARD OSMOSIS

Feed solution preparation:

$$molar\ mass\ of\ Calcium\ Chloride\ dihydrate = 40.08 + 2(35.45) + 2(2(1) + 16)$$
$$= 147.02 g/mol$$

Calculation of the amount of Cl^- required for 1L effluent

$$= \frac{0.7174}{\frac{35.45 \times 2}{147.02}} = 1.488\ g$$

Therefore, for 2L of effluent … $2 \times 1.488 = 2.976 g$

$$molar\ mass\ of\ Calcium\ Sulphate\ dihydrate$$
$$= 40.08 + 32.06 + 4(16) + 2(2(1) + 16) = 172.19\ g/mol$$

Calculation of SO_4^{2-} required for 1L effluent

$$= \frac{0.8558}{\frac{96.07}{172.19}} = 1.535\ g$$

Therefore, for 2L… $2 \times 1.535 = 3.07 g$

$$molar\ mass\ of\ sodium\ hydrogen\ carbonate = 22.99 + 1 + 12.01 + 3(16)$$
$$= 84.01\ g/mol$$

Calculation of CO_3^{2-} required for 1L effluent

$$= \frac{0.2061}{\frac{60.01}{84.01}} = 0.289g$$

Therefore, for 2L … $2 \times 0.289 = 0.578g$

Dilution factor calculations

$$D_f = \frac{Final\ vol\ of\ DS}{Volume\ of\ permeate}$$

For run 1:

Final volume of DS = 1220 mL

Initial volume of DS = 1000 mL (constant throughout)

Volume of permeate = 1220 – 1000 = 220 mL

$D_f = \frac{1220}{220}$ = 5.55

Dilution factors for all runs are shown Table A-2.

Reverse solute flux calculation

Reverse solute flux $(J_s) = \frac{C_f V_f - C_0 V_0}{At} = \frac{Final\ mass\ of\ salt\ in\ FS - initial\ mass\ of\ salt\ in\ FS}{A \cdot t}$

For run 1:

Initial mass of Cl^- in FS = 640 mg = 0.64g

Final mass of Cl^- in FS = 720 mg = 0.72g

Area of membrane = 0.0225 m^2

Experimental time per run = 6 h

$J_s = \frac{0.72-0.64}{0.0225\ x\ 6} = 0.59\ \frac{g}{m^2 \cdot h}$

Values of J_s for each run are shown in Table A-2.

Table A - 2: dilution factor Df and RSD for all FO runs

RUN	DS Df	RSF, g/m^{2}h
1	5.55	0.59
2	3.86	1.04
3	3.56	1.59
4	3.53	1.59
5	2.76	0.96
6	2.81	1.41
7	3.44	0.93
8	2.93	1.89
9	4.04	2
10	6.56	0.81
11	3.33	0.89
12	5.10	0.78
13	3.33	3.44
14	2.94	0.78
15	3.15	0.30

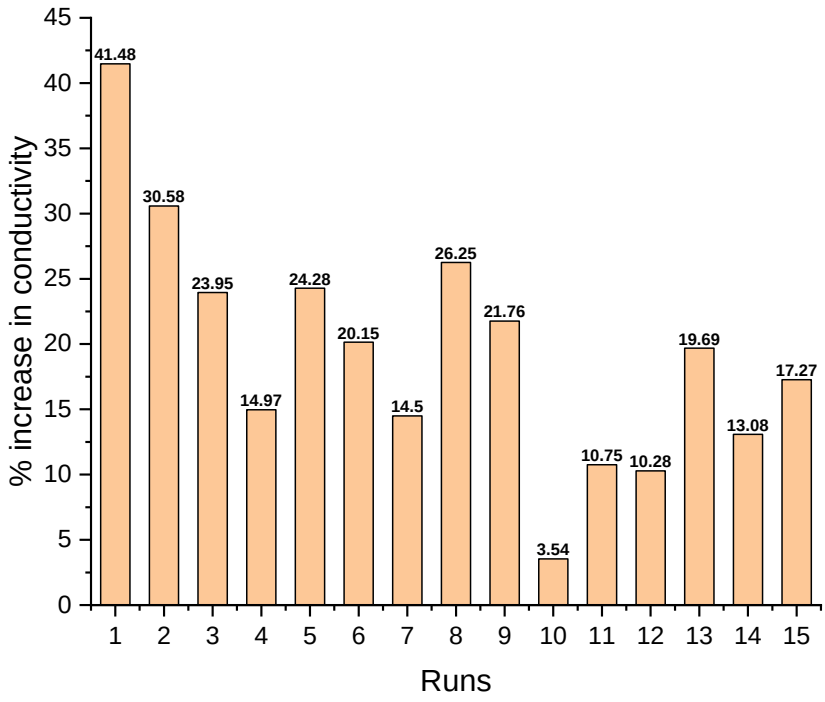

Figure A - 1: Conductivity variations in feed solution for all runs due to ion concentration and RSD

REVERSE OSMOSIS

Feed solution preparation

$$molar\ mass\ of\ Calcium\ Chloride\ dihydrate = 40.08 + 2(35.45) + 2(2(1) + 16)$$
$$= 147.02 g/mol$$

Calculation of the amount of Cl^- required for 1L effluent

$$= \frac{0.7174}{\frac{35.45 \times 2}{147.02}} = 1.488\ g$$

Therefore, for 7 L of effluent … $7 \times 1.488 = 10.416\ g$

$$molar\ mass\ of\ Calcium\ Sulphate\ dihydrate$$
$$= 40.08 + 32.06 + 4(16) + 2(2(1) + 16) = 172.19\ g/mol$$

Calculation of SO_4^{2-} required for 1L effluent

$$= \frac{0.8558}{\frac{96.07}{172.19}} = 1.535\ g$$

Therefore, for 7 L… $7 \times 1.535 = 10.75\ g$

$$molar\ mass\ of\ sodium\ hydrogen\ carbonate = 22.99 + 1 + 12.01 + 3(16)$$
$$= 84.01\ g/mol$$

Calculation of CO_3^{2-} required for 1L effluent

$$= \frac{0.2061}{\frac{60.01}{84.01}} = 0.289 g$$

Therefore, for 7 L … $7 \times 0.289 = 0.578 g$

Appendix B

This section presents raw diagnostic data generated by the DOE software for all responses of FO and RO. These include the actual experimental values, the model-predicted values and the residual values among other diagnostic values that define the validity of the generated models. Under each table, two diagnostic plots are presented viz normal probability plot and the residual vs predicted plots.

The normality plot indicates whether the residuals follow a normal distribution (straight line). Alignment of the data points to the diagonal line indicates equal distribution of the residuals. The residual vs predicted plot test the assumption of constant variance. The plot shows how low or how high the predicted values are, in comparison with the actual results. This is indicated by how far below or above the points are in relation to the horizontal line $y = 0$.

Table B - 1: Forward osmosis: Response 1: Permeation flux

Run Order	Actual Value	Predicted Value	Residual	Leverage	Internally Studentized Residuals	Externally Studentized Residuals	Cook's Distance	Influence on Fitted Value DFFITS	Standard Order
1	1.72	1.74	-0.0163	0.625	-0.247	-0.230	0.013	-0.297	1
2	2.59	2.63	-0.0355	0.643	-0.554	-0.525	0.069	-0.704	2
3	3.05	3.21	-0.1643	0.143	-1.653	-1.961	0.057	-0.800	3
4	3.03	3.06	-0.0275	0.625	-0.418	-0.392	0.036	-0.506	4
5	4.01	3.96	0.0487	0.625	0.742	0.715	0.115	0.924	5
6	4.09	4.10	-0.0080	0.643	-0.125	-0.116	0.004	-0.156	6
7	3.04	3.01	0.0345	0.643	0.537	0.508	0.065	0.682	7
8	2.98	2.90	0.0762	0.625	1.160	1.195	0.280	1.543	8
9	3.71	3.81	-0.0975	0.625	-1.483	-1.659	0.458	-2.141	9
10	1.33	1.34	-0.0050	0.625	-0.076	-0.070	0.001	-0.091	10
11	3.19	3.13	0.0620	0.643	0.966	0.961	0.210	1.289	11
12	2.23	2.27	-0.0437	0.625	-0.666	-0.637	0.092	-0.822	12
13	3.18	3.21	-0.0343	0.143	-0.345	-0.322	0.002	-0.132	13
14	3.36	3.21	0.1457	0.143	1.466	1.631	0.045	0.666	14
15	2.74	2.68	0.0650	0.625	0.989	0.987	0.204	1.274	15

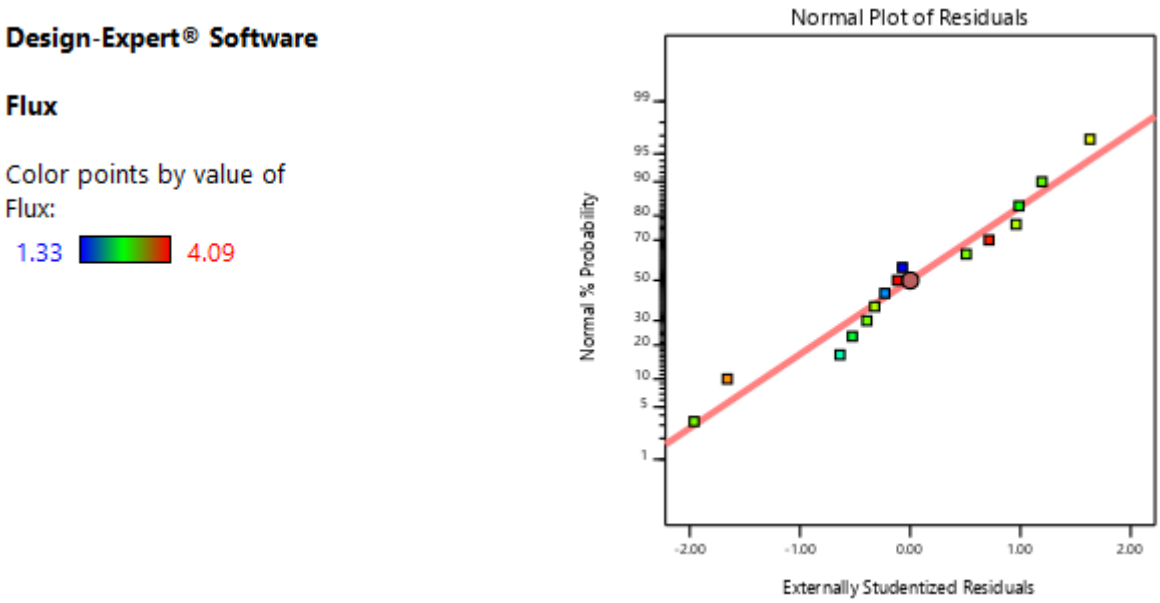

Figure B - 1: Normal probability vs residual plot

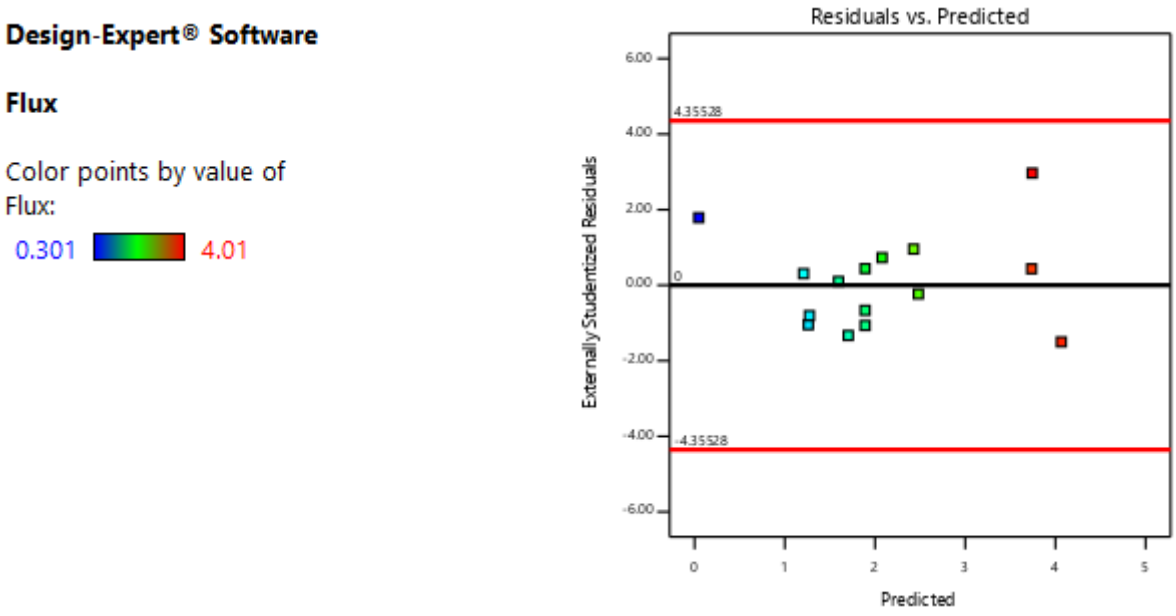

Figure B - 2: Plot of residuals vs Predicted

Table B - 2: Forward osmosis: Response 2: Cl^- enrichment

Run Order	Actual Value	Predicted Value	Residual	Leverage	Internally Studentized Residuals	Externally Studentized Residuals	Cook's Distance	Influence on Fitted Value DFFITS	Standard Order
1	4.48	4.32	0.1581	0.692	0.213	0.197	0.013	0.296	1
2	20.29	20.52	-0.2332	0.692	-0.314	-0.292	0.028	-0.438	2
3	27.90	27.01	0.8892	0.231	0.756	0.731	0.021	0.400	3
4	52.11	52.74	-0.6268	0.442	-0.626	-0.597	0.039	-0.531	4
5	39.33	39.98	-0.6519	0.692	-0.877	-0.860	0.216	-1.290	5
6	35.01	33.79	1.22	0.692	1.646	1.947	0.762	2.920	6
7	41.08	42.80	-1.72	0.692	-2.310	-4.388	1.501(1)	-6.582	7
8	66.01	65.20	0.8056	0.692	1.083	1.099	0.330	1.649	8
9	63.09	62.62	0.4732	0.442	0.473	0.445	0.022	0.396	9
10	29.33	27.82	1.51	0.442	1.504	1.692	0.224	1.507	10
11	31.01	31.27	-0.2607	0.692	-0.350	-0.327	0.035	-0.491	11
12	29.98	31.28	-1.30	0.692	-1.747	-2.154	0.859	-3.231(1)	12
13	26.22	27.01	-0.7908	0.231	-0.672	-0.644	0.017	-0.353	13
14	27.90	27.01	0.8892	0.231	0.756	0.731	0.021	0.400	14
15	17.58	17.94	-0.3643	0.442	-0.364	-0.340	0.013	-0.303	15

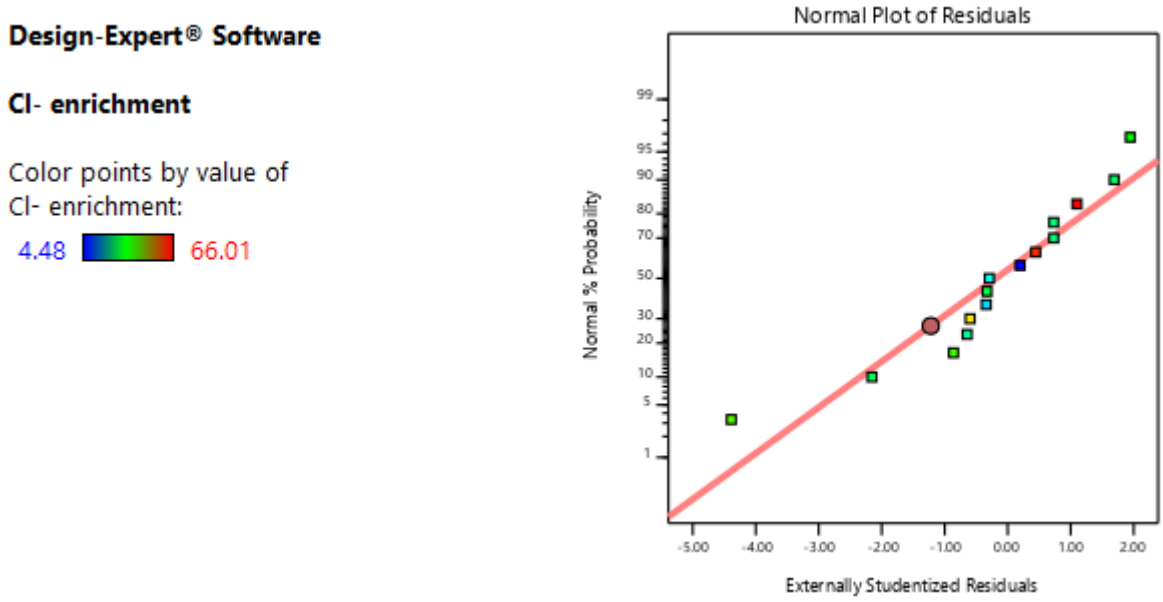

Figure B - 3: Normal probability vs residual plot

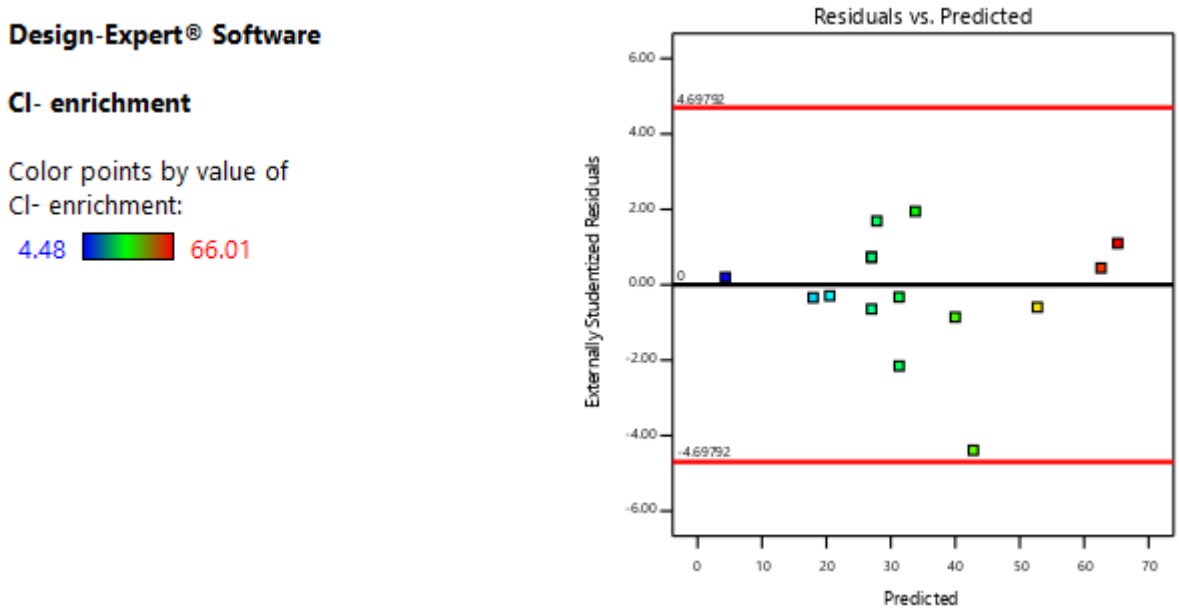

Figure B - 4: Plot of residuals vs Predicted

Table B - 3: Forward osmosis: Response 3: SO_4^{2-} rejection efficiency

Run Order	Actual Value	Predicted Value	Residual	Leverage	Internally Studentized Residuals	Externally Studentized Residuals	Cook's Distance	Influence on Fitted Value DFFITS	Standard Order
1	88.91	89.59	-0.6825	0.625	-0.794	-0.774	0.150	-0.999	1
2	87.03	87.17	-0.1438	0.625	-0.167	-0.157	0.007	-0.202	2
3	96.94	98.48	-1.54	0.143	-1.183	-1.219	0.033	-0.498	3
4	100.00	98.33	1.67	0.393	1.527	1.696	0.215	1.365	4
5	99.05	98.74	0.3100	0.625	0.361	0.340	0.031	0.439	5
6	99.96	100.42	-0.4563	0.625	-0.531	-0.506	0.067	-0.653	6
7	99.22	98.39	0.8287	0.625	0.965	0.960	0.222	1.239	7
8	95.97	95.97	-0.0025	0.625	-0.003	-0.003	0.000	-0.004	8
9	100.00	102.04	-2.04	0.393	-1.864	-2.319	0.321	-1.866	9
10	100.00	98.62	1.38	0.393	1.259	1.315	0.147	1.058	10
11	97.13	96.61	0.5162	0.625	0.601	0.575	0.086	0.743	11
12	97.92	98.29	-0.3700	0.625	-0.431	-0.408	0.044	-0.526	12
13	99.96	98.48	1.48	0.143	1.142	1.167	0.031	0.476	13
14	97.91	98.48	-0.5671	0.143	-0.437	-0.413	0.005	-0.169	14
15	94.53	94.92	-0.3859	0.393	-0.353	-0.333	0.012	-0.268	15

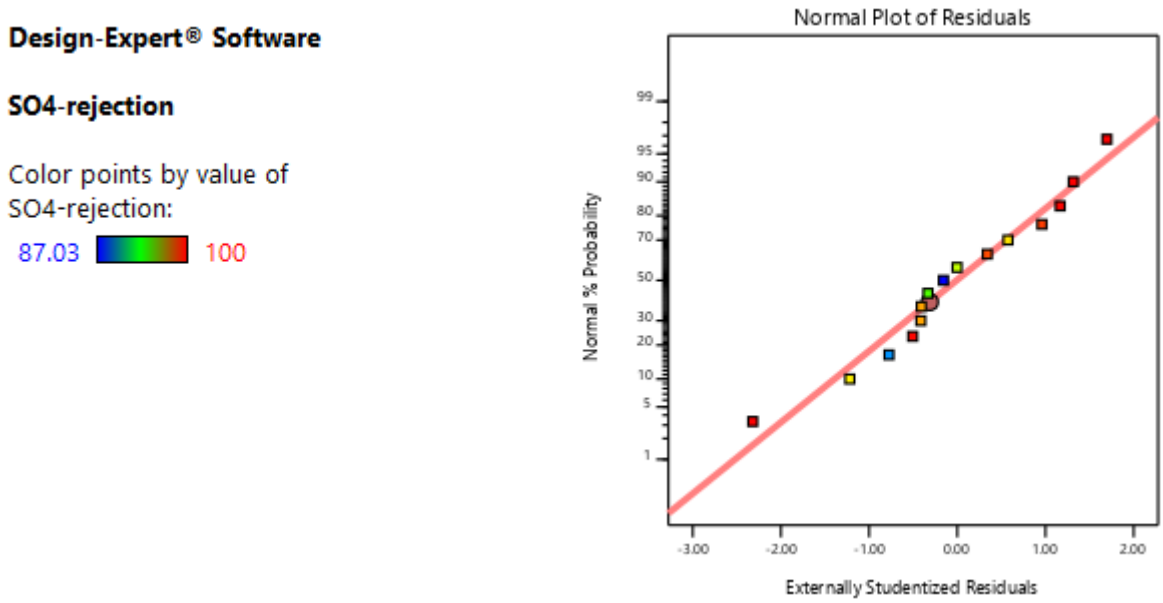

Figure B - 5: Normal probability vs residual plot

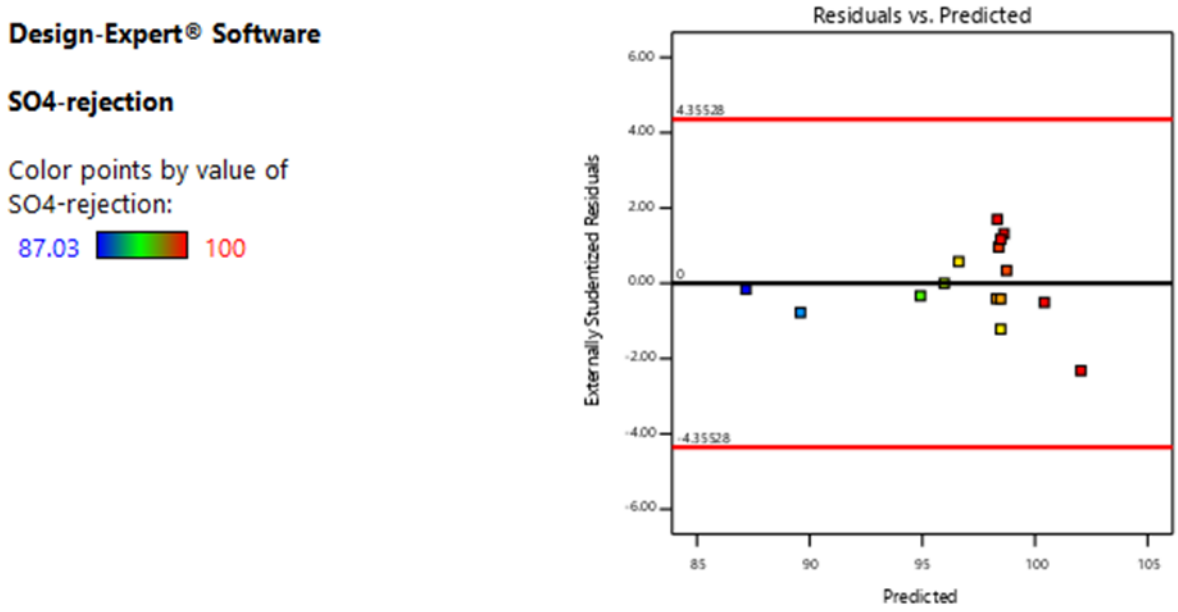

Figure B - 6: Plot of residuals vs Predicted

Table B - 4: Forward osmosis: Response 4: CO_3^{2-} rejection efficiency

Run Order	Actual Value	Predicted Value	Residual	Leverage	Internally Studentized Residuals	Externally Studentized Residuals	Cook's Distance	Influence on Fitted Value DFFITS	Standard Order
1	89.23	88.95	0.2770	0.692	1.313	1.420	0.431	2.130	1
2	92.49	92.92	-0.4283	0.692	-2.030	-3.310	1.030(1)	-4.965(1)	2
3	95.01	94.95	0.0577	0.231	0.173	0.158	0.001	0.087	3
4	93.28	93.39	-0.1120	0.692	-0.531	-0.496	0.070	-0.745	4
5	94.03	93.95	0.0795	0.692	0.377	0.348	0.036	0.522	5
6	96.08	96.23	-0.1458	0.692	-0.691	-0.657	0.119	-0.986	6
7	92.29	92.50	-0.2108	0.692	-0.999	-0.999	0.249	-1.498	7
8	93.89	93.53	0.3620	0.692	1.716	2.195	0.736	3.292	8
9	97.01	97.34	-0.3295	0.692	-1.562	-1.851	0.610	-2.776(1)	9
10	86.89	87.13	-0.2445	0.692	-1.159	-1.201	0.336	-1.801	10
11	91.73	91.66	0.0717	0.692	0.340	0.313	0.029	0.470	11
12	90.99	91.00	-0.0055	0.692	-0.026	-0.024	0.000	-0.036	12
13	95.28	94.95	0.3277	0.231	0.982	0.979	0.032	0.536	13
14	95.28	94.95	0.3277	0.231	0.982	0.979	0.032	0.536	14
15	96.04	96.07	-0.0270	0.692	-0.128	-0.117	0.004	-0.176	15

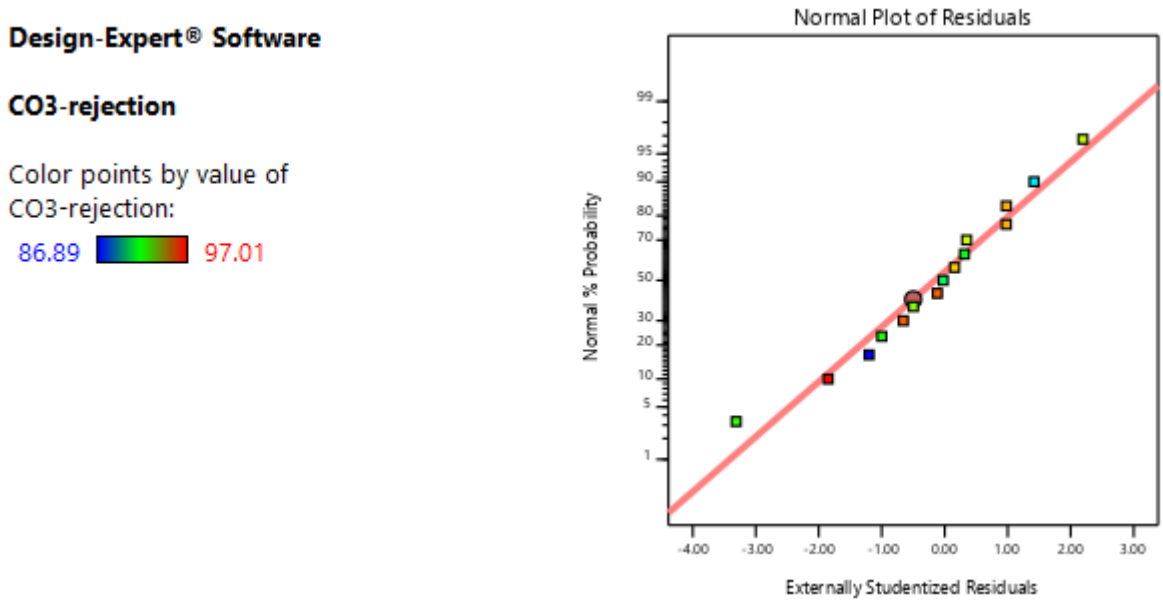

Figure B - 7: Normal probability vs residual plot

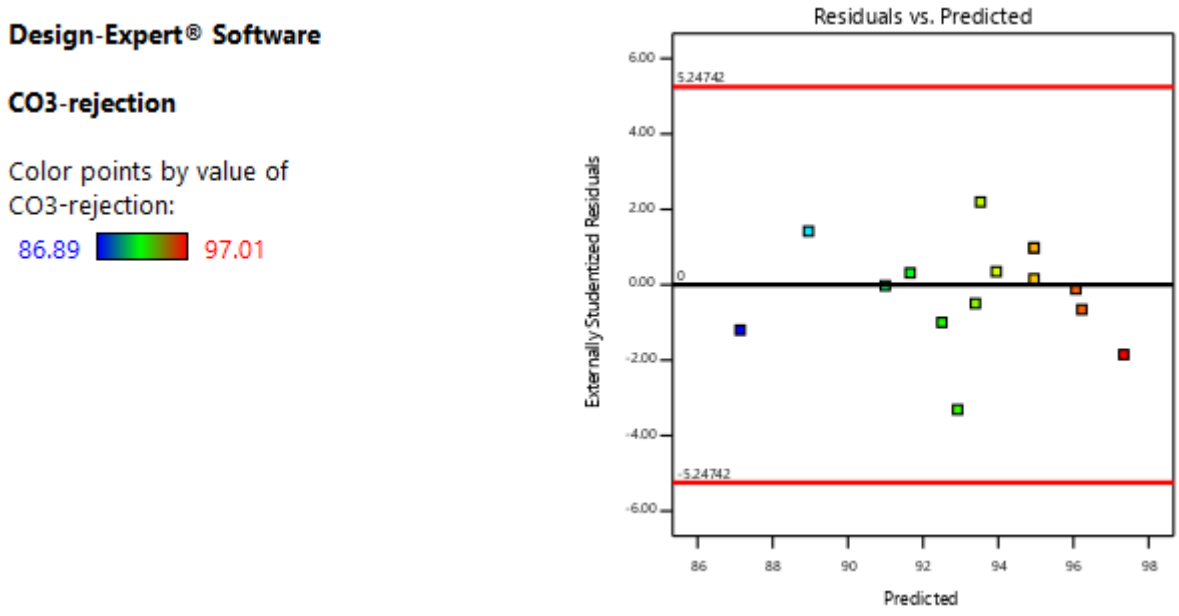

Figure B - 8: Plot of residuals vs Predicted

Table B - 5: Reverse osmosis: Response 1: permeation flux

Run Order	Actual Value	Predicted Value	Residual	Leverage	Internally Studentized Residuals	Externally Studentized Residuals	Cook's Distance	Influence on Fitted Value DFFITS	Standard Order
1	1.13	1.26	-0.1314	0.625	-1.041	-1.047	0.258	-1.352	1
2	0.3010	0.0468	0.2542	0.393	1.583	1.787	0.232	1.437	2
3	1.25	1.21	0.0411	0.625	0.326	0.307	0.025	0.396	3
4	3.89	4.07	-0.1761	0.625	-1.396	-1.501	0.464	-1.938	4
5	1.98	1.89	0.0884	0.143	0.464	0.440	0.005	0.179	5
6	3.81	3.74	0.0737	0.393	0.459	0.435	0.019	0.350	6
7	1.69	1.89	-0.2016	0.143	-1.057	-1.066	0.027	-0.435	7
8	1.17	1.27	-0.1039	0.625	-0.823	-0.805	0.161	-1.039	8
9	4.01	3.74	0.2664	0.625	2.111	2.967	1.061[1]	3.830	9
10	1.50	1.70	-0.2041	0.393	-1.271	-1.331	0.149	-1.071	10
11	1.76	1.89	-0.1316	0.143	-0.690	-0.665	0.011	-0.272	11
12	2.20	2.08	0.1209	0.393	0.753	0.731	0.052	0.588	12
13	2.45	2.48	-0.0311	0.625	-0.247	-0.232	0.014	-0.299	13
14	1.61	1.60	0.0136	0.625	0.108	0.101	0.003	0.130	14
15	2.55	2.43	0.1214	0.625	0.962	0.957	0.220	1.235	15

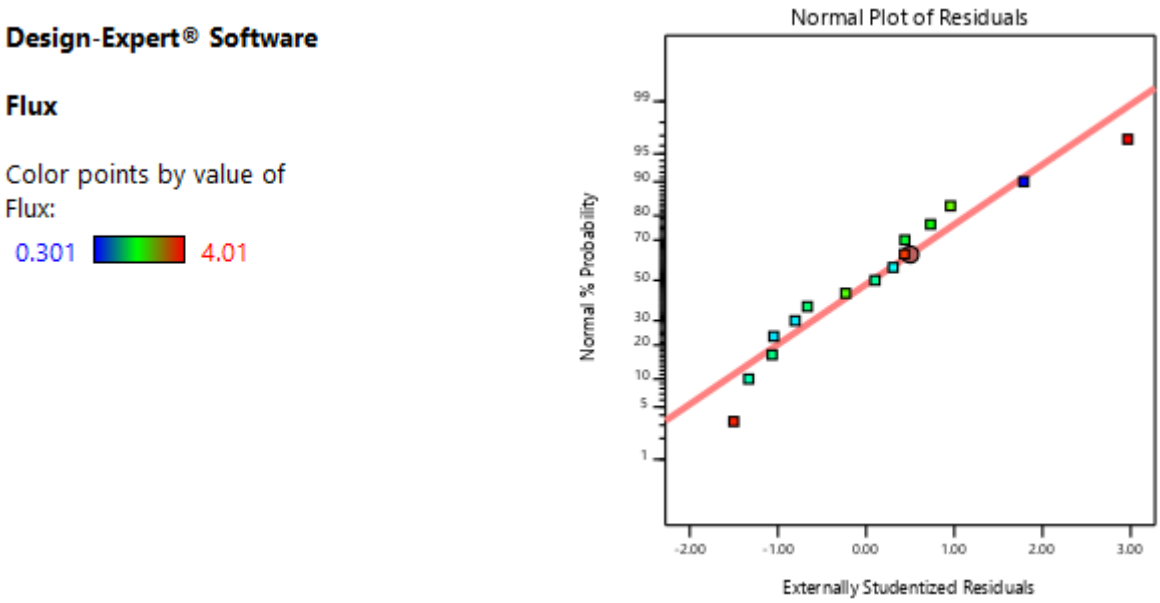

Figure B - 9: Normal probability vs residual plot

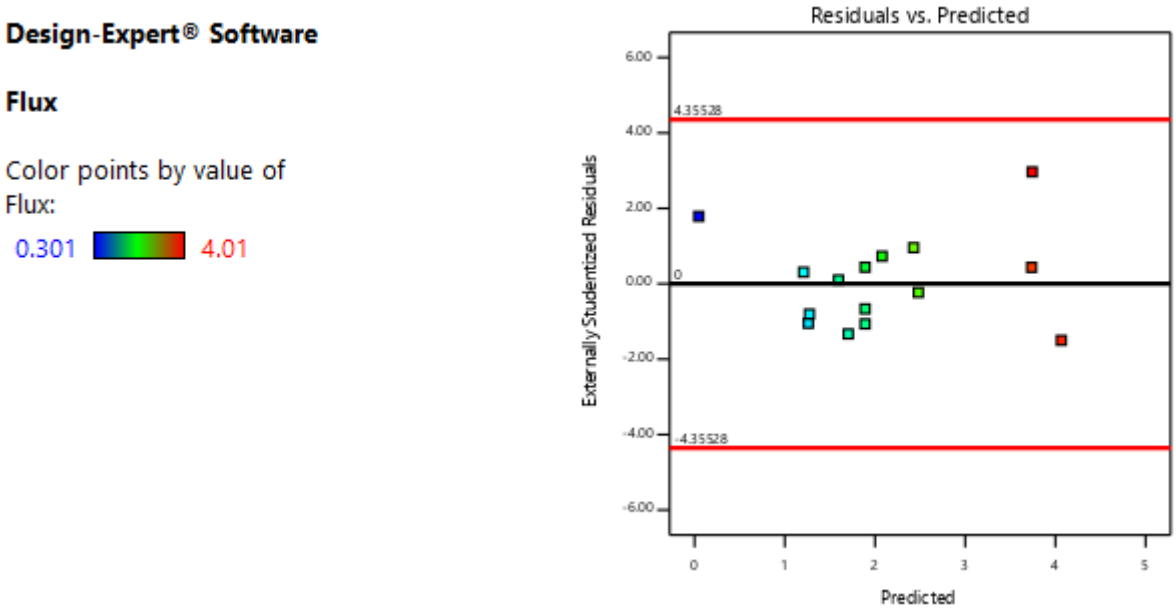

Figure B - 10: Plot of residuals vs Predicted

Table B - 6: Reverse osmosis: Response 2: Cl^- rejection efficiency

Run Order	Actual Value	Predicted Value	Residual	Leverage	Internally Studentized Residuals	Externally Studentized Residuals	Cook's Distance	Influence on Fitted Value DFFITS	Standard Order
1	75.00	74.99	0.0150	0.750	0.032	0.030	0.000	0.052	1
2	90.00	89.52	0.4813	0.500	0.732	0.705	0.067	0.705	2
3	89.96	91.40	-1.44	0.500	-2.185	-3.586	0.597	-3.586	3
4	70.12	70.60	-0.4787	0.500	-0.728	-0.701	0.066	-0.701	4
5	77.90	77.33	0.5733	0.333	0.755	0.730	0.036	0.516	5
6	67.88	68.33	-0.4462	0.500	-0.679	-0.650	0.058	-0.650	6
7	77.08	77.33	-0.2467	0.333	-0.325	-0.303	0.007	-0.214	7
8	97.08	96.61	0.4663	0.500	0.709	0.682	0.063	0.682	8
9	85.01	85.03	-0.0150	0.750	-0.032	-0.030	0.000	-0.052	9
10	94.83	94.34	0.4888	0.500	0.743	0.717	0.069	0.717	10
11	77.00	77.33	-0.3267	0.333	-0.430	-0.404	0.012	-0.286	11
12	62.98	63.50	-0.5237	0.500	-0.797	-0.774	0.079	-0.774	12
13	66.83	65.38	1.45	0.500	2.204	3.687	0.607	3.687[1]	13
14	91.40	91.37	0.0275	0.750	0.059	0.055	0.001	0.095	14
15	90.95	90.98	-0.0275	0.750	-0.059	-0.055	0.001	-0.095	15

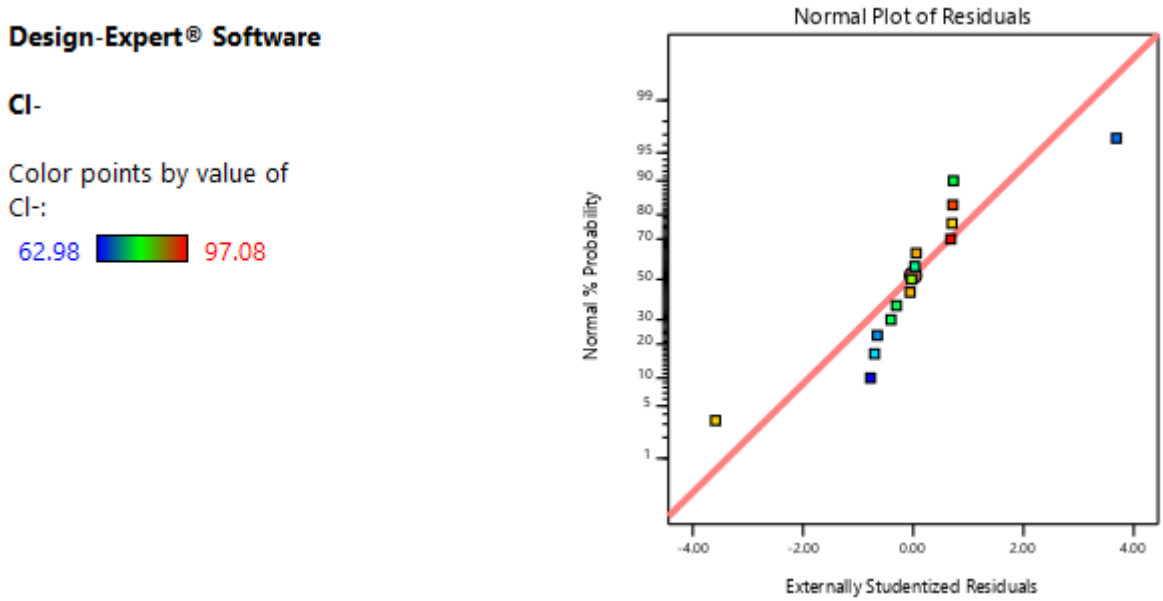

Figure B - 11: Normal probability vs residual plot

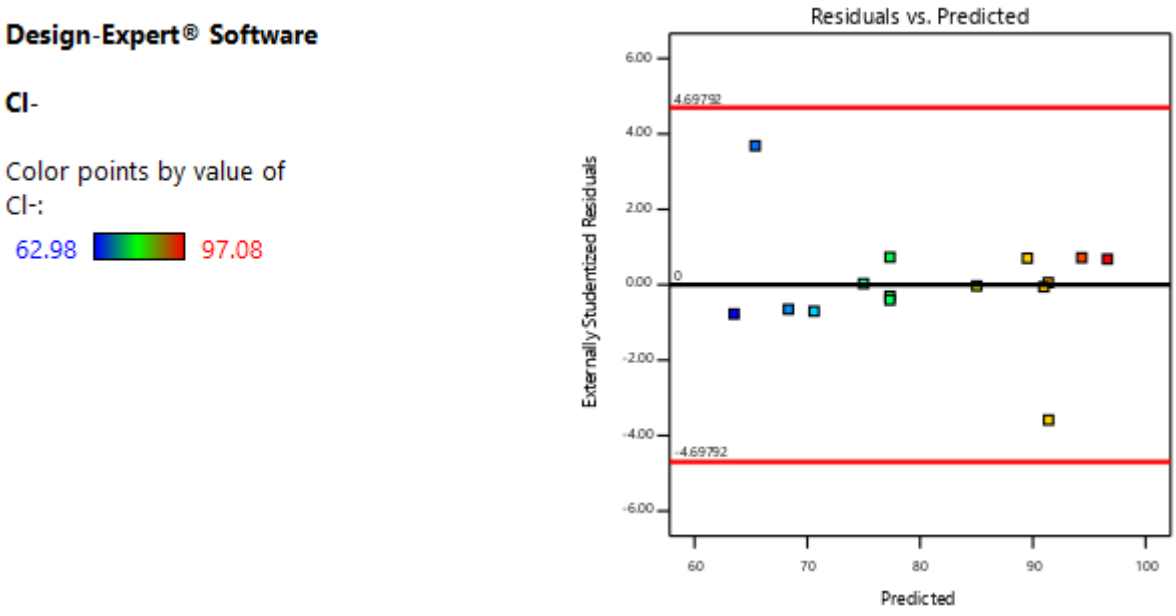

Figure B - 12: Plot of residuals vs Predicted

Table B - 7: Reverse osmosis: Response 3: SO_4^{2-} rejection efficiency

Run Order	Actual Value	Predicted Value	Residual	Leverage	Internally Studentized Residuals	Externally Studentized Residuals	Cook's Distance	Influence on Fitted Value DFFITS	Standard Order
1	86.40	86.85	-0.4467	0.692	-1.892	-2.381	1.151	-3.571	1
2	95.01	94.87	0.1380	0.442	0.434	0.411	0.021	0.366	2
3	94.02	93.68	0.3355	0.442	1.055	1.064	0.126	0.948	3
4	83.99	84.10	-0.1120	0.442	-0.352	-0.332	0.014	-0.296	4
5	86.92	86.66	0.2577	0.231	0.690	0.666	0.020	0.365	5
6	85.13	85.46	-0.3345	0.442	-1.052	-1.061	0.125	-0.944	6
7	87.01	86.66	0.3477	0.231	0.931	0.923	0.037	0.505	7
8	96.53	96.85	-0.3170	0.442	-0.997	-0.997	0.113	-0.888	8
9	93.82	93.35	0.4733	0.692	2.004	2.657	1.291	3.986[1]	9
10	98.00	98.21	-0.2095	0.442	-0.659	-0.634	0.049	-0.565	10
11	86.11	86.66	-0.5523	0.231	-1.479	-1.624	0.094	-0.889	11
12	82.48	82.13	0.3530	0.442	1.110	1.129	0.140	1.006	12
13	80.98	80.94	0.0405	0.442	0.127	0.119	0.002	0.106	13
14	94.57	94.61	-0.0442	0.692	-0.187	-0.176	0.011	-0.263	14
15	94.86	94.79	0.0708	0.692	0.300	0.282	0.029	0.423	15

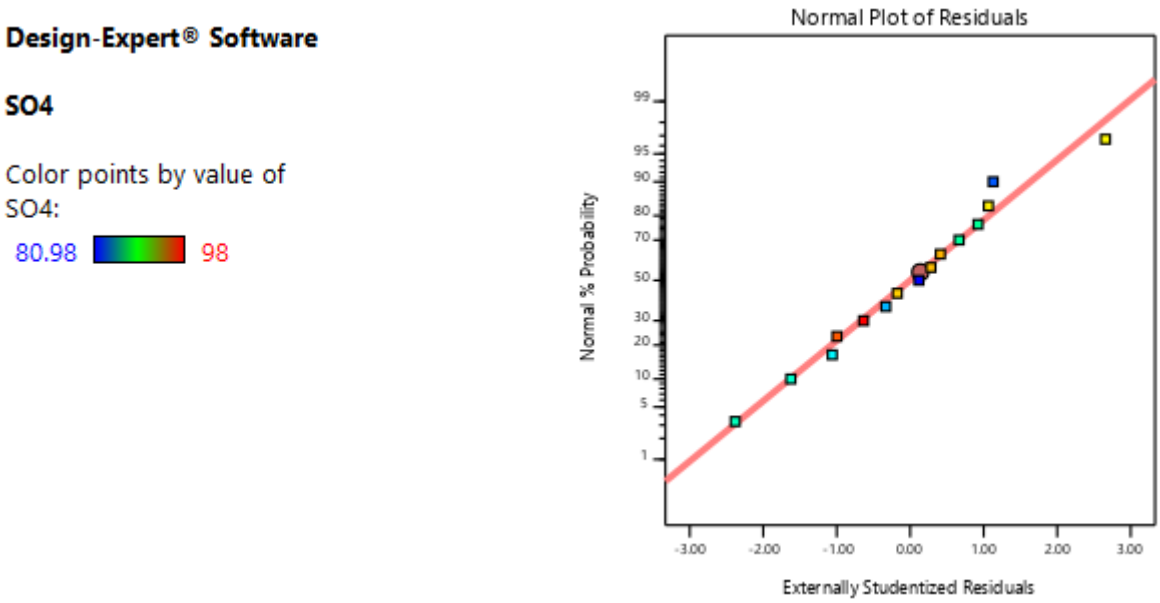

Figure B - 13: Normal probability vs residual plot

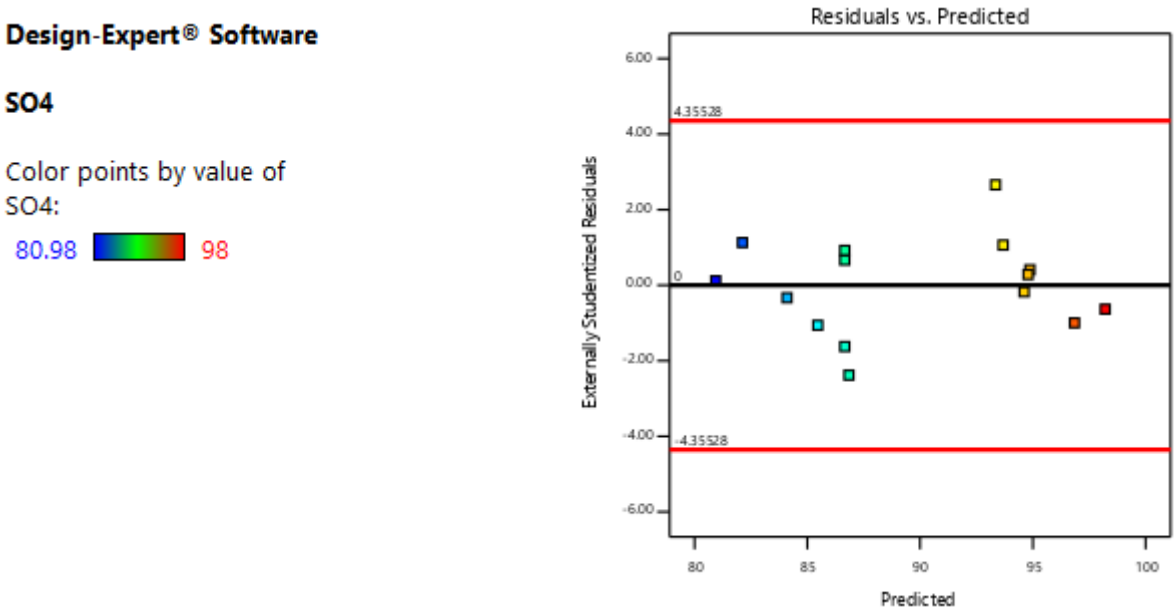

Figure B - 14: Plot of residuals vs Predicted

Table B - 8: Reverse osmosis: Response 3: CO_3^{2-} rejection efficiency

Run Order	Actual Value	Predicted Value	Residual	Leverage	Internally Studentized Residuals	Externally Studentized Residuals	Cook's Distance	Influence on Fitted Value DFFITS	Standard Order
1	98.73	98.83	-0.0963	0.750	-1.415	-1.582	0.667	-2.740	1
2	99.38	99.33	0.0500	0.750	0.735	0.703	0.180	1.218	2
3	98.84	98.67	0.1737	0.500	1.806	2.439	0.362	2.439	3
4	98.33	98.25	0.0812	0.500	0.844	0.821	0.079	0.821	4
5	93.78	93.84	-0.0567	0.333	-0.510	-0.476	0.014	-0.337	5
6	98.33	98.38	-0.0500	0.750	-0.735	-0.703	0.180	-1.218	6
7	93.82	93.84	-0.0167	0.333	-0.150	-0.137	0.001	-0.097	7
8	98.84	99.01	-0.1713	0.500	-1.780	-2.364	0.352	-2.364	8
9	99.08	98.98	0.0962	0.750	1.415	1.582	0.667	2.740	9
10	98.63	98.68	-0.0525	0.750	-0.772	-0.742	0.198	-1.285	10
11	93.91	93.84	0.0733	0.333	0.660	0.626	0.024	0.442	11
12	98.16	98.11	0.0525	0.750	0.772	0.742	0.198	1.285	12
13	97.82	97.90	-0.0838	0.500	-0.870	-0.850	0.084	-0.850	13
14	98.87	98.88	-0.0063	0.750	-0.092	-0.084	0.003	-0.145	14
15	98.35	98.34	0.0062	0.750	0.092	0.084	0.003	0.145	15

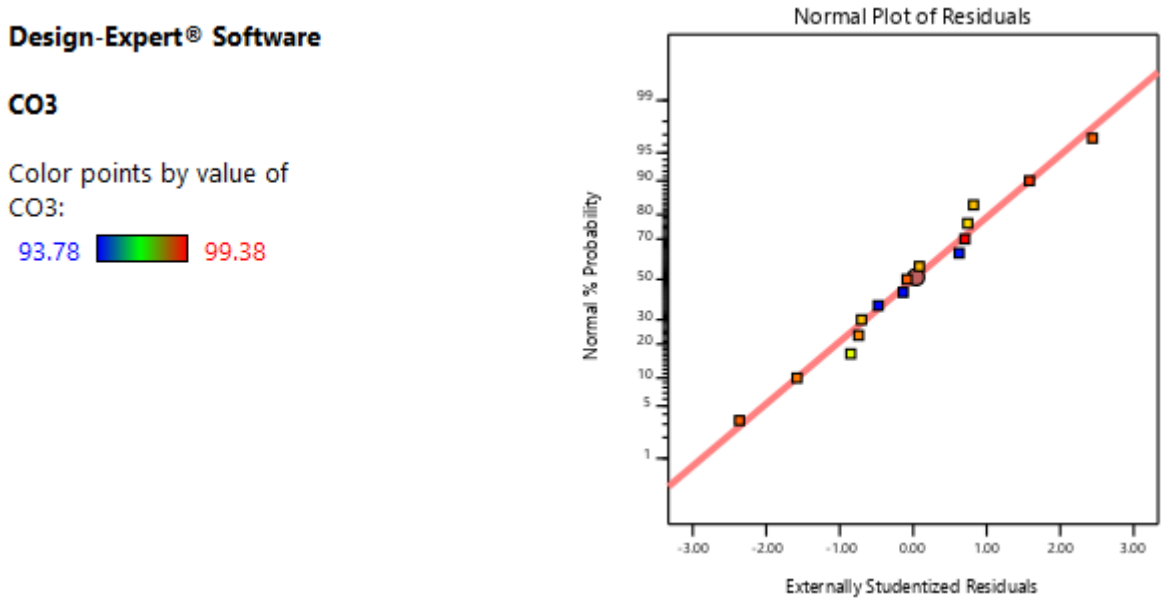

Figure B - 15: Normal probability vs residual plot

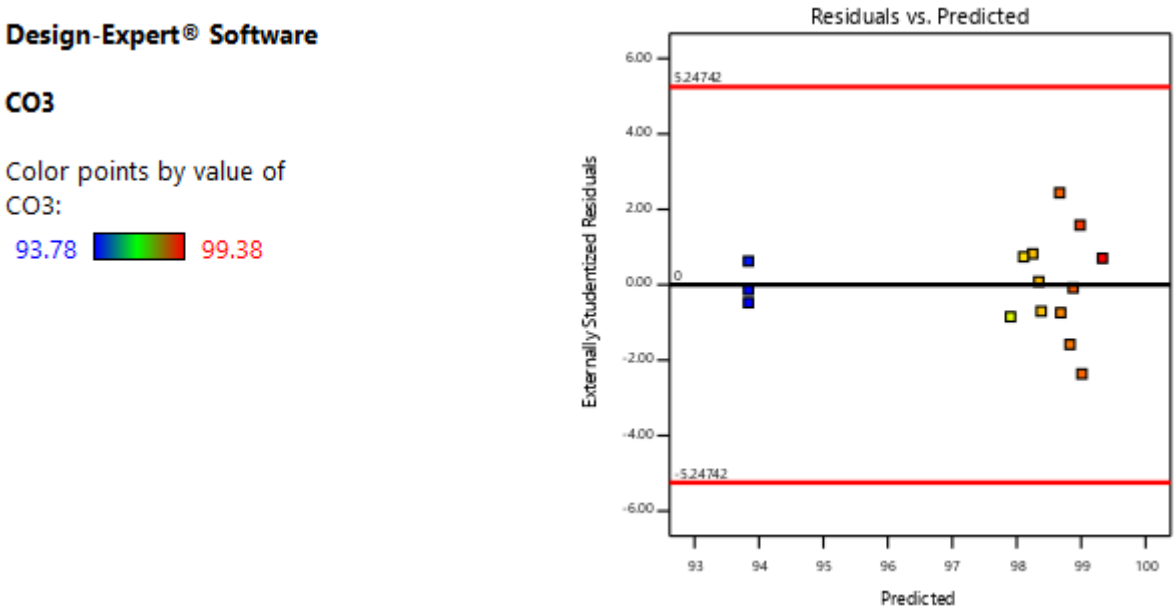

Figure B - 16: Plot of residuals vs Predicted

Appendix C

COMPONENTS OF MEMBRANE RIGS

This section provides description and labeled pictures of the membrane test rigs for both forward osmosis and reverse osmosis. The section also displays some photographs of some relevant equipment used in this study.

Forward osmosis

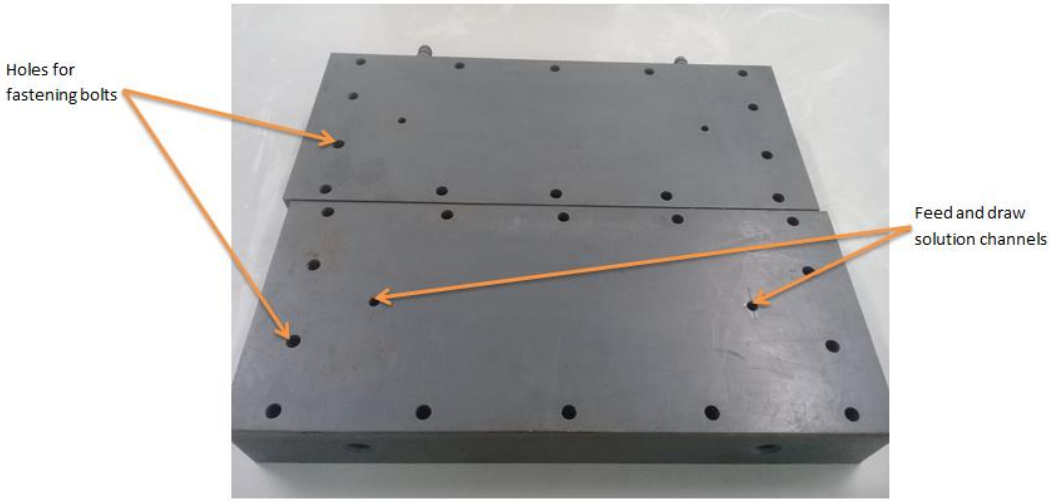

Figure C - 1: PVC blocks showing feed and draw solution channels and holes for fastening bolts

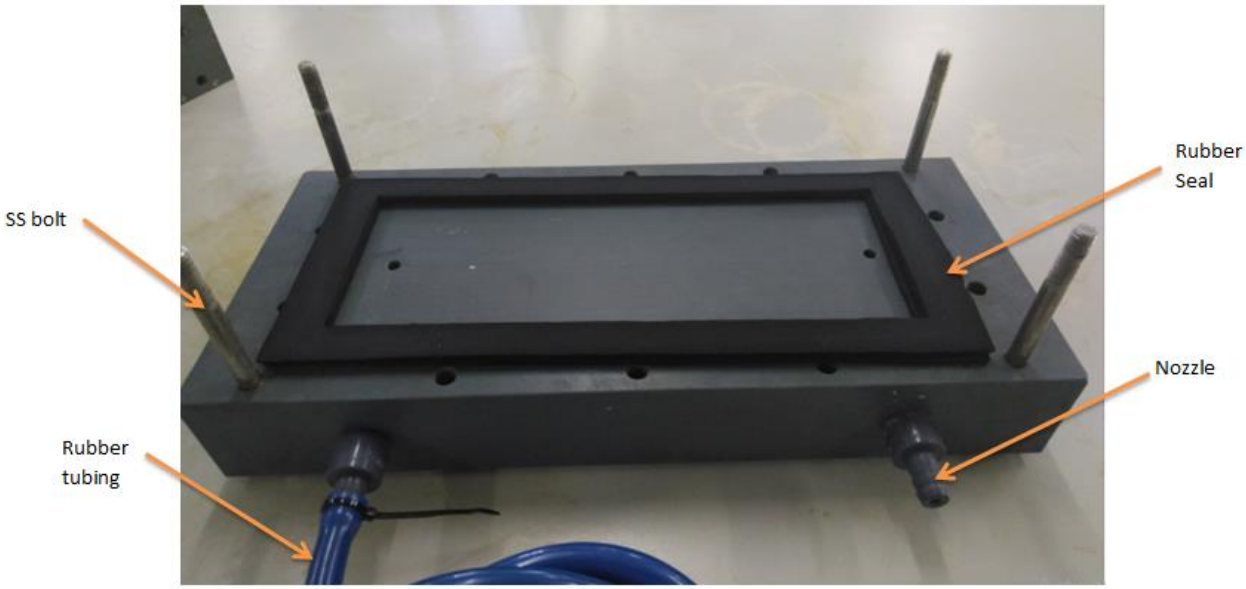

Figure C - 2: FO – membrane cell showing the nozzle, rubber seal and fastening bolts

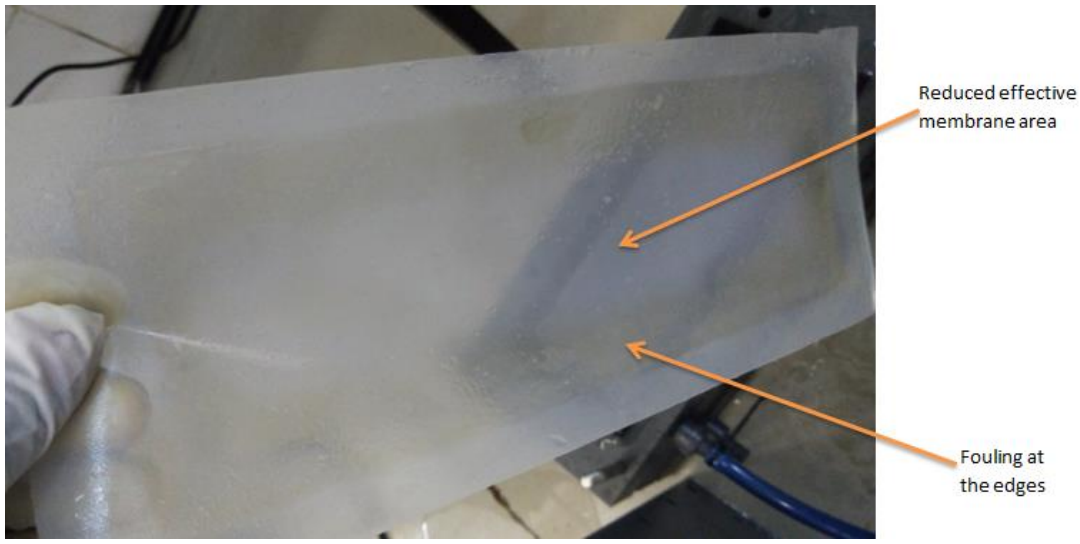

Figure C - 3: Fouled FO membrane showing reduced effective membrane area.

Figure C - 4: Peristaltic pump with connected rubber tubing

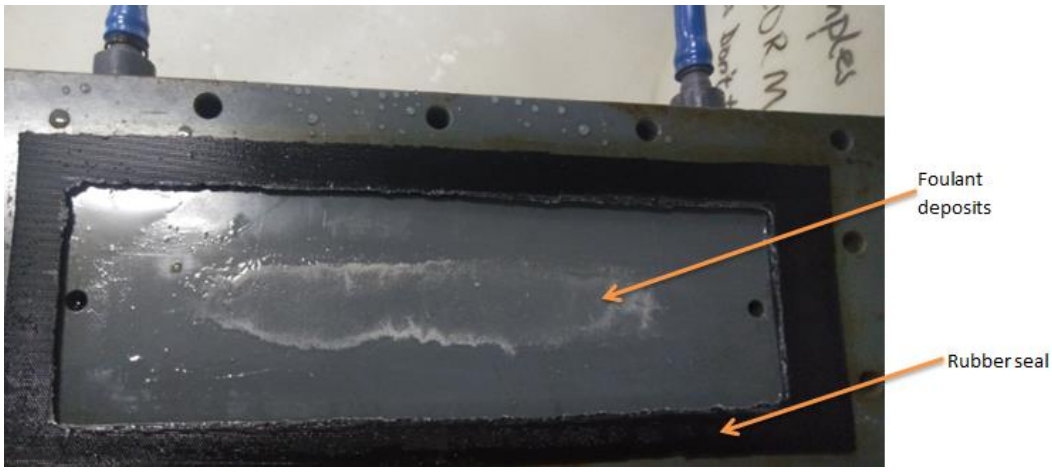

Figure C - 5: FO – membrane cell showing foulant deposits

Reverse osmosis

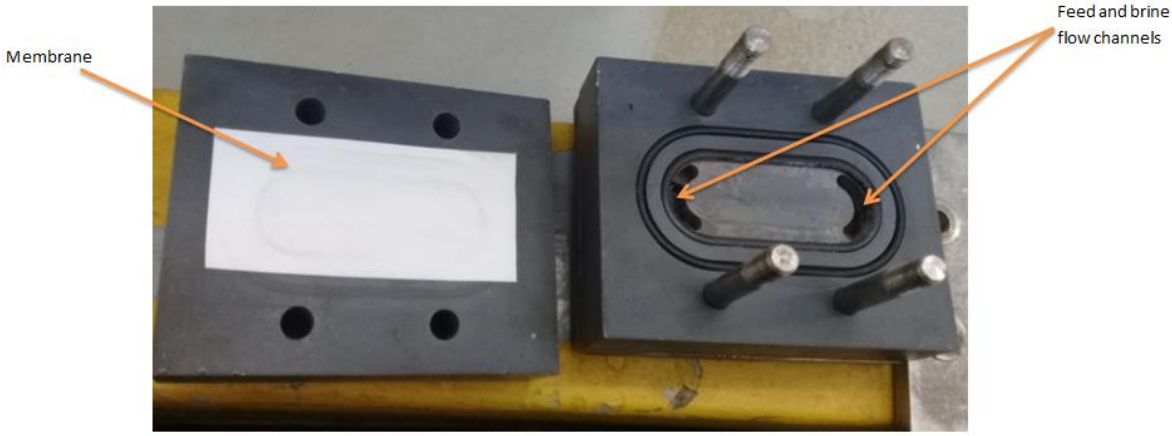

Figure C - 6: RO membrane cell showing TFC membrane, feed and brine flow channels

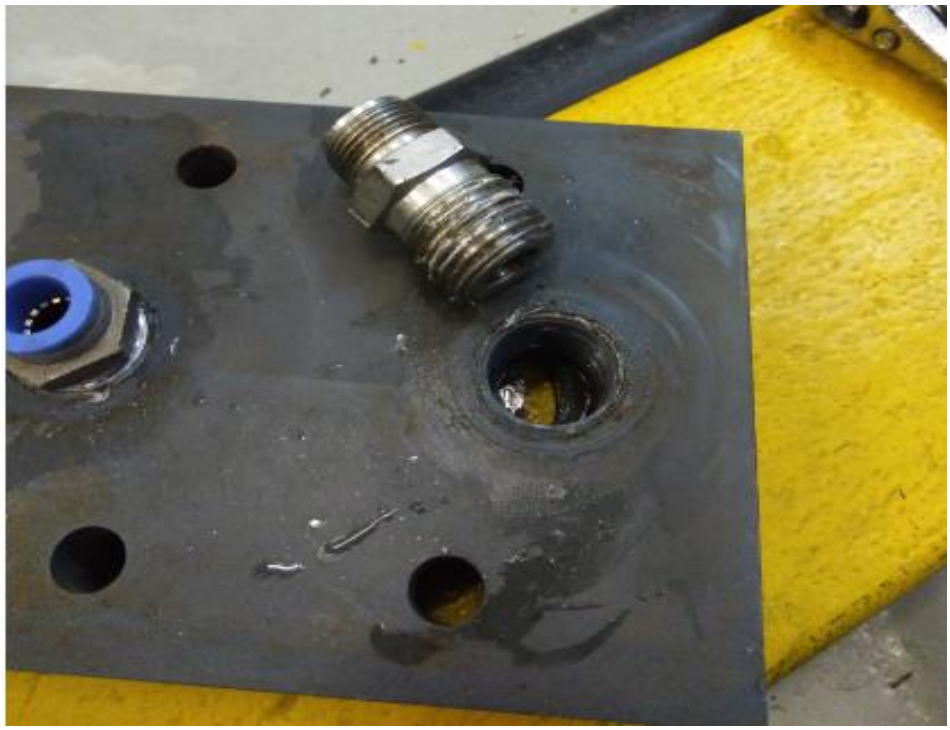

Figure C - 7: Constructing the RO membrane test cell

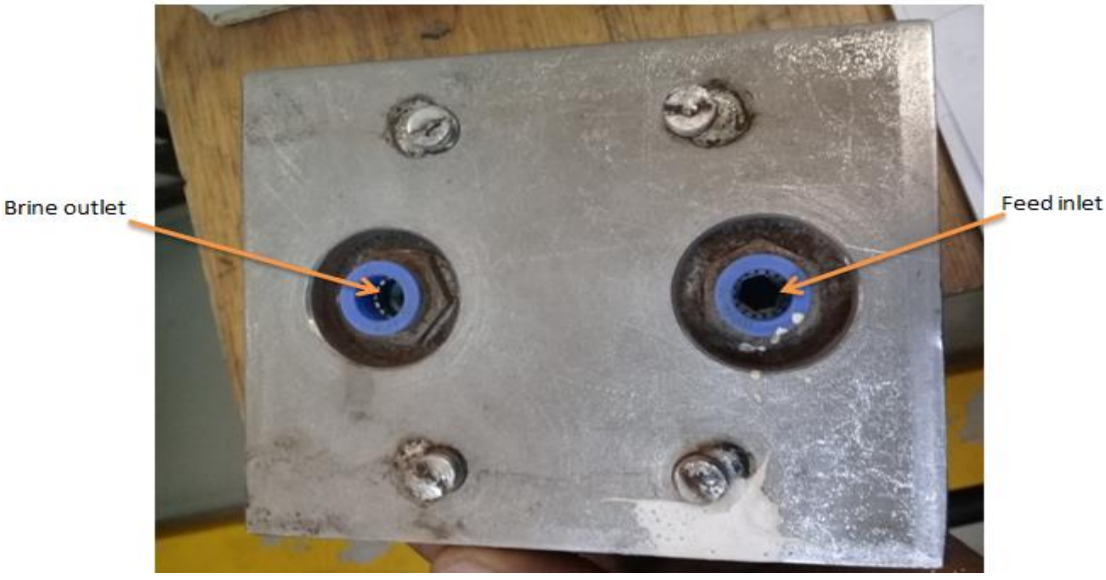

Figure C - 8: RO test cell showing feed inlet and brine outlet

Figure C - 9: RO membrane rig showing the high-pressure pump, pressure gauge and pressure control valve

Figure C - 10: Fouled RO membrane

Relevant photographs of experimental equipment and materials

Figure C - 11: HACH DR 3900 spectrophotometer

Figure C - 12: Pre-filtration of raw ORE

Figure C - 13: ELGA PURELAB Option-Q water deionizer